TWO DIMENSIONAL SELF-PRESERVING TURBULENT WAKES

BY

V.A. VAINAS

A thesis submitted to the Faculty of Graduate Studies and Research in partial fulfilment of the requirements for the degree of Master of Engineering

Department of Mechanical Engineering
McGill University
Montreal, Quebec
CANADA

August, 1978

ABSTRACT

The equations governing the mean motion of symmetrical, two dimensional turbulent wakes and jets in streaming flow indicate that these flows can be self-preserving when subjected to appropriately tailored pressure gradients. This class of flow was investigated experimentally for a jet and two wakes with different values of deficit-to-free-stream velocity ratio. The data are presented in the form of non-dimensional plots of mean velocity distribution, rate of growth of the wakes and the jet, velocity decay rate and components of the turbulent stress tensor.

For one wake self-similarity of only the mean flow parameters was achieved. For the other wake and the jet self-preservation of all flow parameters including the stress tensor was achieved. The flows were satisfactorily two dimensional. Comparisons of the experimental results to theory show that Vogel's theory predicts satisfactorily the rate of growth and the shear stress parameters for these flows.

SOMMAIRE

Un écoulement symétrique à deux dimensions contenant des jets et sillages turbulents fut mis en présence de changement de pression graduel pour prouver que la turbulence peut s'auto-préserver comme indiqué par l'équation de mouvement des fluides.

Les résultats expérimentaux démontrent la distribution de vitesse non-dimensionnelle, le taux de croissance des sillages et des jets turbulents, le taux de décroissance de vitesse et les composantes du vecteur de contrainte, pour deux cas différents de déficience moyenne de vitesse en rapport avec la vitesse moyenne d'écoulement. Toutes ces variables sont non-dimensionnalisées par la déficience moyenne de vitesse locale.

Le fait que l'écoulement est à deux dimensions fut bien démontré (une fois que le taux de changement de pression fut établi) et les conditions d'auto-préservation furent obtenues pour les jets et le deuxième sillage pour le vecteur de contrainte, et pour les paramètres moyens de l'écoulement. Le premier sillage démontra des similitudes avec les paramètres de l'écoulement moyen mais le vecteur de contrainte n'était qu'approximativement similaire. En comparant la théorie de Vogel avec les résultats expérimentaux l'on peut constater qu'elle prédit raisonnablement bien le taux de croissance et les paramètres des contraintes de cisaillement pour les jets et sillages auto-préservants à deux dimensions.

ACKNOWLEDGEMENTS

The author is very much indebted to Dr. G.I. Fekete for his guidance, interest, his valuable suggestions and for the useful criticism which he has offered during the course of this work. The author would like to thank Dr. Fekete for supplying him with his computer programs, which were used in analyzing and plotting the results. The traversing gear, used by the author, was designed and built by Dr. Fekete.

Many thanks are due to Mr. Joe Dubik for his assistance and technical advice during the experiments and for machining different wake forming bodies.

Thanks are also due to the members of the Aero Group, Professor B. G. Newman, R. Murray and J. Robert for many interesting informal discussions which were of great help.

---

* The work was supported by the Defence Research Board of Canada under D.R.B. Grant Number 9550-59.

TABLE OF CONTENTS

NOTATION

A	-	Lateral rate of strain, $\frac{\partial U}{\partial y}$
B	-	Longitudinal rate of strain, $\frac{\partial U}{\partial x}$
b	-	Slot width for the jet or width of body producing two-dimensional wake
C_1	-	Scale factor from $U_1 = C_1 \ (X_{TE} + X_0)^m$
C_0	-	$(\frac{dL_0}{dx})$ Growth parameter for wake or jet
f	-	Function of η for the mean velocity profile
F	-	$(\frac{dL_0}{dx})$ (Figures 51 and 52) of jet in still air $(G = \infty)$
G	-	Jet excess or wake deficit to free stream velocity ratio $\frac{U_0}{U_1}$
g	-	Functions of η for components of the turbulence stress tensor
g_0	-	Shear stress parameter at $y = L_0$ $(\eta=1)$
H	-	$(q_0^2)^{\frac{1}{2}}/U_0$
H_s^2	-	Suffix s = jet in still air
k	-	ln2
k	-	(Figure 11) Constant in longitudinal cooling law
L_0	-	Scaling length for the mean-velocity and the turbulence; interpreted as the value of y where $U = U_1 + U_0/2$

m	-	Growth exponent for self-preserving flow $U_1 \propto (X_{TE} + X_0)^m$
P_s	-	Reference static pressure
q^2	-	$u^2+v^2+w^2$ twice the kinetic energy of turbulence per unit mass
q_0^2	-	Twice kinetic energy of turbulence at $y = 0$
R_T	-	Eddy viscosity Reynold's number $(\frac{U_0 L_0}{\nu})$
U	-	Mean velocity in x-direction
U_m	-	Maximum or minimum velocity see Figure (1)
U_0	-	Velocity scale for the mean velocity and the turbulence; difference between velocity at centerline of jet or wake and the free stream velocity
U_j	-	Jet exit velocity at the tunnel exit plane
U_w	-	Wake velocity at centerline at the exit plane of the tunnel
U_1	-	Free stream velocity in x-direction
U_{0TE}	-	Velocity scale for the mean velocity at the tunnel exit
U_{1TE}	-	Free stream velocity at the tunnel exit
u	-	Fluctuating velocity about the mean in x-direction
V	-	Mean velocity in y-direction
v	-	Fluctuating velocity about the mean in y-direction
W	-	Mean velocity in z-direction
w	-	Fluctuating velocity about the mean in z-direction
X_{TE}	-	Streamwise distance measured from tunnel exit plane
X_0	-	x-position of the virtual origin of the flow from the tunnel exit plane

X - ($X_{TE}+X_0$) Coordinate direction (downstream distance measured from virtual origin)

y - Cross-stream distance measured from the axis of symmetry where V=0

Z - Coordinate direction

COMPUTER NOTATION	EQUIVALENTS	
$RMSU/_{U1}$	$\sqrt{\overline{u^2}}/U_1$	Longitudinal turbulent intensity (non-dimensional)
$RMSU/_{UO}$	$\sqrt{\overline{u^2}}/U_0$	Longitudinal turbulent intensity (non-dimensional)
$RMSV/_{UO}$	$\sqrt{\overline{v^2}}/U_0$	Cross-stream turbulent intensity (non-dimensional)
$RMSW/_{UO}$	$\sqrt{\overline{w^2}}/U_0$	Lateral turbulent intensity (non-dimensional)
$SQorQ2/_{SUO}$	$\overline{q^2}/U_0^2$	Twice kinetic energy of turbulence (non-dimensional)
$UW/_{SUO}$	$\overline{uw}/U_0^2$	Non-dimensional shear stress
$UV/_{SUO}$	$\overline{uv}/U_0^2$	Non-dimensional shear stress
$Y/_{LO}$	y/L_0	Non-dimensional cross-stream coordinate
MUV	$\overline{uv}$	Shear stress calculated from momentum equation
SUO	U_0^2	Scaling velocity squared
XTE		Streamwise distance measured from the tunnel exit plane
$X/_B$	$\frac{x}{b}$	Distance measured from virtual origin to slot width ratio $\frac{(X_{TE}+X_0)}{b}$

DLX	$\frac{dL_0}{dx}$ Rate of jet or wake growth - C_0
REF.	Reference station number
REF. ORDINATE	Reference hot-wire position measured in y-axis
UV1 UV2	RMS voltage readings of slanted wire (u, v-plane)
UW1 UW2	RMS voltage readings of slanted wire (u, w-plane)
YCL	Reference centerline of the flow, measured in y-axis

GREEK LETTERS

α , β	-	Constants relating g_0 to mean rates of strain used by Vogel Figures (51, 52) Also see Fekete (1970) pages 49-51
η	-	Similarity parameter (Y/L_0)
ν	-	Kinematic viscosity of fluid
ρ	-	Density of fluid

1. INTRODUCTION

Self-preserving flows have particular importance in the study of turbulent shear flows because of their relative simplicity. When a flow is self-preserving, the governing equations which describe the flow, become considerably simplified. Partial differential equations are replaced by ordinary differential equations, all properties scale with a single velocity and length scale, and the non-dimensional properties of the turbulent structure can be related to the properties of the mean flow. (Gartshore 1967, Gartshore and Newman 1969). The experimental study of self-preserving wakes and jets is of considerable interest since they represent a situation in which one is able to compare the actual and the predicted relationships of the rates of spread of the flows and the stress tensor to the local mean flow parameters. By the use of this information modelling of more complicated flows of engineering significance becomes feasible. Such flows are of practical interest in the design of jet pumps, thrust augmentors and in models of combustion chambers. This class of flows is also similar to the outer part of the flow in a jet-augmented boundary layer.

Theoretical and experimental work has been carried out in the study of two dimensional wall jets by Gartshore (1965), and of free jets, jets in uniform streaming flow and adverse pressure gradient by Newman (1967). No experimental data are available, however, for two dimensional self-preserving wakes.

Two fundamental flow parameters, the rate of spread, $\frac{dL_0}{dx}$ and the shear stress parameter, $\left.\frac{\overline{uv}}{U_\delta^2}\right|_{L_0}$, of self-preserving two dimensional jets and wakes, were predicted theoretically by Newman (1968) and Vogel (1969). Measurements of the rate of spread in jets (Fekete, 1970) and in wakes (Gartshore, 1967) are in good agreement with Newman's (1968) theory. However, the measured shear stress parameter for the jet and the two wakes show better agreement with Vogel's theory, although Gartshore's wake measurements show almost 50% higher values than those indicated by Vogel's theory. It should be noted that Gartshore's wakes were only approximately self-preserving.

The major objective of the present research was to obtain reliable shear stress measurements in self-preserving wakes and to compare the results with the existing theories and Gartshore's measurements. The detailed objectives of this work can be set as follows:

(a) to establish two-dimensional flows

(b) to adjust the pressure gradient in order to obtain self-preserving flows, as the mean flow parameters indicate,

(c) to carry out measurements in a two-dimensional self-preserving jet and compare the results to those measured by Fekete (1970) in order to gain confidence in the hot wire techniques in measuring turbulence,

(d) to measure the mean velocity, the rate of growth and the stress tensor for two-dimensional wakes,

(e) to prove that self-preservation does in fact exist for the stress tensor,

(f) to, compare the experimental results with Newman's (1968) and Vogel's (1969) theories and with Gartshore's (1967) and Fekete's (1970) measurements.

2. THEORY

2.1 Conditions for self-preservation

A self-preserving flow is one in which the mean velocity U and all other mean quantities such as the Reynolds stresses have the same profiles at every value of the downstream coordinate x, when they are made non-dimensional by using suitable length and velocity scales.

The necessary conditions for the exact self-preservation of turbulent jets and wakes, based on Townsend's approach, have been given by Patel and Newman (1961) and by Newman (1967). The conditions for self-preservation in two-dimensional flows are obtained from the mean flow momentum equation and the turbulence energy equation.

Considering a symmetrical, two dimensional jet or wake (Figure 1), the momentum equation in the downstream direction x, may be written as

$$U \frac{\partial U}{\partial X} + V \frac{\partial U}{\partial y} + \frac{\partial}{\partial X} (\overline{u^2} - \overline{v^2}) + \frac{\partial}{\partial y} (\overline{uv}) = U_1 \frac{dU_1}{dx} + \frac{\partial^2 U}{\partial y^2} \quad (1)$$

where U and V are the mean velocities in the x- and y-directions, u and v, are the associated turbulent fluctuations about the mean and U_1 is the velocity of the external irrotational flow.

Following Townsend (1956) the following self-preserving and similarity forms are assumed:

$$U = U_1 + U_0 f(\eta) \tag{2a}$$

$$\overline{u}^2 = U_0^2 g_{11}(\eta) \tag{2b}$$

$$\overline{v}^2 = U_0^2 g_{22}(\eta) \tag{2c}$$

$$\overline{uv} = U_0^2 g_{12}(\eta) \tag{2d}$$

where $\eta = (y/L_0)$, the bars denote time averages, and the functions f and g are functions of η only.

The scaling velocity U_0 and the length scale L_0 are shown in Figure 1. The scale U_0 is by definition the maximum velocity deficit in a wake, and the maximum velocity increment in a jet. The length scale L_0 is the distance from the centerline of the jet or wake to the point where the velocity increment or decrement is half the maximum value.

The functions f and g are independent of both x and y for a given self-preserving flow. It has been found experimentally that the function f can be adequately expressed by $\exp(-k\eta^2)$, where $k = \ln 2$ by the definition of L_0 and U_0.

The time average continuity equation for two-dimensional flow is

$$\frac{\partial U}{\partial x} + \frac{\partial V}{\partial y} = 0 \tag{3}$$

Substituting equations 2 into equation 3 gives:

$$V = -L_0 \eta \frac{dU_1}{dx} - \frac{d}{dx}(L_0 U_0) \int_0^\eta (f d\eta) + U_0 \frac{dL_0}{dx}(\eta) f \tag{4}$$

The momentum equation, Eq. (1) combined with equations (2), (3) and (4) leads to Newman (1967)

$$\left\{\frac{L_0}{U_0}\frac{dU_0}{dx}\right\}\left[f^2+2(g_{11}-g_{22})\right]+\left\{\frac{L_0}{U_0^2}\frac{d}{dx}(U_1U_0)\right\}\left[f\right]$$

$$-\left\{\frac{1}{U_0}\frac{d}{dx}(U_1L_0)\right\}\left[\eta f'\right]$$

$$-\left\{\frac{1}{U_0}\frac{d}{dx}(U_0L_0)\right\}\left[f'\int_0^\eta f\,d\eta\right]-\left\{\frac{dL_0}{dx}\right\}\left[\eta(g'_{11}-g'_{22})\right]$$

$$+\left[\frac{d}{d\eta}g_{12}\right]$$

$$-\left\{\frac{\nu}{U_0L_0}\right\}\left[f''\right] \qquad (5)$$

where primes denote differentiation with respect to η.

The terms in the square brackets are functions of η only and the terms in the curly brackets are functions of x only.

At large Reynold's numbers $\frac{U_0L_0}{\nu}$ based on the length scale and velocity deficit or increment, the term on the right-hand side of equation (5) approaches zero and may be neglected.

Following Newman (1968) self-preservation is possible only if the terms

$$\frac{L_0}{U_0}\frac{dU}{dx}\ ,\ \frac{L_0}{U_0^2}\frac{d(U_1U_0)}{dx}\ ,\ \frac{1}{U_0}\frac{d}{dx}(U_1L_0)\ ,\ \frac{1}{U_0}\frac{d}{dx}(U_0L_0),$$

$$\frac{dL_0}{dx}\ ,\ \left(\frac{\nu}{U_0L_0}\right)\text{(viscous term can be neglected)}$$

are constant.

All the above terms are constant if:

$$\frac{dL_0}{dx} \quad , \quad \frac{U_0}{U_1} \quad , \quad \text{and} \quad \frac{L_0}{U_0}\frac{dU_0}{dx}$$

are constant.

It follows directly that:

$$\frac{U_0}{U_1} = \text{constant} = G \qquad \text{-ve for wakes} \tag{6}$$

$$L_0 \propto (X_{TE} + X_0) \tag{6a}$$

$$U_0 \propto (X_{TE} + X_0)^m \tag{6b}$$

$$U_1 \propto (X_{TE} + X_0)^m \tag{6c}$$

2.2 Vogel

Vogel (1968) developed a closed form solution for the rate of growth and the shear stress parameter of symmetric, self-preserving wakes and jets in streaming flow.

The growth parameter obtained as:

$$C_0 = \frac{dL_0}{dx} = \frac{0.0738|G|(2G+4.242)}{(1.424G^2+5.01G+4.401)} \tag{7}$$

is plotted in Figure 51 for two values of α and β.

The growth exponent obtained for self-preserving flow is:

$$m = -\frac{(\sqrt{2}+G)}{(3\sqrt{2}+2G)} \tag{8}$$

and the shear stress parameter

$$\left.\frac{\overline{u\,v}}{U_0^2}\right|_{\eta = 1} = \frac{0.0738(0.405G^2+1.493G+1.414)(\text{sign } G)}{(1.424G^2+5.015G+4.401)} \tag{9}$$

is presented in Figure 52.

3. EXPERIMENTAL ARRANGEMENT

3.1 The wind tunnel, the jet, and the wake forming bodies.

The wake and jet measurements described herein were carried out in the McGill University open-circuit, blower-type wind tunnel, which has been described by Wygnanski and Gartshore (1963). The general layout of the apparatus is shown in Figure 2. A 25 HP, constant speed AC motor drives the centrifugal fan which has variable inlet vanes for speed control. At the exit from the tunnel, velocities between 6 and 40 meters/sec may be maintained, with a maximum spatial variation in velocity of 1.2%, outside the boundary layer. The turbulence level is reduced by a honeycomb and three screens in the settling chamber, upstream of the 6:1 area ratio contraction section. The tunnel air is filtered using American Air Filter bag type filters and fiberglass prefilters. Turbulence intensity on the centre-line of the tunnel varries from a maximum of 1.3% at low velocities to approximately 0.3% at high velocities. In order to reduce the turbulent intensity well below 1% at low velocities, (Patel 1970), a 5HP variable speed D.C. motor drive has been added.

The working section (Figure 3) is 76 cm. wide by 43 cm. high and 2.3 m. long. The side wall boundary layers are bled through 6 mm. wide vertical slots at 30, 108, and 186 cm.

downstream of the tunnel exit plane on both sides of the section. For the present experiments a perforated plate with a 40% open area ratio was fastened over the downstream end to build up the pressure in the working section. The pressure gradient was tailored using adjustable louvres in the top and the bottom of the working section as shown in Figures 4a and 4b.

3.1.1 The jet box

The jet box (Figure 5b) used for the self-preserving jet measurements, was described in detail by Fekete (1970). The air for the jet was supplied by a centrifugal compressor. The air passed through a water cooled heat exchanger (Figure 8b) and the air temperature could be adjusted to equal that of the wind tunnel. The jet velocity was controlled by means of a throttle valve in the ducting which carried the air to the two ends of the jet box (Figures 5c and d). The air streams entered the opposite ends of a 4.4 cm. high by 10.2 cm. wide channel, the front of which consisted of a two-dimensional orifice plate, designed to give uniform flow along the slot. The outside of the jet box was made as uniformly as possible in cross section along the length of the box. The jet was installed in the contraction section of the tunnel in order to give rise to a well behaved two-dimensional flow in the free stream. Jet box reference pressures were measured at two static-pressure taps, one at each end of the settling chamber of the jet box.

3.1.2 Wake forming bodies

In the process of setting up the wakes several wake producing bodies were tried. The jet blowing against the oncoming stream and a 2 cm. diameter rod were investigated. The aim was to produce as strong a wake as possible. The jet set-up was unsatisfactory, the 2 cm. rod was better. It appears that the strong eddies behing a bluff body are very effective at distributing momentum across the flow, and make for a wide, shallow wake. A 1.9 cm. square rod was also tried and proved satisfactory. The square rod (Figure 6a) was attached with one flat face normal to the oncoming stream to the mid points of the sides of the wind tunnel. A wake deficit to free stream velocity ratio of G = -0.181 was reached, but the flow as will be discussed later, was not self-preserving. To further try and reduce the component of separated flow in the wake, and thus possibly obtaining a deeper wake, a (J) shape channel as shown in (Figure 6b) was used and a self-preserving wake of G =-0.193 was produced.

3.2 The traversing gear

The traversing gear (Figure 7) was basically the same one designed and used by Fekete (1970). It consisted of a lead-screw driven by a synchro-receiver (Figure 3) wired to a synchro-transmitter which was driven by a small D.C. motor. The transmitter was coupled directly to a mechanical counter

which indicated the position of the hot wire probes. The traversing gear was checked for accurancy and was found to be accurate within 0.03 mm. over a range of 10 cm. of vertical travel. Hot-wire probes were supported at the end of a long boom made of thin walled steel tubing, the probe lead wires being carried back through the tube (Figure 3). The boom was clamped to the traversing gear slide in such a manner that it could be moved manually a total distance of 50 cm. along the x-axis. Screws located at the back of the slider made possible the alignment of the boom and hence the alignment of the wires with the mean flow direction. The traversing gear could also be slid manually from one side of the working section to the other. This permitted the checking of the two-dimensionality of the flow.

3.3 Instrumentation

The hot wire equipment used for measuring mean velocities, normal and turbulent shear stresses consisted of standard DISA units; five gold plated (55F12) slanting wires, three Pt-Plated tungsten (55A22) and two (55F11) normal wires (ref. DISA manual) were used. A schematic diagram of the instrumentation is shown in Figure 9 and the general layout in Figure 8a. A constant temperature DISA 55 D01 anemometer unit, two 55D10 linearizers and a 55D35, R.M.S. unit were used. One of the linearizers was calibrated for the use of the normal wires only, while the other one was calibrated for the use of the slanting ones as

different gain settings were needed to optimize sensitivity. For the DISA probes (Figure 10) and control units the linearizer exponent used lay between 2.3 and 2.4, the precise setting value depending on the probe.

During the experiments the linearizers were adjusted to the right setting and the probe was then aligned in the centerline of the flow by adjusting the yaw angle until the linearizer output, averaged over a minute, was effectively unchanged when the probe was rotated in its holder through 180°. Root mean square voltages were measured using the circuit in the DISA 55D35 R.M.S. meter. This meter has a low frequency cut off of 5Hz. An HP-2212A voltage to frequency converter was used in conjunction with an HP-5216A digital counter to record both the mean flow and turbulence data. Integration times for mean voltages were 10 seconds and the R.M.S. circuit was set to a 3 second time constant, the output being sampled ten times at about 1 second intervals and then averaged. A small range HP oscillator was also connected to the HP digital counter to provide a time gate in excess of 10 seconds when this was required for signal averaging of the slanting wire measurements. R.M.S. and mean voltages measurements were read directly from the Hewlett Packard 2212A VF converter/5216A electronic counter combinations. The results were recorded by hand and fed later into the computer program, Figures 53a, b, c, and d in data form.

The jet box reference temperature, working section reference pressure and the reference temperature of the working section were monitored visually at frequent intervals to ascertain constancy of flow conditions throughout each test run. The pressures were measured by a vertical water filled manometer and an inclined alcohol filled "Lambrecht" manometer respectively, while a conventional mercury thermometer was used to indicate the working section temperature.

3.4 Shear stress measurements in fully developed pipe flow

To check the experimental procedure and data reduction, an experiment was performed in fully developed pipe flow in a 7.62 cm. diameter 11 m. long smooth brass pipe at a Reynolds number of $Re_D = 3.76 \times 10^5$. The wall shear stress was measured via the pressure drop along the pipe and compared with that measured by the hot wire. The shear stress agrees well with those predicted (Figure 11) and is in very close agreement with those of Patel (1968) and Irwin (1972).

3.5 Hot wire calibration

Platinum plated tungsten DISA 55A22 and 55F11 normal and DISA 55F12 slanting hot wires with gold plated inactive ends were used for all the measurements (Figures 10a and 10b). The hot wires were operated at an overheat ratio of 1.8 resulting in wire operating temperatures which were about 200°c above

the ambient temperature. The angle of yaw (ψ) between the wire and the axis of rotation of each slanting wire probe was measured with a NIKON profile projector with magnification of 50. The wires were examined under a microscope before and after each test to check for any accumulation of dust and wire distortion.

A round nozzle mounted on top of a 45 gallon oil drum which acted as a settling chamber, was used for hot wire calibration (Figure 8b). A sketch is given in (Figure 12). The drum was connected to the jet air supply and the air flow rate to the drum was controlled by means of a slide valve. The velocity range which could be obtained with this arrangement was 0.1-100m/sec. A mechanism mounted on top of the drum allowed the probe axis to be positioned accurately parallel to the nozzle axis. One normal and one slanting wire was calibrated at the beginning of each run. At least 10 points were taken and to these a "Least-Squares" straight line was fitted (Figure 13). Each wire (ie normal and slanting) had its own linearizer unit and was normalized to an output of 8 volts at a free stream velocity of 25m/sec. for the jet experiment and to an output of 5 volts at 15/m sec. free stream velocity for the wake measurements. Correct alignment of the slanting wire probe with the calibration drum flow centerline, was assumed when the mean voltage reading was independent of the rotation of the wire.

4. EXPERIMENTAL PROCEDURE

4.1 Pressure gradient

All self-preserving jets and wakes of pratical interest, except the small deficit wakes, require an adverse pressure gradient; consequently the working section of the wind tunnel must provide for an adjustable decrease in velocity along the working section. The roof and the floor of the tunnel working section consisted of louvres which could be adjusted to bleed air from the tunnel. This, in conjunction with a 40% open area perforated plate fastened over the downstream end of the section, did create the required adverse pressure gradient. The following procedure was followed to set up the self-preserving flow.

The louvres on the top and bottom of the working section were-preset following Fekete (1970) and Vogel (1974) to give an adverse pressure gradient (Figures 4 and 14).

For a particular value of $\frac{U_{0TE}}{U_{1TE}}$ at the tunnel exit plane, the value of m was calculated from equation (8). A suitable free stream velocity at the tunnel exit U_{1TE} was then chosen. Using equations

$$U_1 = (X_{TE} + X_0)^m \quad \text{and}$$

$$U_{1TE} = (X_0)^m$$

$$\frac{U_1}{U_{1TE}} = \left(1 + \frac{X_{TE}}{X_0}\right)^m \qquad (10)$$

It was then possible to calculate the free stream velocity U_1 at various stations $\frac{X_{TE}}{X_0}$. The value of X_0 was determined approximately by extrapolating Fekete's results. Using the approximate values of U_1 and assuming that the flow at any section was one dimensional the mass flow at each section was calculated to establish the amount of excess air to be bled from the top and bottom louvres. Assuming that the louvre profiles were sufficiently streamlined to ensure that the flow left smoothly and without a vena contracta, it was possible by iteration (Vogel 1970) to determine the louvre setting to give the required pressure gradient (Figure 55).

For similar profiles, $(\frac{U_0}{U_1})$ is constant and in order to check that the pressure gradient was producing similar profiles, pitot-static tubes were used to measure U_0 and U_1 at different downstream distances in the working section. The positions of these pitot-static tubes were staggered on either side of the tunnel centre line so as to reduce the wake interference of one tube upon another.

From these readings the value $\frac{U_0}{U_1}$ was determined and the louvres were finally adjusted so that this ratio was constant down the working section. The constancy of the excess to free stream velocity ratio down the tunnel was then checked by hot wire measurement. It was found that Newman's criterion, equation (6), for self-preservation was satisfied (Figure 16). To generate the appropriate pressure gradient for the two wakes a

similar procedure was followed. The two wakes investigated required a different louvre space setting. It was found impossible to succeed in building-up an adverse pressure gradient in order to maintain a constant wake deficit to free stream velocity ratio higher than 0.2. The aim was to produce as strong a wake as possible, but although several wake producing bodies in combination with different louver settings were tried, unsatisfactory results were obtained, as the wakes produced were broad and very shallow. For a wake more adverse pressure gradient than required for self-preservation increases the magnitude of the ratio $\frac{U_0}{U_1}$ and slows down the wake more than the free stream. Thus a more and more negative value of G is produced and the value of m calculated from equation (8) gets smaller and smaller. This means that deviation from self-preserving conditions tends to produce a flow that is even farther from self-preservation making the flow "unstable". It is not implied that the wake is impossible to set up in practice, because changes of shear stress will occur to counteract the changes of G. The present argument, however, helps to explain why the wake was a more difficult flow to stabilize. It is interesting to note, however, that Townsend (1970) predicts from a study of the mechanism of entrainment in shear flow that the small deficit wake can never become self-preserving in zero pressure gradient.

4.2 Measurements and accurancy

Symmetry in the flow was ensured in a number of ways. First of all considerable care was taken to provide symmetry in the geometry of the apparatus. The jet or the wake producing apparatus having no support struts was carefully centered in the tunnel and the spacing of the top and bottom louvres was symmetrical.

In practice, the primary decision on whether or not a satisfactory flow had been achieved was based on G becoming nearly constant for a significant length of flow. Having L_0 varying linearly with x was also important but this was not always satisfactory although G was almost constant (Figures 16, 27 and 38).

Each test run was carried out in the following manner. The hot-wire instrumentation shown in Figure 9 was checked out, zeros, set points and gain settings were adjusted. Constant room and tunnel air flow temperatures were achieved as follows. The flow was traversed with the hot wire, and its cold resistance was measured at various stations in the jet and free stream regions, while the heat exchanger water supply was altered until no difference could be detected in the cold resistance measurements.

For any given traverse the first measurement was made at the center line, the flow was traversed from bottom to top and a final reading was taken at the centre line. For normal wire traverses both the mean and the R.M.S. voltages

were recorded and the averaging time for both signals was 10 seconds. The cold resistance of the wire was measured before the first and last center line reading always maintaining the same overheat ratio at the different streamwise locations. After the last measurement the wire was calibrated again and its cold resistance was compared with the cold resistance measured in the flow. Following this, slanted wire profiles were taken at the same downstream stations. The procedure followed was the same as the normal wire measurements, except that four traverses were made at each streamwise station, the wire being rotated 90^{o} between traverses. Correct alignment of the slanted wire probe with the working section flow center line, was assumed when the mean voltage reading was independent of the rotation of the wire.

The hot wire results for $\overline{uv}$, $\overline{v^2}$, $\overline{w^2}$, were corrected for longitudinal cooling using Champagne's (1965) correction. Preliminary measurements indicated that the turbulence intensities were less than 15%. Hence there was no need to worry about high intensity turbulence corrections (Guitton, 1968).

The recorded data was fed later into the computer and all mean flow quantities, turbulence intensities and shear stresses were calculated and the results were printed and plotted out.

The basic data and the calculated results are available in numerical tables, and Figures 54a, b, and c show examples of the numerical information. Figure 54a shows basic information

about the hot wire and voltages, Figure 54b presents dimensional calculated results without the longitudinal cooling correction and Figure 54c shows the non-dimensional results including the effects of the longitudinal cooling.

5. EXPERIMENTAL RESULTS AND DISCUSSIONS

5.1 Two-dimensionality and self-preservation of the flows

Figures 15 and 37 show the two-dimensionality investigation of the jet and the second wake, G = -0.193 respectively. Velocity profiles were taken at different positions across the flow, at a downstream distance of 1.3 m. Within 15 cm. of the center line the profiles are almost identical across the flow and indicate only ± 0.90 per cent variation in maximum velocity. Another, perhaps better measure of the existence of the two-dimensionality is shown in the comparison between the measured shear stress and that calculated from the integral momentum equations. This is a very severe criterion for the evaluation of the two-dimensionality because the existence of even a limited degree of three-dimensionality in a flow will cause momentum inbalance and noticeable digagreement between the calculated and measured shear stress values. The work of Bradshaw (1963) and Patel (1964) also points this out. Based on the measurements, the flow was considered to be effectively two-dimensional for the range of measurements which are presented here.

The theory predicts that if $U_1 \propto (X_{TE} + X_0)^m$ then G = constant down the flow, L_0 varies linearly with x, and the non-dimensionalized velocity profiles are the same at all stations. These conditions seem to be met satisfactorily for two of the

flows measured, the jet G = 0.79 and the wake G = -0.193 (Figures 17, 18 and 39, 40 respectively).

The non-dimensionalized profiles of all the terms in the Reynolds stress tensor should also be invariant down the flow when the flow is self-preserving. The longitudinal turbulence intensity $\left(\sqrt{u^2}/U_0\right)$ was taken as a measure of the self-preservation. For the two flows, the jet and the wake of G = -0.193, the turbulence intensity reached a self-preserving form, Figures 21 and 43 respectively. For the three flows the other two normal stress terms were also measured at more than one station, and here the similarity of the profiles at the different stations is not as good, especially for the two wakes. Figures (33-34) and (44-45).

For the same flows the shear stress measurements were made at a number of stations, and the fact that the measurements collapse onto one curve can be taken as another indication that the flows are self-preserving in the stress tensor term.

5.2 Results for the self-preserving jet and the two wakes in streaming flow with an adverse pressure gradient

The data for the jet and the two wake flows are presented in one table and eleven figures each. Table I and Figures (15 to 26) for the jet, table II and Figures (27 to 36) and table III and Figures (37 to 48) for the two wakes respectively.

The first three figures for each flow show the development of the mean flow. The first of each group of figures shows the value of G and the second presents the value of L_0 as a function of downstream distance X. Lines are drawn to give the average value of G, the slope of the L_0 line and X_0 (the virtual origin of the flows). The deviation of G in each case is no more than a few per cent from the average value and that of the L_0 from the line $L_0 = C_0 (X_{TE} + X_0)$ is 1 per cent for the jet and 1.6 per cent for the self-preserving wake, G = -0.193. The virtual origin X_0 is upstream of the outlet of the jet box and the leading edge of the wake forming body. Close to the jet outlet the jet grows at a larger rate, gradually reducing to the lower rate for the particular value of G for that flow. This would produce the observed effect on position of the virtual origin relative to the jet outlet. For the wake case, G = -0.193 the virtual origin defined by the values of U_0 is very close to that defined by L_0. For the jet X_0 is quite dependent on the internal boundary layers in the slot. However, if the flows eventually reach constant-momentum-increment or constant-momentum-deficit conditions at some downstream location, then this is a necessary condition that the velocity and the length scale must both have the same X_0.

Experimental values of $\log(U_1)$, $\log(U_0)$ and $\log(U_m)$ plotted against $\log(X_{TE} + X_0)$ are presented in the third figure of each group. Best lines are drawn through the experimental points and the slope is indicated. Since $U_1 \propto (X_{TE} + X_o)^m$

these points should lie on a straight line and the slope be equal to the value of m predicted by equation (8). Generally the fit to the log (U_1) log (U_m) and log (U_0) points is very good.

The next figure in each set presents the normalized mean velocity profiles. It is seen that for each flow they all collapse satisfactorily onto one curve, and, as was assumed in the theoritical development, the curves are identical for each flow. The assumed Gaussian profile used in the theory is also plotted on each of these figures. It is seen to be in close agreement over most of the width of the flow, but overestimates the amplitude in the outer part. The next figure presents the longitudinal turbulent intensity non-dimensionalized with U_1 and the next six figures present the measured Reynolds stress profiles of each flow non-dimensionalized with U_0.

The curves of the shear stress profiles calculated from the integrated momentum equation, the measured growth rates and the experimentally obtained excess or deficit to free stream velocity ratios of the flows, are drawn on the figures showing the non-dimensional shear stress $(\frac{\overline{uv}}{U_0^2})$ experimental data. The curves were calculated assuming self-preservation and Gaussian velocity profiles, and the experimental values of G and $\frac{dL_0}{dx}$ were used for each case.

For the flows with G = 0.79 and -0.193 the agreement between the data points and this profile line (Figures 26 and 48)

respectively is good out to the value of η at which the measured mean velocity and the Gaussian profile starts to differ. (Figures 19 and 41). The other two normal stress terms ($\sqrt{\overline{v^2}}/U_0$ and $\sqrt{\overline{w^2}}/U_0$) were also measured. (Figures 22, 23 and 44, 45). There is considerably more scatter in the data than for the $\sqrt{\overline{u^2}}/U_o$ values, Figures 21 and 43.

Figures 24 and 46 show the three normal stresses collected together and plotted as twice the turbulent kinetic energy ($\overline{q}^2/U_0{}^2$). Profiles of $\overline{uw}/U_0{}^2$ are plotted in Figures 25 and 47. From symmetry considerations these measured values should be zero, and this seems to be the case for the measured jet and the wake with G = -0.193.

As expected in the first non self-preserving wake G = -0.181, the agreement between predicted and measured shear stress is not as good, the measured values being higher and vary from the average by ± 8.1% to 25% at $\eta = L_0$ and $X/B = 76$ to 91 stations. This assymetry of the flow is also apparent in Figures 32 to 36. Investigation showed that the wake forming body was set at a slight angle to the oncoming flow and it was not centered properly, probably causing the rather large assymetry.

For the two wakes of G = -0.181 and G = -0.193, the Reynold's numbers are approximately 2.0 and 4.0 x 10^3 respectively, based on model dimensions b. These Reynold's numbers

are high enough that the obvious characteristics of the vortex street which develops close to the body are lost within 10 or 20 body widths. (Townsend 1956). No evidence of a periodic wake was observed, probably because the investigation was limited to $\frac{X_{TE}}{b} > 20$.

6. DISCUSSION

The main objective of this research work was to obtain experimental results for deep, self-preserving, two-dimensional wakes. However, in order to prove the instrumentation and experimental techniques, a self-preserving, two-dimensional jet flow was first investigated as there existed experimental data for comparison (Fekete, 1970).

The experimental results for the jet flow are presented in Figures 15 to 26. It can be seen that the flow was two-dimensional and self-preserving even in the components of the stress tensor sufficiently far downstream of the jet slot. When one compares the data of Figures 16 to 26 to the corresponding figures of Fekete (1970), one finds them to be in reasonable agreement. This is not entirely surprising as the excess to free stream velocity ratio G was 0.79 for both cases (Figure 49). The rate of growth $\frac{dL_0}{dx}$ of the jet was found to be 0.0308 as compared to Fekete's result of 0.0333, Figure 49. The linearity of the curves, rate of growth and velocity decay, Figures 49 and 50 respectively, indicate preservation of momentum, as was expected. There is a discrepancy in the measured non-dimensional shear stress parameter, $g_0 = \frac{\overline{uv}}{U_0^2}\Big|_{L_0}$, the value of the present measurements being 0.0187, (Figure 26), as compared to Fekete's value of 0.0212.

The velocity decay comparison, Figure 50, indicates that although the two tests had almost identical $\frac{U_0}{U_1}$ ratio's of 0.79 the scaling velocities were slightly different. The discrepancy between the two tests in the shear stress term $\frac{\overline{uv}}{U_0^2}\Big|_{y=L_0}$ is about 10 per cent. This discrepancy is most likely due to errors which resulted from imperfect alignment of the slanting wire with the mean flow direction in the present measurements. In spite of this discrepancy the results are in general consistent and give, therefore, confidence in the soundness of the experimental procedures and techniques.

The first wake investigated, G=-0.181, was produced by a 1.9 cm. square rod attached with one flat face normal to the oncoming stream to the mid-points of the sides of the tunnel. The normalized mean velocity profiles are given in Figure 30. They all collapse satisfactorily onto one curve. The curve $(e^{-k\eta^2})$ is also plotted in Figure 30 and agrees well with the measured values for (y/L_0) less than about 1.5. For values (y/L_0) greater than 1.5, Figures 19 and 41, also show that the exponential curve slightly overestimates the actual mean velocity; this is the usual mode of departure. Thus mean velocity measurements all indicate that this wake (G = -0.181) has a tendency towards self-preservation.

However, when the turbulence measurements, Figures 32 to 35 are examined, the evidence contradicts this assumption. The values of the turbulence intensities do not reach a self-preserving form and do not even seem to be tending towards a

stable value. Clearly, then, this flow is not self-preserving. This observation is also substantiated by the growth rate of the wake shown in Figure 28. In addition to noting that this wake does not exhibit self-preservation it can also be observed that the flow is not symmetrical. It may be worth noting, however, that the normalized stress tensor and shear stress values change with downstream distance in a consistent manner (Figures 32 to 34). The measurements could not be carried out further downstream than 91 wake producing body widths due to the limitations imposed by the tunnel length.

The second wake, G = -0.193, was produced by a smaller (⊐) shaped channel which was concave upstream as it is shown in Figure 6b. The ratio of maximum velocity deficit to free stream velocity is almost constant, Figure 38, and Figure 39 indicates that the experimental wake growth of L_0 varies approximately linear with downstream distance X_{TE}.

Although the mean velocity profiles in a wake may appear self-preserving, it is usual to find that the distribution of turbulent velocities is not self-preserving until some further distance downstream, (Townsend 1956).

Figure 43 shows distribution of $\frac{\sqrt{\overline{u^2}}}{U_0}$ at a number of stream-wise locations, $189 < \frac{x}{b} < 225$, and confirms the slow approach of the turbulent velocity components towards self-preservation.

The turbulent shear stress distribution was measured and the results are shown in Figure 48. In plotting these results

it has been assumed that the centre of the wake is at the point of zero shear. By means of the momentum integral equation, a calculation has been made of the shear stress distributions at the stations where the shear stress was measured. The experimental distributions of $\frac{dL_0}{dx}$ and of $\frac{U_0}{U_1}$ were used in this calculation, as was the assumption that the velocity profile was given by the exponential equation of the form

$$(U_1 - U_0) = U_0 \exp-[\ln 2 \left(\frac{y}{L_0}\right)^2] \qquad (11)$$

Since integration for the calculating curve was always started from lower limit y = 0, any departures in velocity profile from the assumed distribution of equation (11) have a cumulative effect, and are most apparent for large Y. The measured and calculated values of shear stress therefore depart more and more from one another as y increases ; (Figures 48 and 28 for the wake and the jet respectively)

However, it is evident from Figures 38 to 48 that the wake, G = -0.193, was symmetrical, two-dimensional and also fully self-preserving, the measurements have been carried out to 225 wake producing body widths, downstream. The results represent therefore useful information.

The bands of growth and shear stress parameter values of Vogel's theory (1968) are plotted in Figures 51 and 52. Newman's predicted values for the growth parameter, the value of C_0 for the jet measured by Fekete (1970), the results of the present measurements and the values of C_o for the two wakes measured by Gartshore (1970) are also plotted in Figure 51.

Examination of Figure 51 shows only a slight variation between Newman's and Vogel's theories for the growth parameter for self-preserving two-dimensional jets and wakes. The experimental growth results fit both Newman's and Vogel's theories fairly well, Vogel's theory predicts the measured growth parameter within about 15%.

A comparison of the predicted and the experimentally measured values of the shear stress parameter $g_0 = (\frac{\overline{uv}}{U_0^2})$ at $y = L_0$ are plotted in Figure 52. The results indicate that Fekete's experimental data straddle the curve presented by Vogel's theory (1968). The result of the present jet, shear measurements lies in Newman's bounds. The wake result, however, favours the trend of Vogel's theory.

The discrepancy between Vogel's theory and the experimentally measured values is less than 15% for the wake ($G = -0.193$) and 18% for the jet results.

It would also be important to note here that, it was assumed in this work that the levels of free stream turbulence encountered did not have a noticeable effect on the above parameters.

One may conclude, therefore, that from a pragmatic point of view Vogel's theory based on Townsend's large eddy equilibrium hypothesis will give reasonable results.

To be more certain one would have liked to have measured several wakes instead of only one. Indeed several attempts

were made, using a variety of wake bodies, to produce deep wakes with large velocity deficit, but without any success. It is implied, therefore, that it was much more difficult to set up a deep wake flow than the jet. Part of this may be due to the fact that there was no easy, independent way of adjusting wake strength as there is for the jet.

7. CONCLUSIONS

The principal objectives of the investigation have been achieved. A two-dimensional jet and one wake have been set up according to the constrains of the mean momentum and turbulence energy equations for self-similar flow.

The measurements indicated that the two flows, the jet and the wake with G = -0.193 were satisfactorily self-preserving in both mean velocity and longitudinal turbulence.

The wake with G = -0.183 was lacking self-preservation and the results were not satisfactory.

The results obtained for the self-preserving two-dimensional jet were in substantial agreement with Fekete's (1970) measurements providing a measure of confidence in experimental procedures and the turbulence measurements.

Measured distributions of shear stress across the wake and the jet compare favorably with distributions calculated from the momentum equation and the known flow development.

The experimentally measured values of the self-preserving wake were compared to Gartshore's results, Newman's and Vogel's theories. The rate of growth and the measured shearing stresses were in reasonable agreement with Gartshore's measurements.

The experimental results favour Vogel's theory which predicts reasonably well the rate of growth and the shear stress parameter for two-dimensional self-preserving jets and wakes.

Large deficit two-dimensional self-preserving wakes could not be established.

REFERENCES

Bradshaw, P. — The effect of wind tunnel screens on "two-dimensional" boundary layers N.P.L. Aero Report 1086 ARC 25 402 1963.

Champagne F. H. (1968) — Turbulence measurements with inclined hot wires. Boeing Scientific Research Laboratories. Document D1-82-0491.

Fekete G.I. (1970) — Two-dimensional, self-preserving turbulent Jets in streaming flow. Report No 70-11. M.E.R.L. McGill University.

Gartshore Ian (1965) — The streamwise development of two-dimensional wall jets and other two-dimensional shear flows (Ph.D Thesis August 1965).

Gartshore Ian (1967) — Two-dimensional turbulent wakes J. Fluid Mechanics (1967) Vol 30 part 3 p.p 547-560.

Gartshore I. S. and Newman, B. G. (1969) — Small perturbation jets and wakes which are approximately self-preserving in a pressure gradient. CASI Trans. 2 No 2, 101.

Gartshore I. S. (1972) — The interaction between turbulent wakes and boundary layers, CASI Trans 5 49.

Guitton D.E. (1968) — Correction of Hot-wire data for high intensity turbulence, longitudinal cooling and probe interference. McGill University, Dept. Mechanical Engineering Report 68-6.

Guitton D. E. (1970) — Some contribution to the study of equilibrium and non-equilibrium turbulent to wall jets over curved surfaces. McGill University (Ph. D. Thesis)

Hinze J. O. (1959) 'Turbulence' McGraw Hill Book Company Inc. New-York, Toronto, London.

Irwin, H. P. A. H. (1972) The longitudinal cooling correction for wires inclined to the prounges and some turbulence measurements in fully developed pipe flow! Mech. Eng. Res. Lab. Tech. Note 72-1, McGill University.

Irwin, H. P. A. H. (1974) Measurements in Blown Boundary layers and their prediction by Reynolds stress Modelling. Ph. D., Thesis McGill University.

Newman B. G. (1967) Turbulent jets and wakes in a pressure gradient. Fluid Mechanics of internal flow. Elsevier Publishing Company-Amsterdam 1967.

Newman B. G. (1968) The Growth of Self-preserving Turbulent Jets and Wakes. Report no (68-10) McGill University R.L.

Patel R.P. and Newman B.G. (1961) Self-preserving, two-dimensional turbulent jets and wall jets in a moving stream. McGill University. M.E.R.L.

Patel, R.P. (1970) A study of Two-dimensional, Symmetric and Asymmetric Turbulent Shear Flows. McGill University, Mech. Eng. Dept. Ph. D. Thesis, 1970.

Patel R.P. (1968) Reynolds Stresses in Fully Developed Turbulent Flow Down a Circular Pipe Report no 68-7 McGill University M.E.L.R.

Patel R.P. (1964) The effects of Wind Tunnel Screens and Honeycombs on the Spanwise variation of Skin friction in "Two-dimensional" Turbulent Boundary Layers; Mech Eng. Research Labs. T.N. 64-7 McGill University (1964).

Streiger and Chen (1965)	AIAA J., Vol 3, No 528, 1965.
Townsend A. A. (1956)	The structure of Turbulent shear flow; Cambridge University Press (1956)
Townsend A. A.(1961)	J. of Fluid Mechanics Vol II, p 97 (1961)
Townsend A. A.(1970)	Entrainment and the Structure of Turbulent Flow. J. Fluid Mech, Vol 41.
Vogel W. M. (1968)	Exact solution of Growth Parameters for two-Dimensional and Axismmetric self-preserving Turbulent Jets and Wakes Report 68-5 M.E.R.L. (August 1968)
Vogel W.M. (1974)	Axisymmetric turbulent jets and wakes that are self preserving June (1974) Ph. D. thesis.
Vogel W. M. (1969)	An analytic solution for flow development of symmetric self-preserving jets and wakes using an integral method.CASI Trans. 2 No 2, 105.
Wygnanski, I. and Gartshore, I. S. (1963)	General description and calibration of the McGill 17 x 30 in. Blower Cascade Wind Tunnel. Mech. Eng. Rep. Lab. Tech. Note 63-7, McGill University
Wygnanski I. and Feidler, H. (1969)	'Some measurements in the self-preserving jet'. J. Fluid Mechanics 38, 577.
DISA manual	Hot wire probes; probe catalog No 603 DISA ELEKTRONIK A/S DK 2730 HERLEV DENMARK.

TABLE I

GROWTH INFORMATION FOR SELF-PRESERVING JET, G = 0.790

Width of jet outlet (b) = 0.25 in. or 0.635 cm.

Jet pressure (at jet inlet) = 47.8 cm water

X_0 (virtual origin) = 24.87 in. or 63.0 cm.

m (best fit to $U_1 \propto (X_{TE}+X_0)^m$) = -0.379

m (best fit to $U_0 \propto (X_{TE}+X_0)^m$) = -0.379

m (calculated for G = 0.790) = -0.379

$C_0 (L_0 = C_0(X_{TE}+X_0))$ = 0.030

VALUES AT MEASURED STATIONS

X_{TE} (cm) STATION	$X_{TE}+X_0$ (cm)	$\frac{X_{TE}+X_0}{b}$	U_m (m/sec)	U_1 (m/sec)	U_0 (m/sec)	G	L_0 (cm)	$Re(U_0 L_{0/\nu})$ (x 10^{-5})	XTE(in) Station
101.6	165.1	259.	22.0	12.2	9.8	0.799	5.105	0.353	40
109.2	172.7	271.	21.6	12.0	9.7	0.808	5.384	0.368	43
114.3	177.8	279.	21.4	11.9	9.5	0.804	5.486	0.368	45
119.4	182.8	287.	21.0	11.8	9.3	0.786	5.638	0.370	47
124.5	187.9	295.	20.9	11.7	9.2	0.780	5.842	0.379	49
134.7	198.1	311.	20.4	11.4	9.0	0.784	6.146	0.390	53

TABLE II

GROWTH INFORMATION FOR SELF-PRESERVING WAKE, G =-0.181

Width of wake forming body (b) = 1.90 cm.

Pressure difference P_s = 3.5 cm.alch.(incl."Lambrecht" manometer)
(P_s working section - P_s tunnel)

X_0 - (virtual origin) = 0.872 m.

m - (best fit to $U_1 \propto (X_{TE}+X_0)^m$) =-0.317

m - (calculated for G =-0.181) =-0.317

C_0 - ($L_0 = C_0(X_{TE}+X_0)$) = 0.034

VALUES AT MEASURED STATIONS

XTE (cm) Station	$\frac{(X_{TE}+X_0)}{b}$	U_m (m/sec)	U_1 (m/sec)	U_0 (m/sec)	G	L_0 (cm)	$Re(U_0 L_0/\nu)$ ($\times 10^{-5}$)	XTE(in) Station
40.6	67.2	13.80	17.09	3.18	-0.18	4.41	0.098	16
45.7	70.0	13.72	16.75	3.04	-0.181	4.34	0.093	18
50.8	72.5	13.57	16.55	2.98	-0.180	4.42	0.093	20
58.4	76.0	13.40	16.32	2.93	-0.180	5.10	0.105	23
63.5	79.2	13.33	16.28	2.95	-0.181	5.48	0.114	25
73.7	84.0	12.99	15.83	2.83	-0.179	5.63	0.112	29

TABLE III

GROWTH INFORMATION FOR SELF-PRESERVING WAKE, G =-0.193

Width of wake forming body (b) = 1.27 cm.

Pressure difference P_s (P_s working section- P_s tunnel) = 3.50 cm.alch.(incl.'Lambrecht' manometer)

X_0 (virtual origin) = 1.51 m.

m (best fit to $U_1 \propto (X_{TE}+X_0)^m$) =-0.3166

m (calculated for G =-0.193) =-0.3166

C_0 ($L_o = C_0(X_{TE}+X_0)$) = 0.0218

VALUES AT MEASURED STATIONS

X_{TE} (cm) Station	$\frac{(X_{TE}+X_0)}{b}$	U_m (m/sec)	U_1 (m/sec)	U_0 (m/sec)	G	L_0 (cm)	$Re(U_0 L_0/\nu)$ ($\times 10^{-5}$)	XTE(in) Station
88.9	189.0	12.80	15.91	3.11	0.195	5.029	0.110	35
96.5	195.0	12.78	15.82	3.04	0.192	5.480	0.121	38
104.2	201.0	12.53	15.54	3.00	0.193	5.740	0.121	41
111.8	207.0	12.20	15.16	2.95	0.195	5.638	0.117	44
119.4	213.0	12.07	14.93	2.85	0.191	5.92	0.115	47
129.6	221.0	11.96	14.86	2.90	0.195	6.190	0.126	51

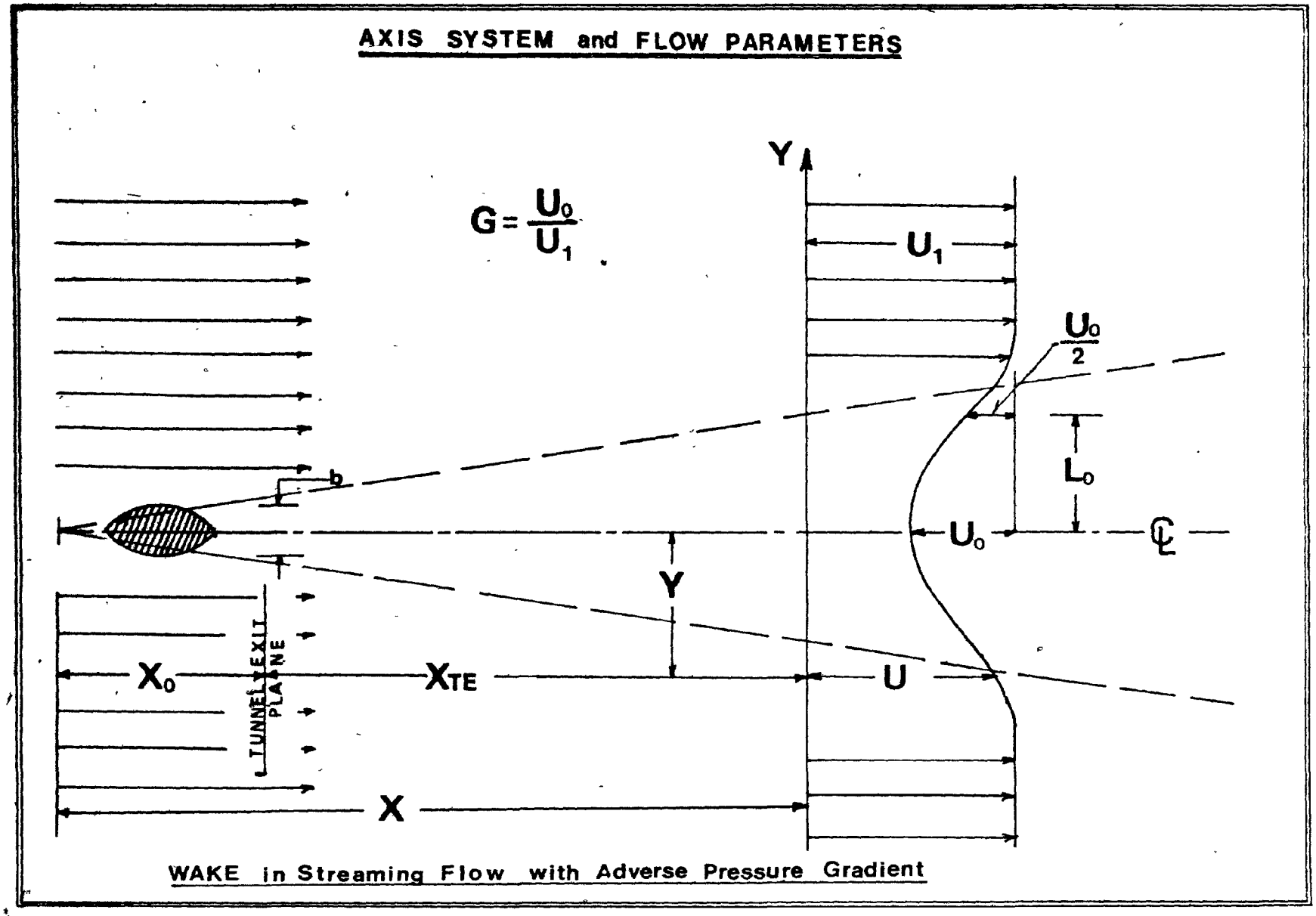
AXIS SYSTEM and FLOW PARAMETERS
$G = \frac{U_0}{U_1}$
Y
U_1
$\frac{U_0}{2}$
L_0
b
U_0
Y
X_0
TUNNEL EXIT PLANE
X_{TE}
U
X
WAKE in Streaming Flow with Adverse Pressure Gradient

fig.1

GENERAL LAYOUT OF BLOWER CASCADE WIND-TUNNEL

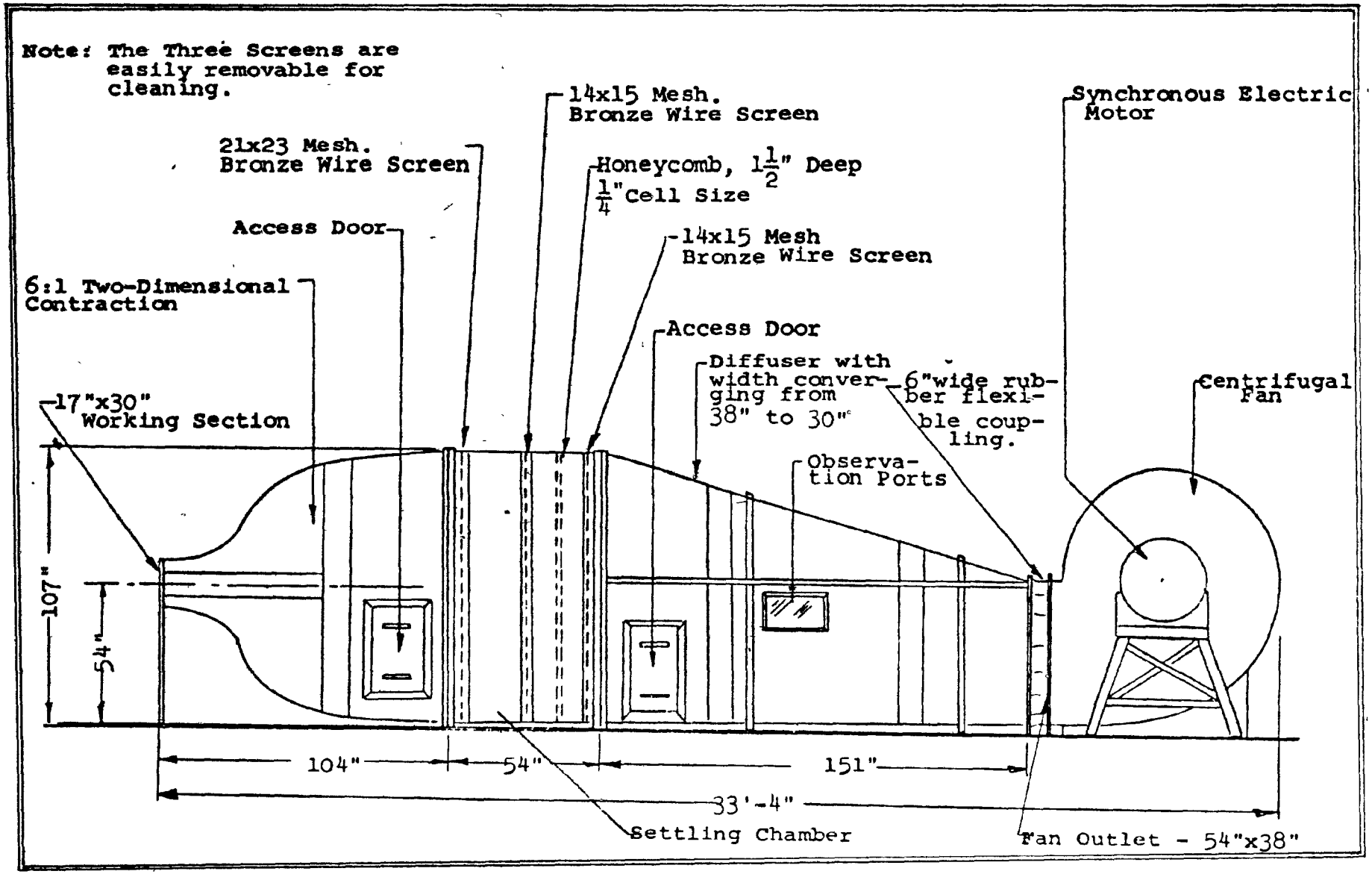

FIG. 2

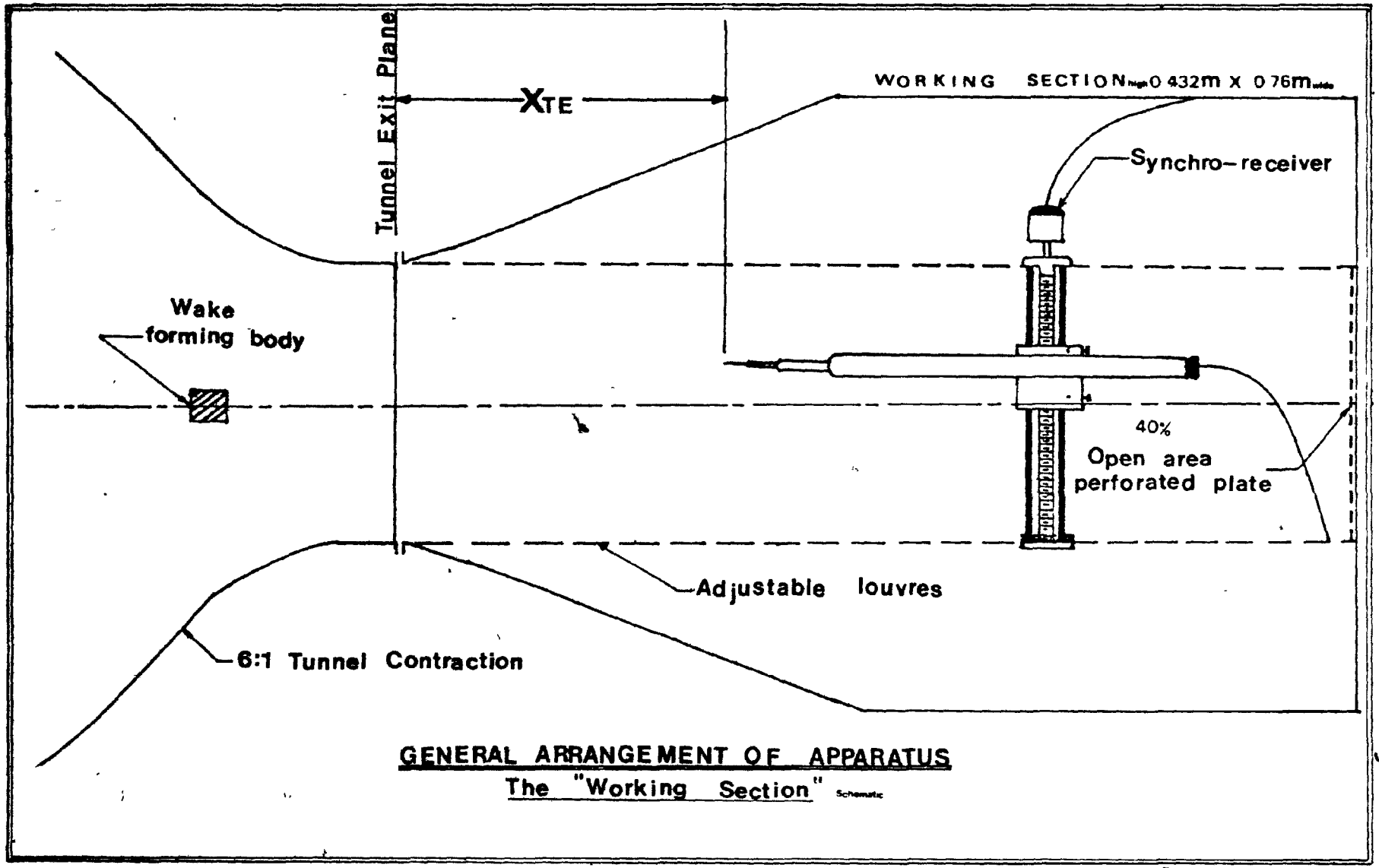

GENERAL ARRANGEMENT OF APPARATUS

The "Working Section" Schematic

Fig.3

Fig.4

(a)

(b)

Louvre Arrangement for Adverse Pressure Gradient

Fig.5

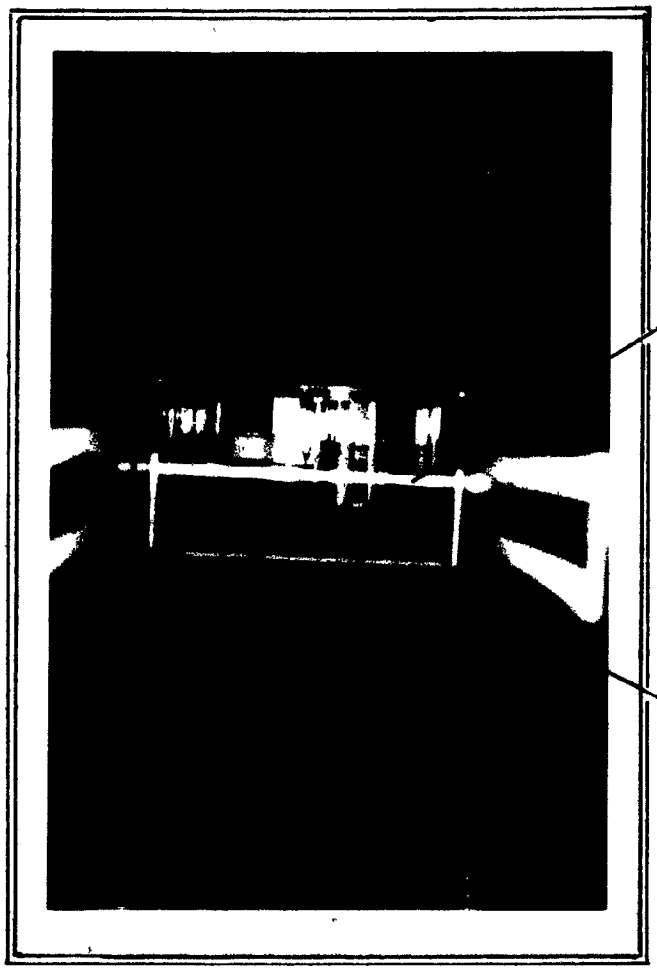

(a)

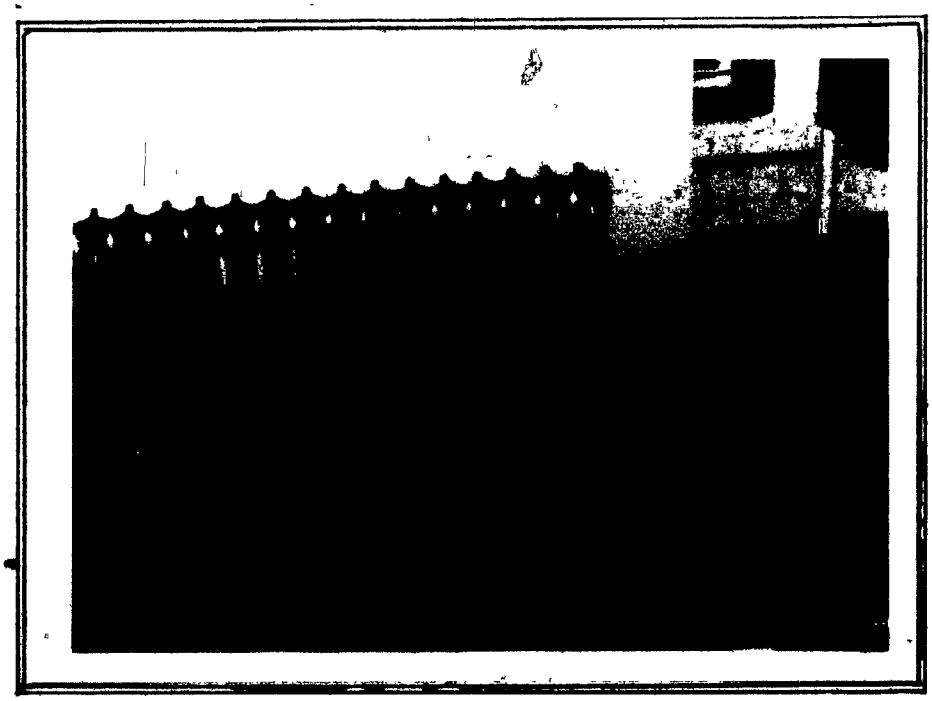

(b)

Jet Box

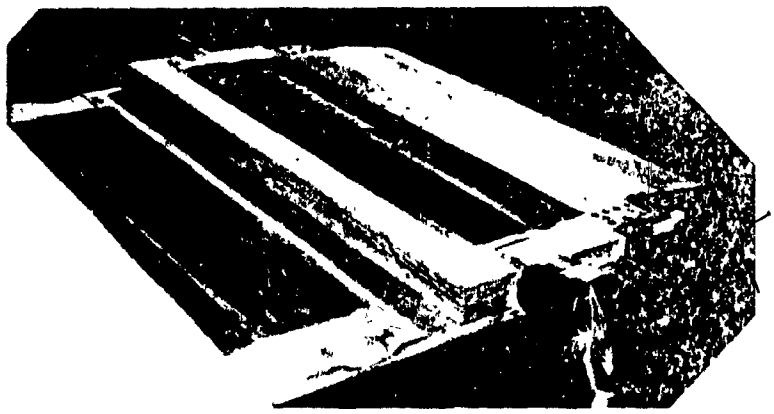

Fig.5c Photograph of jet box with top cover plate removed.

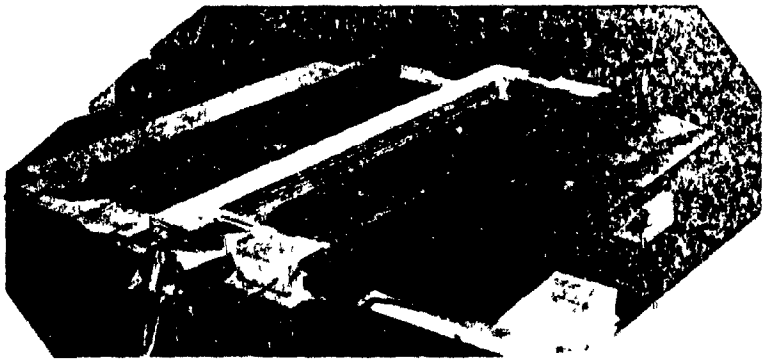

Fig.5d Photograph of jet box with top cover plate removed.

Wake Forming Bodies

(Cross Sections)

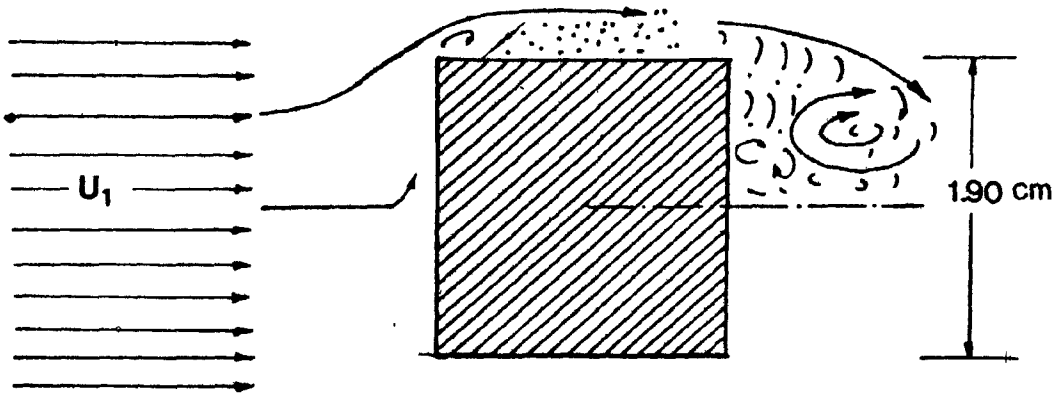

a) 1.90 cm. **Square Rod**; $C_D = 2.05$

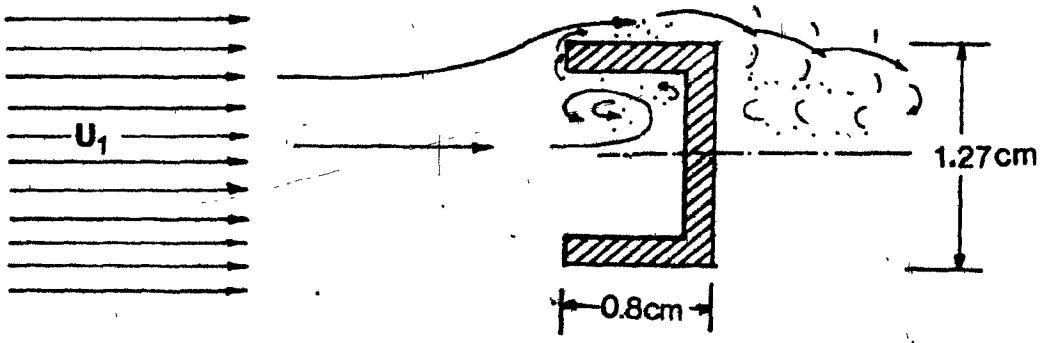

b) 0.8x1.27cm, **Concave Upstream Channel**; $C_D = 2.30$

Fig.7

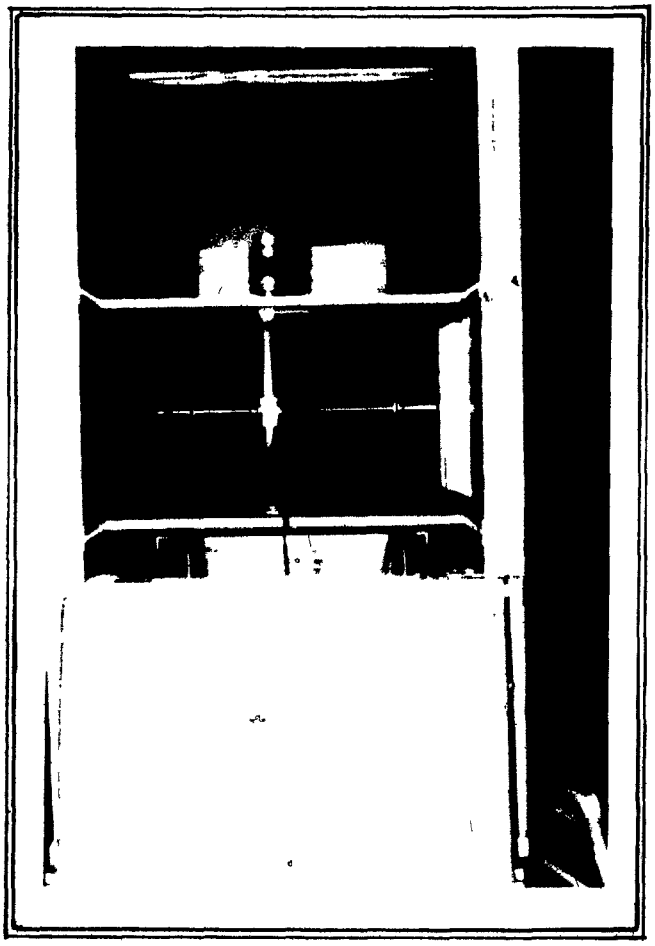

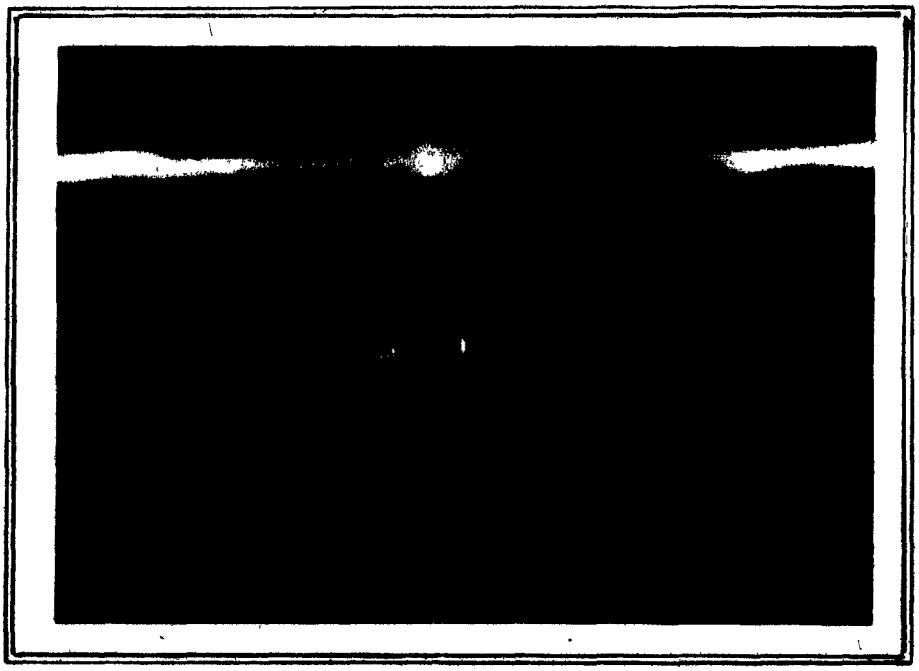

Traversing Gear

Fig.8

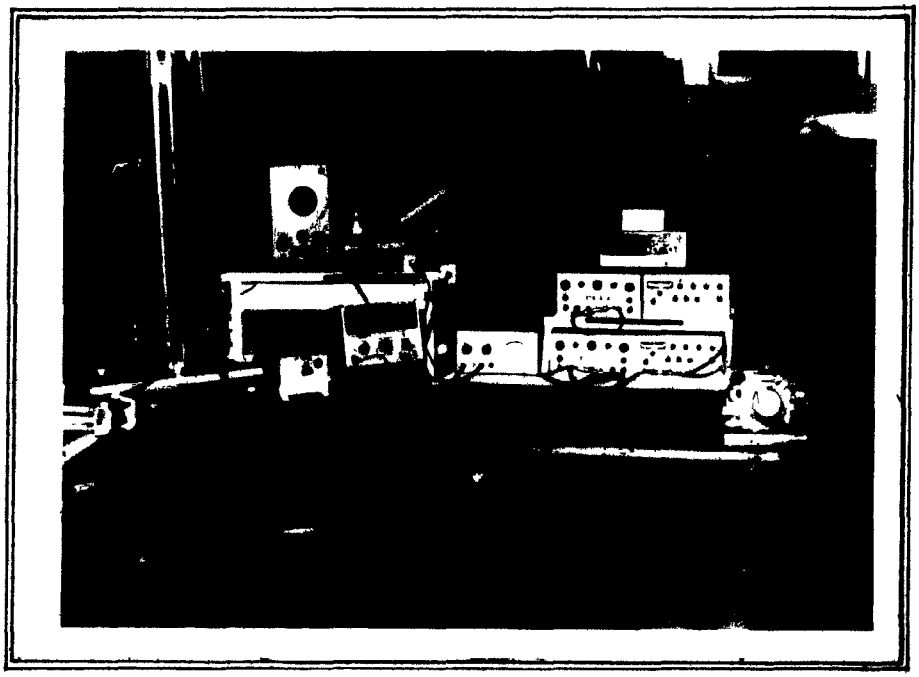

a) Instrumentation

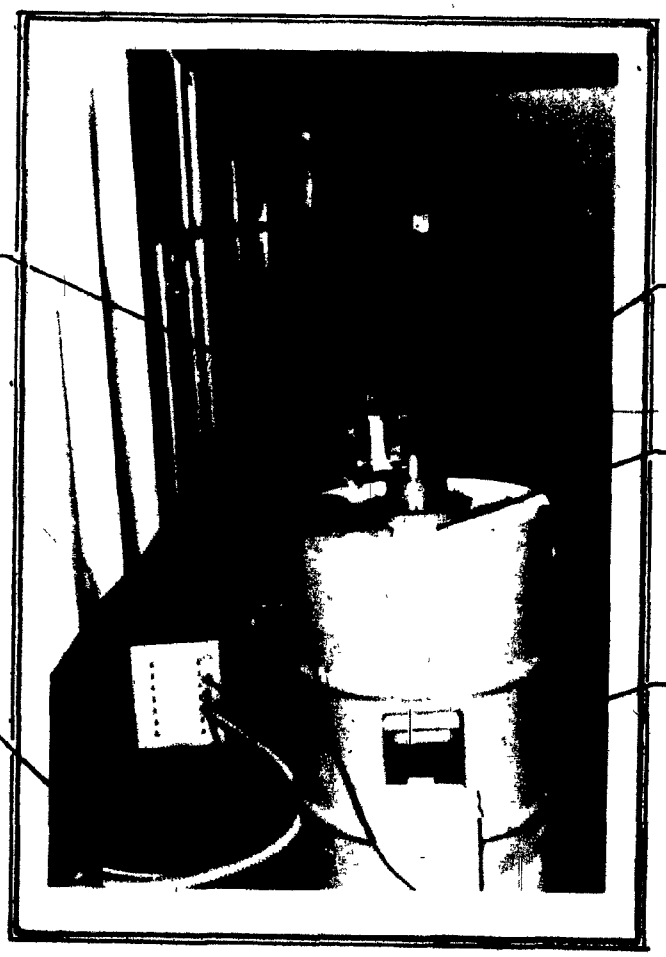

b) Hot-wire Calibration

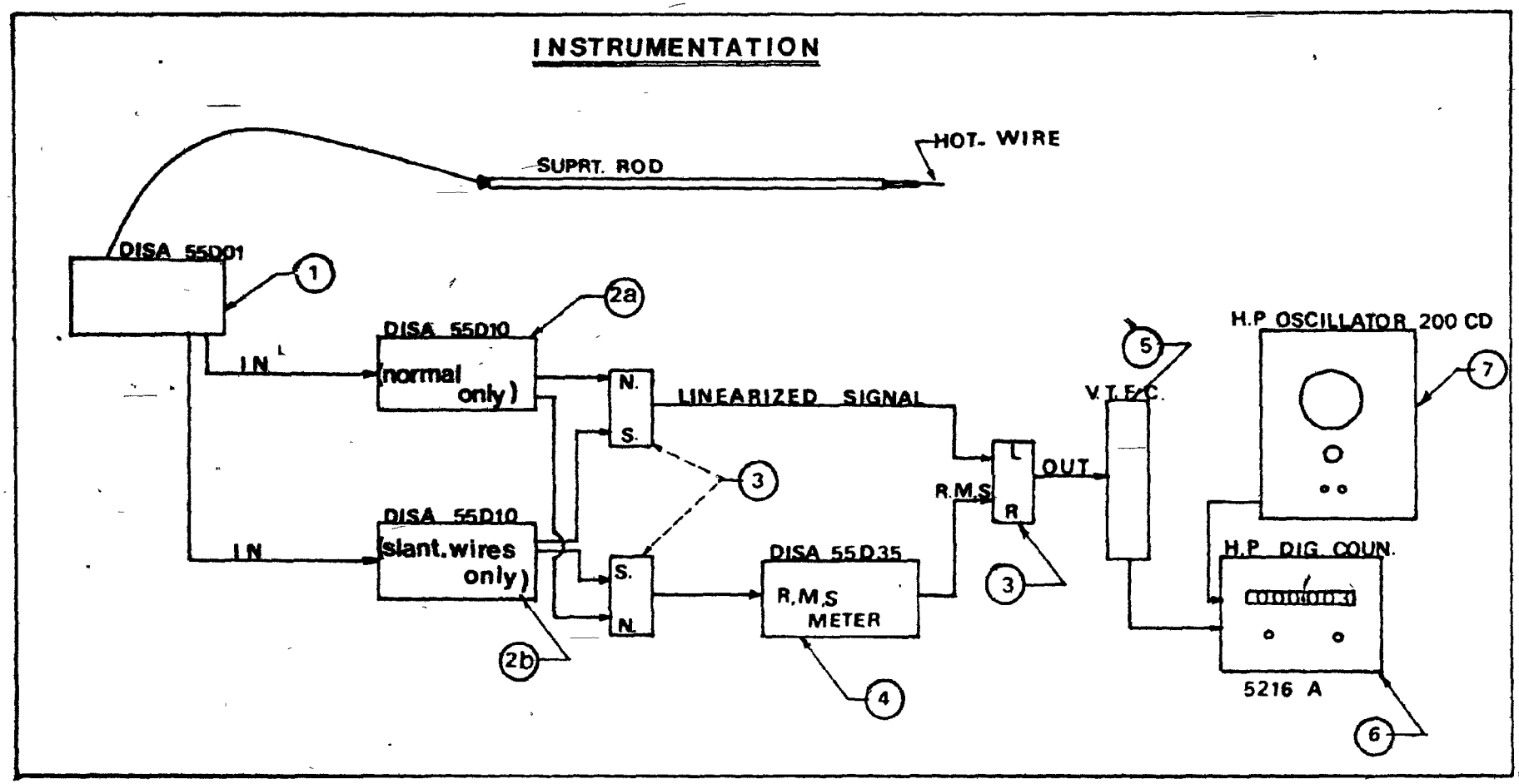

Fig.9

1. Constant Temperature Anemometer Unit
2a. Linearizer Unit(normal wires only)
2b. Linearizer Unit.
3. Switches
4. R.M.S Unit
5. (Voltage-to-frequency converter)
6. Digital counter
7. External gate for long time integration

Fig. 10

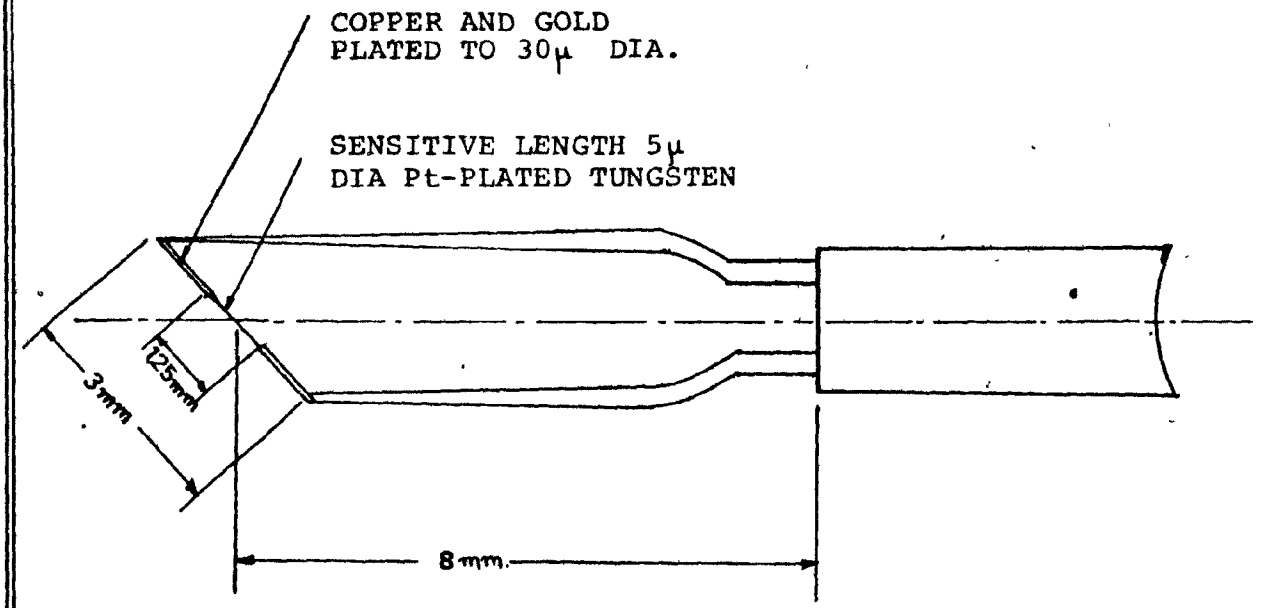

a) PROBE WITH PLATED ENDS

NOTE: Probe dimensions in this figure are the nominal dimensions quoted in the DISA manuals

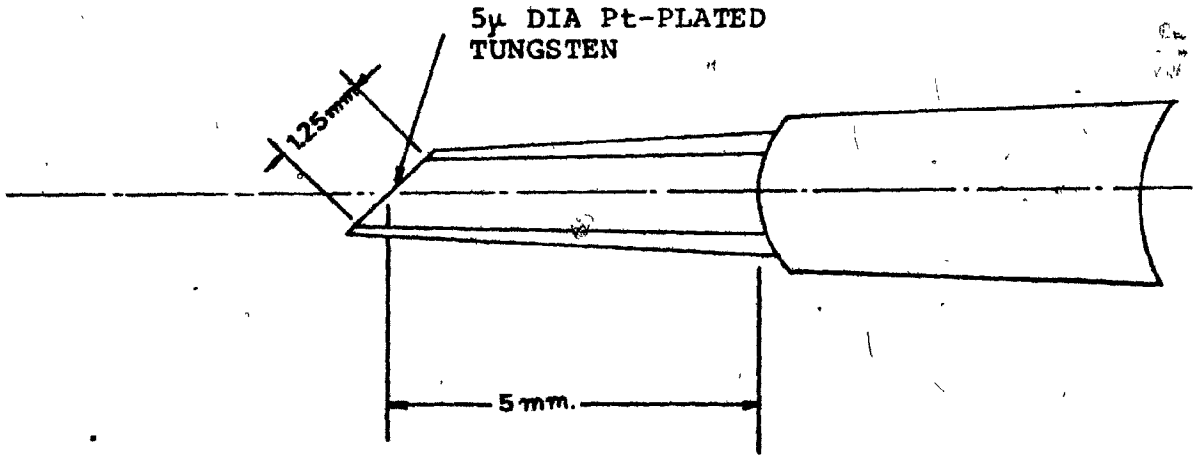

b) PROBE WITHOUT PLATED ENDS

HOT WIRE PROBES

Fig.11

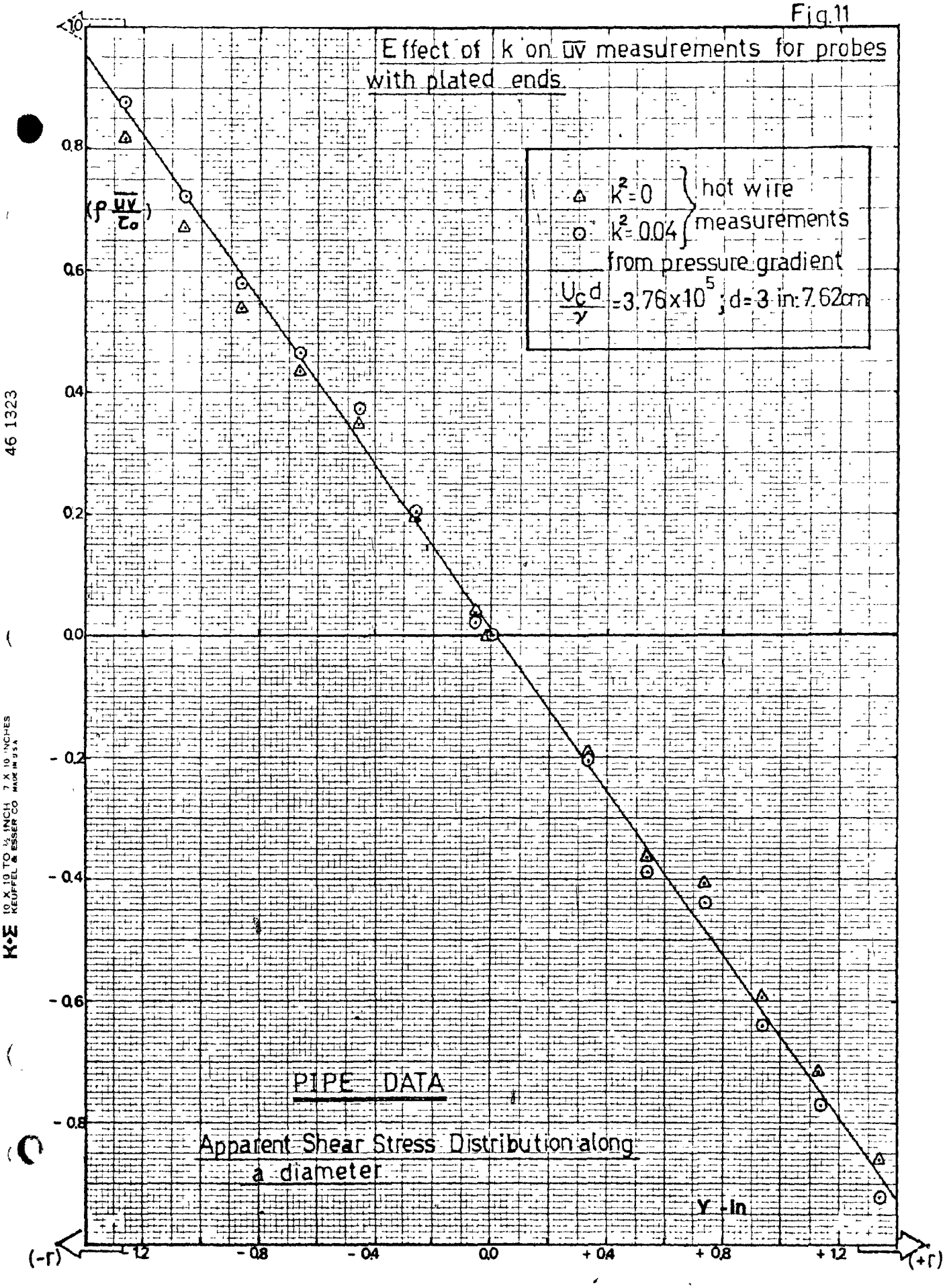

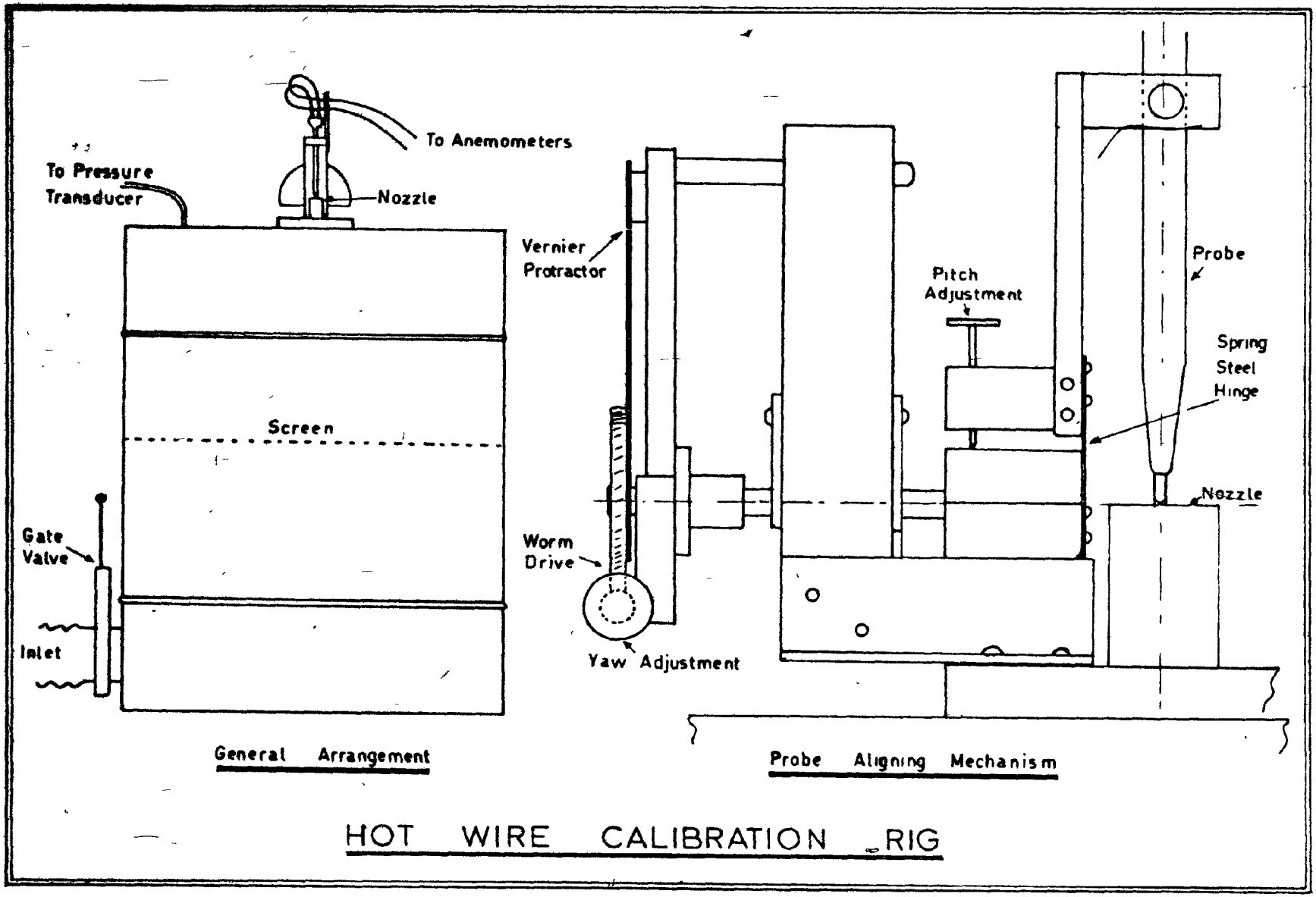

HOT WIRE CALIBRATION RIG

Fig 12

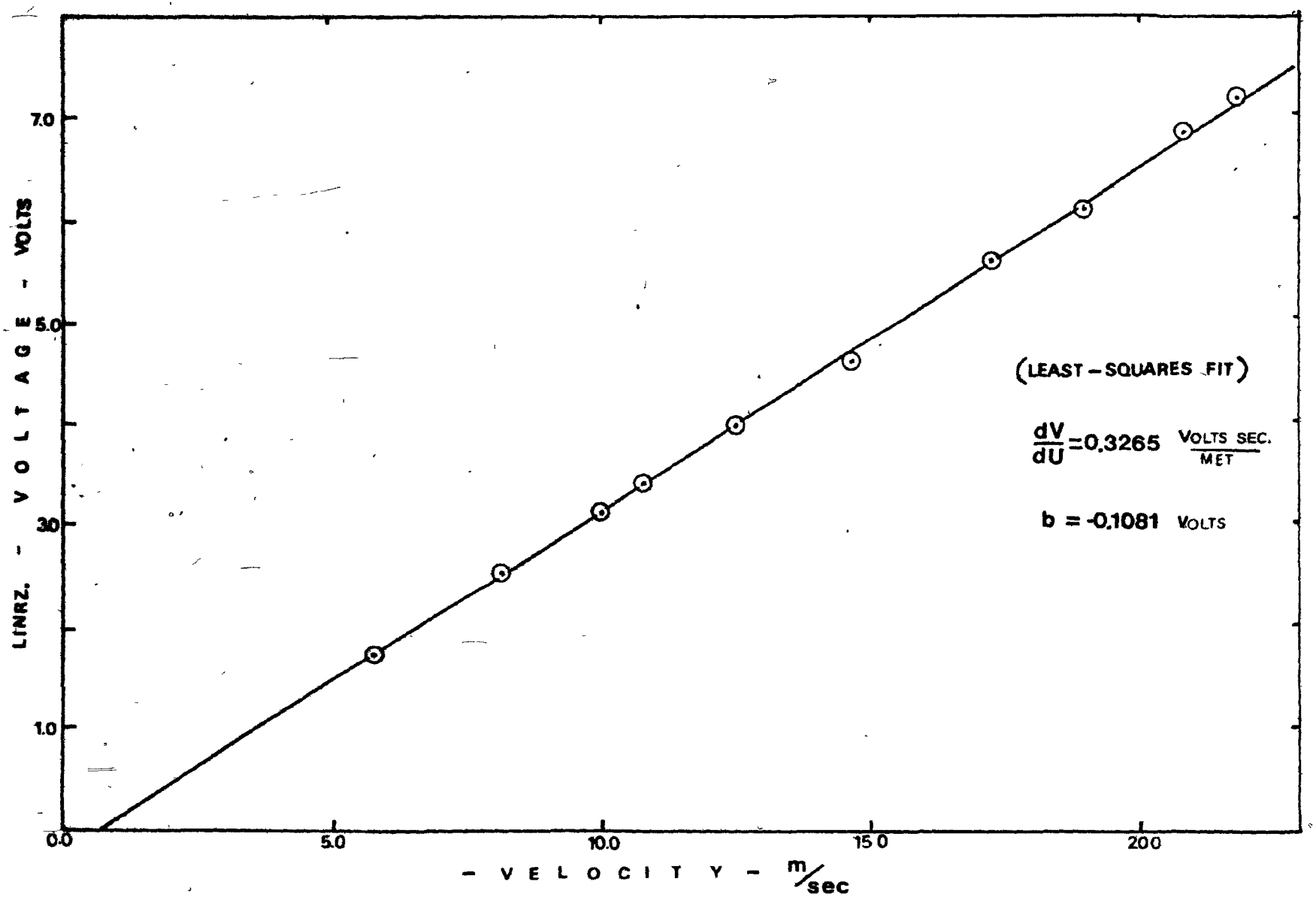

HOT-WIRE Calibration graph

Fig.13

Fig.14

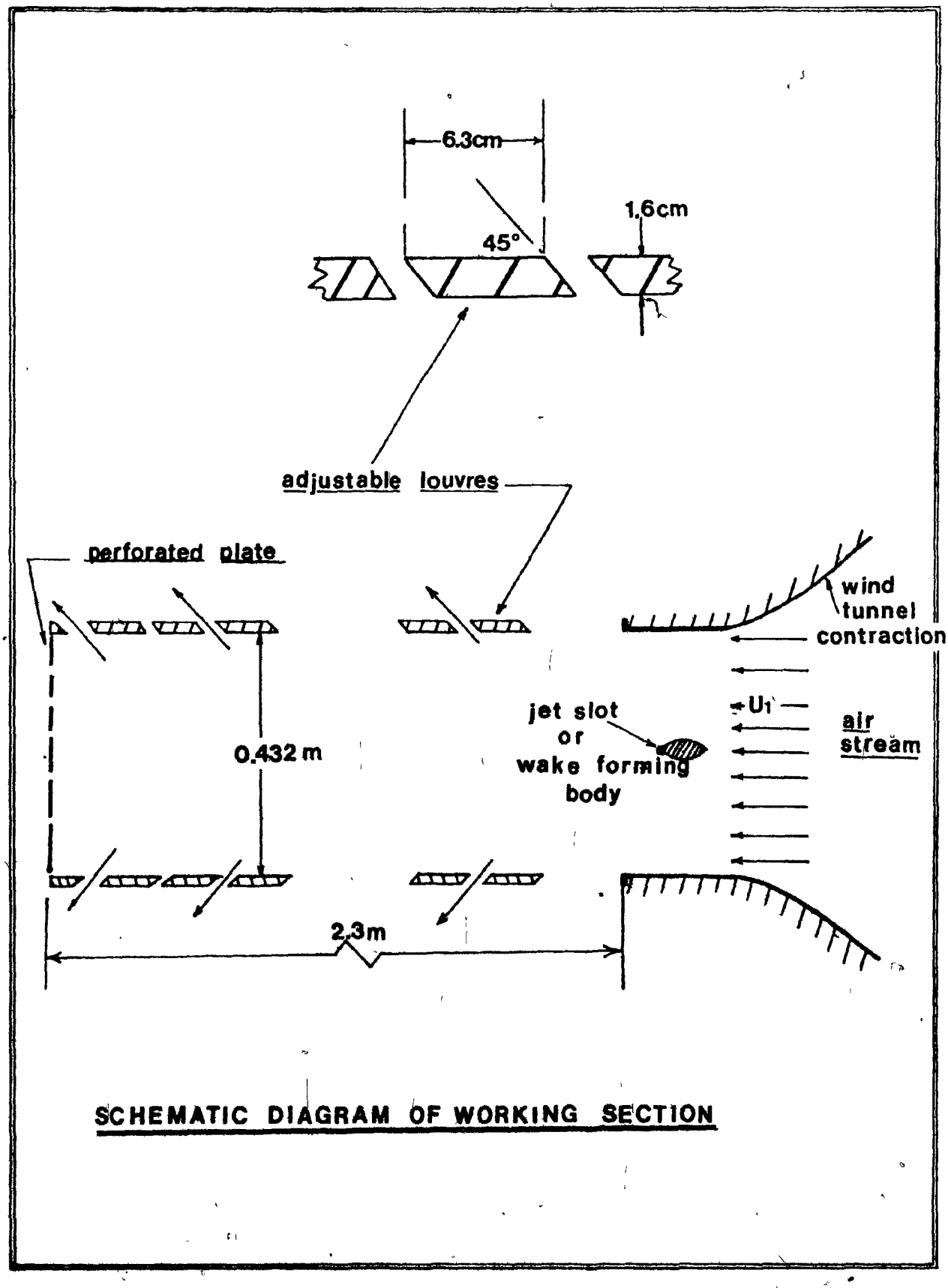

SCHEMATIC DIAGRAM OF WORKING SECTION

Fig. 15

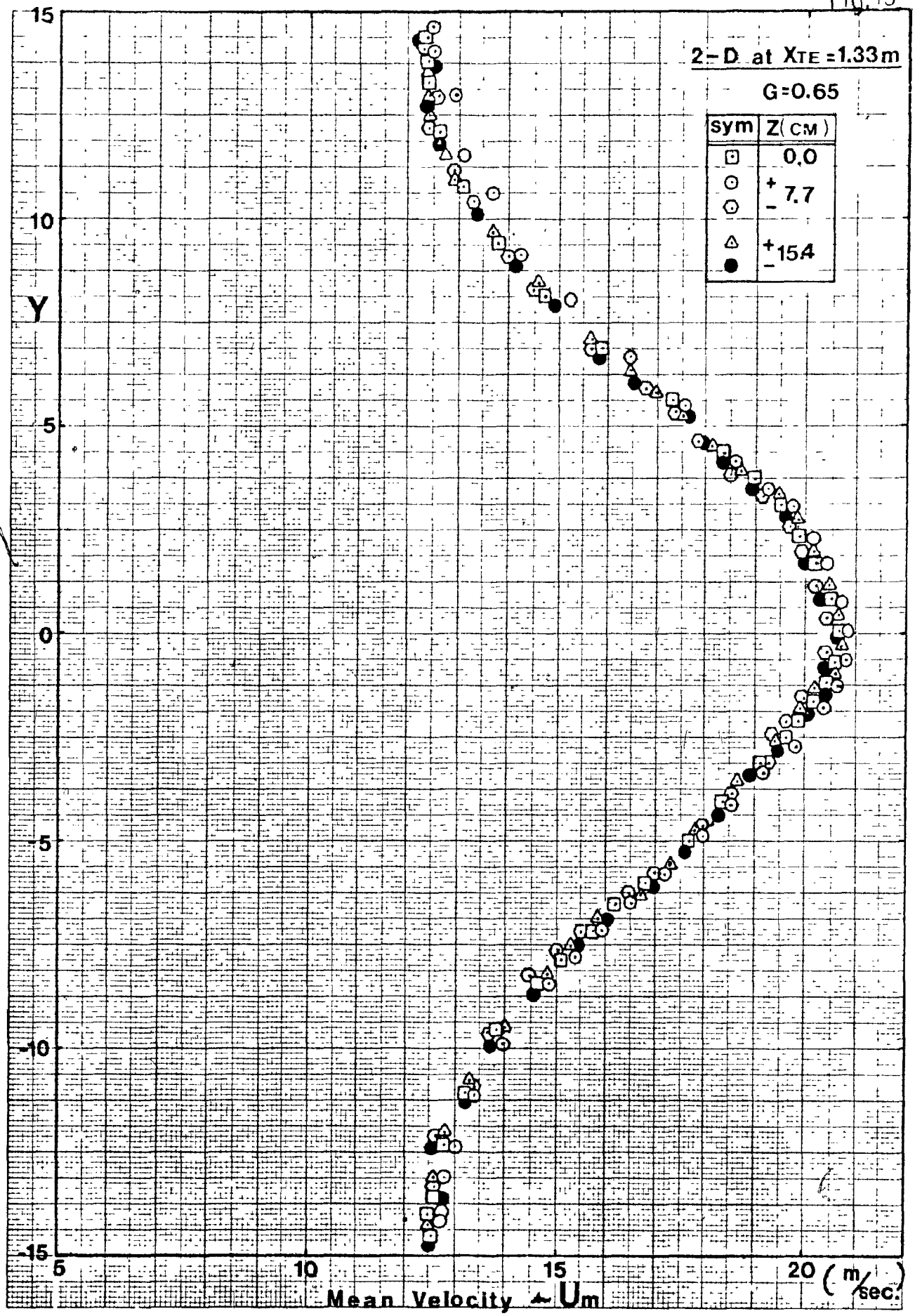

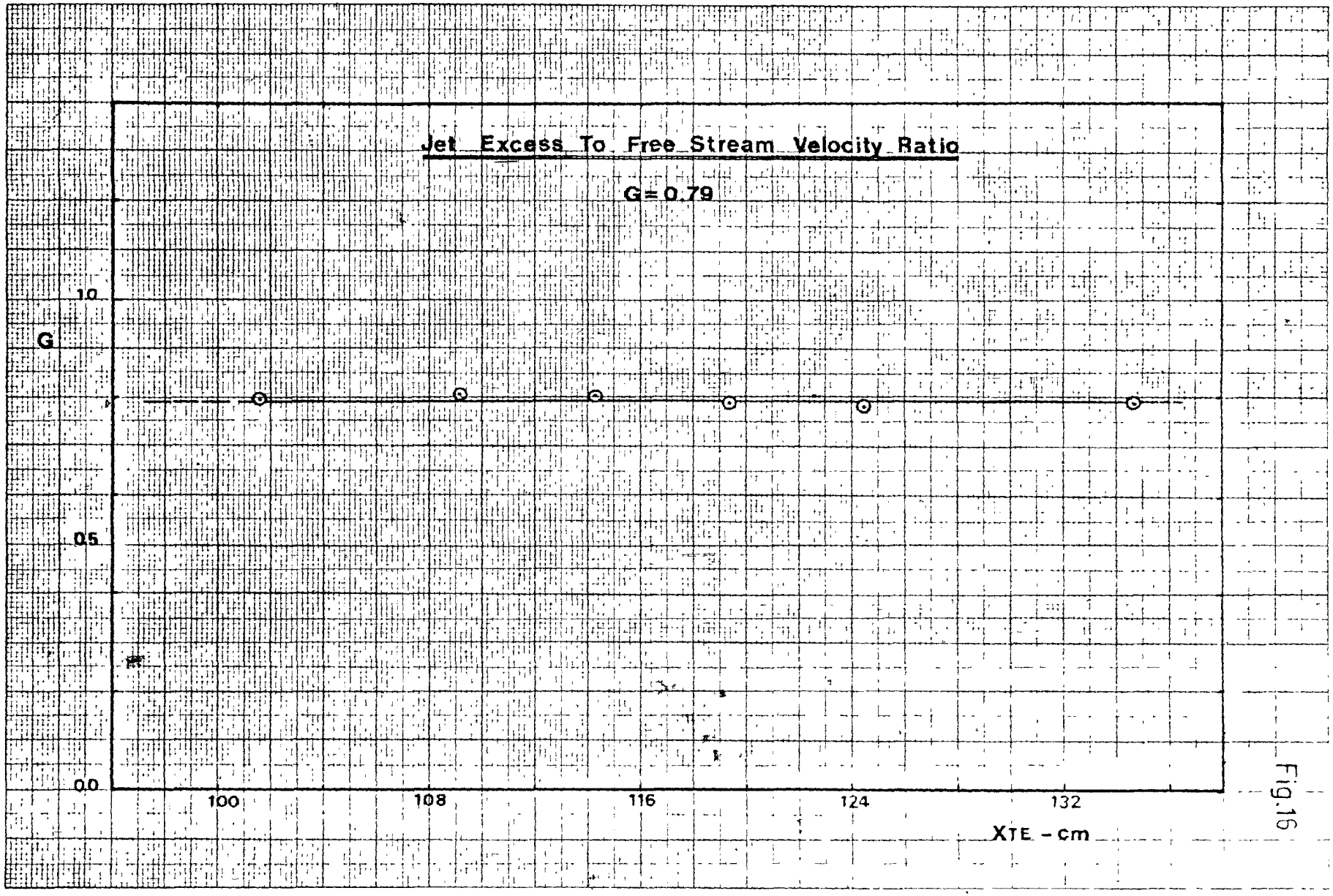

Fig.16

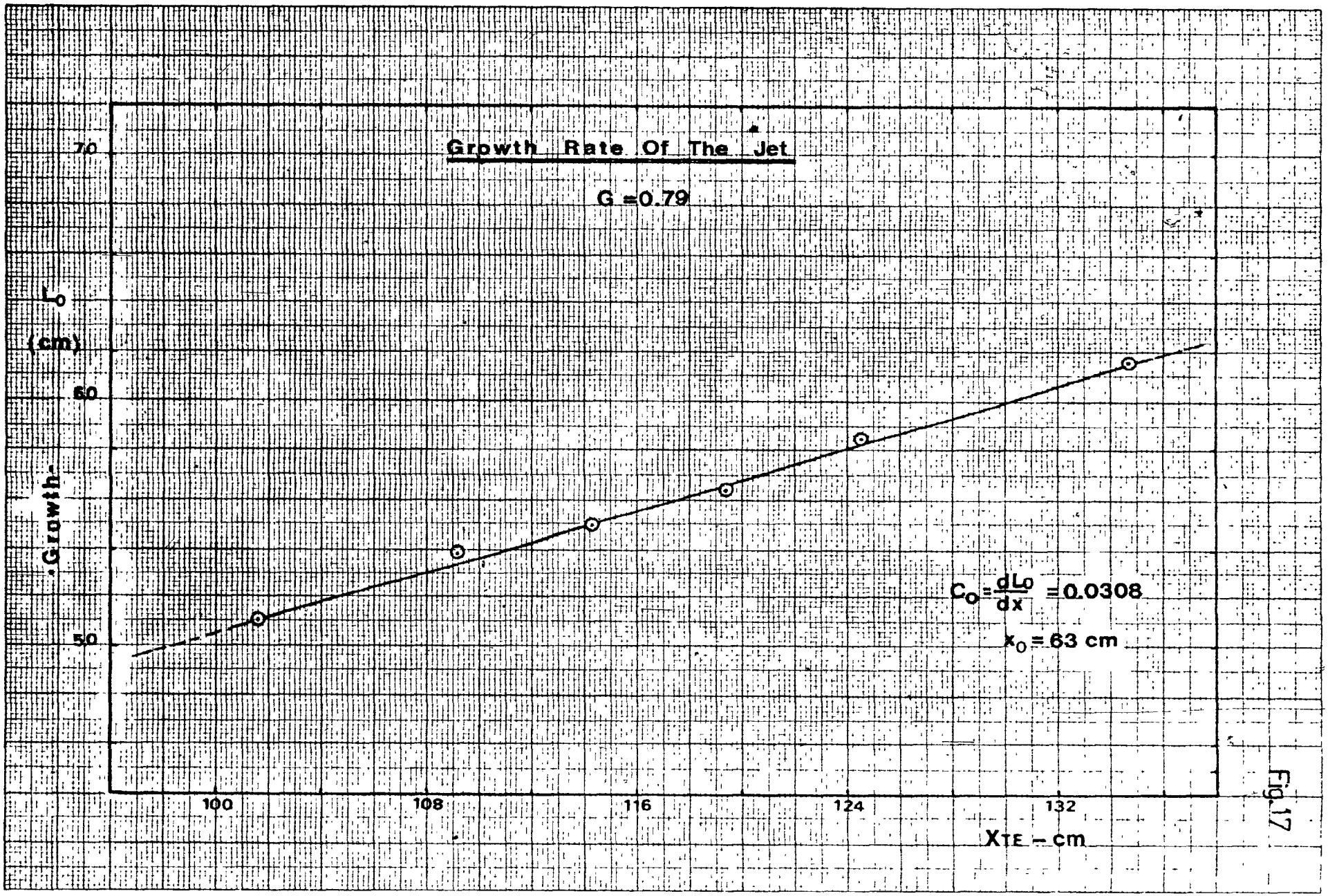
Growth Rate Of The Jet
G = 0.79
70
60
50
L_o (cm)
Growth
100
108
116
124
132
X_{TE} – cm
$C_o = \frac{dL_o}{dx} = 0.0308$
$x_o = 63$ cm

Fig. 17

Fig.18

VELOCITY DECAY

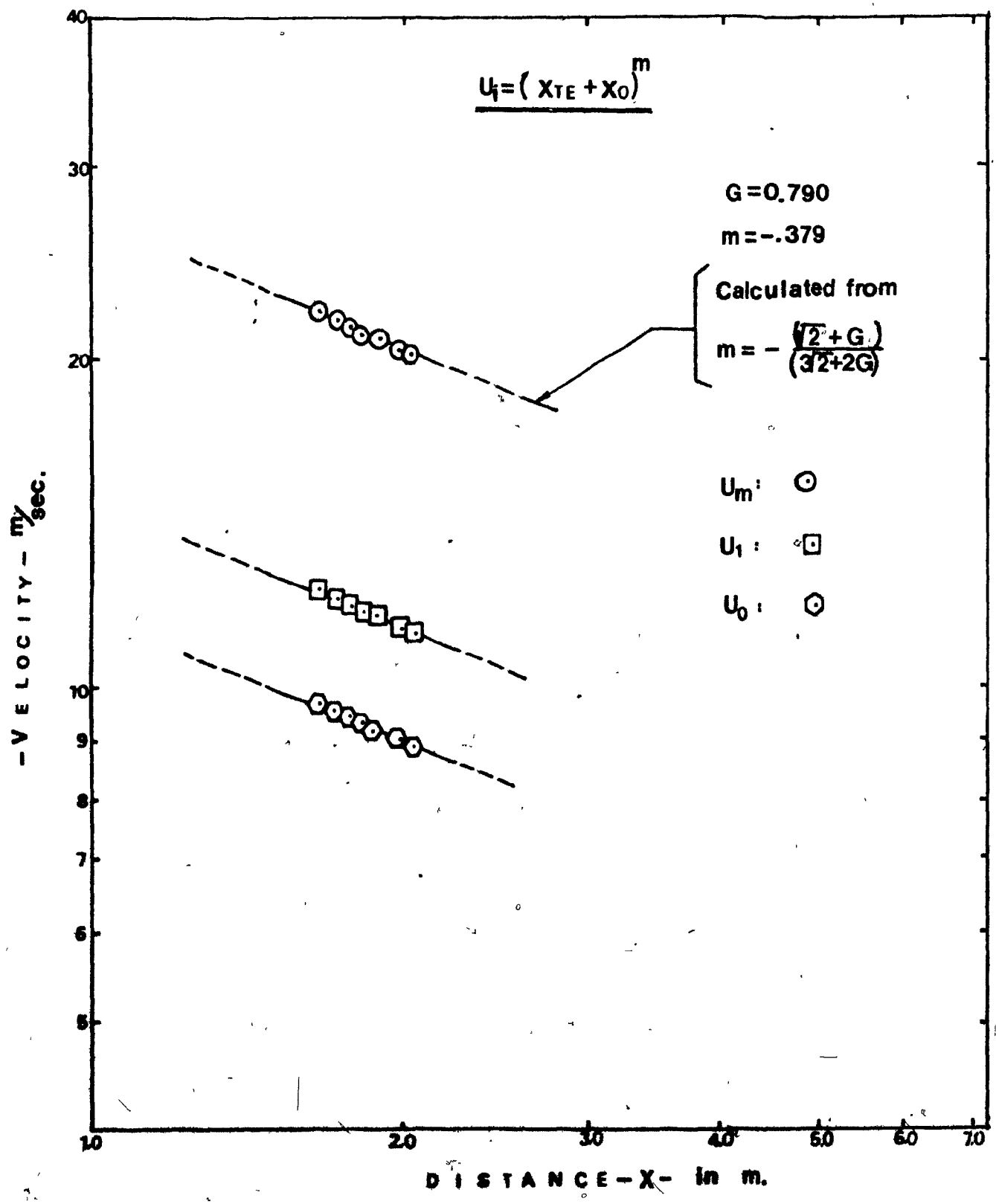

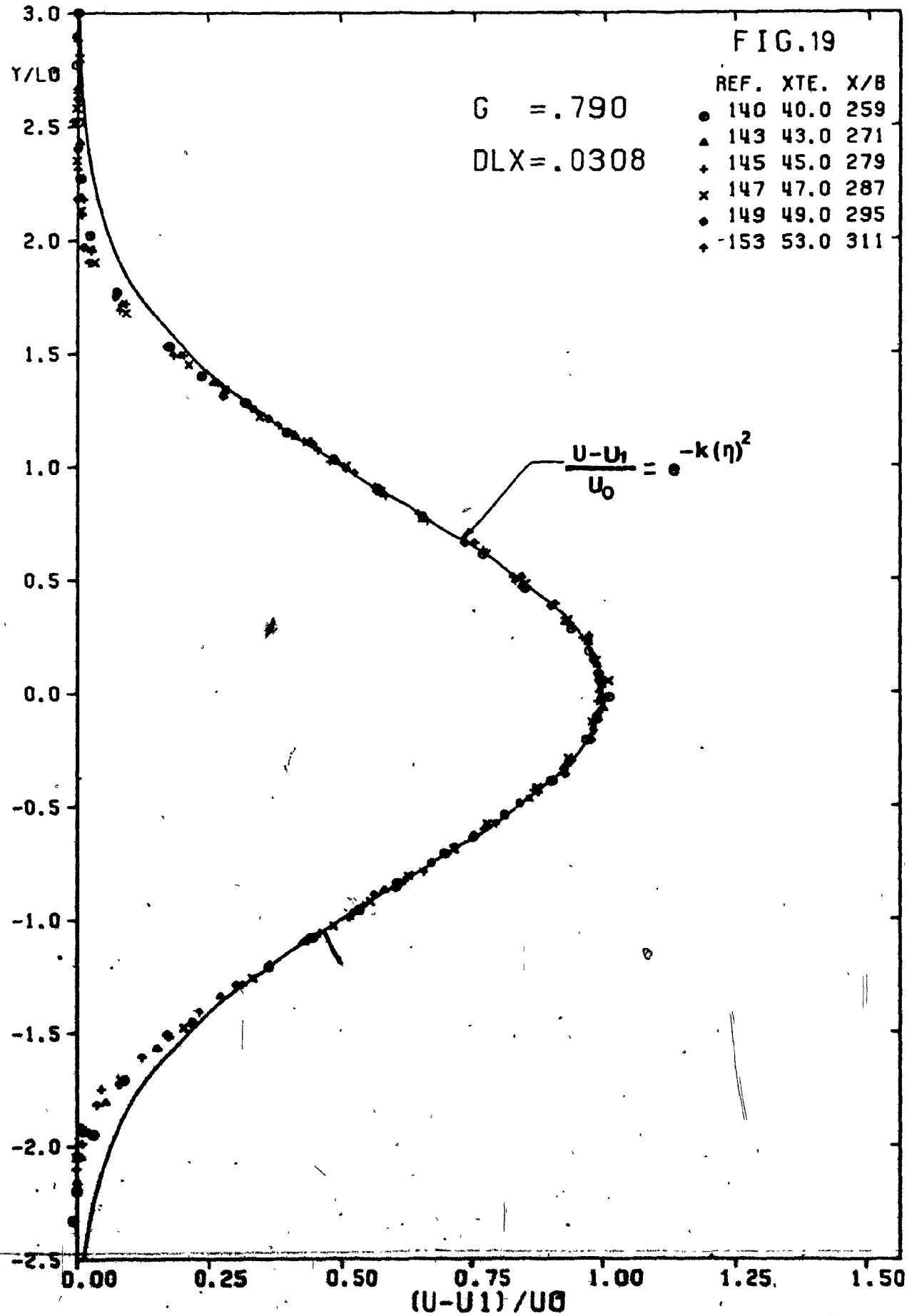
FIG.19
G =.790
DLX=.0308
REF. XTE. X/B
140 40.0 259
143 43.0 271
145 45.0 279
147 47.0 287
149 49.0 295
153 53.0 311
$\frac{U-U_1}{U_0} = e^{-k(\eta)^2}$
Y/L0
3.0
2.5
2.0
1.5
1.0
0.5
0.0
-0.5
-1.0
-1.5
-2.0
-2.5
0.00
0.25
0.50
0.75
1.00
1.25
1.50
(U-U1)/U0

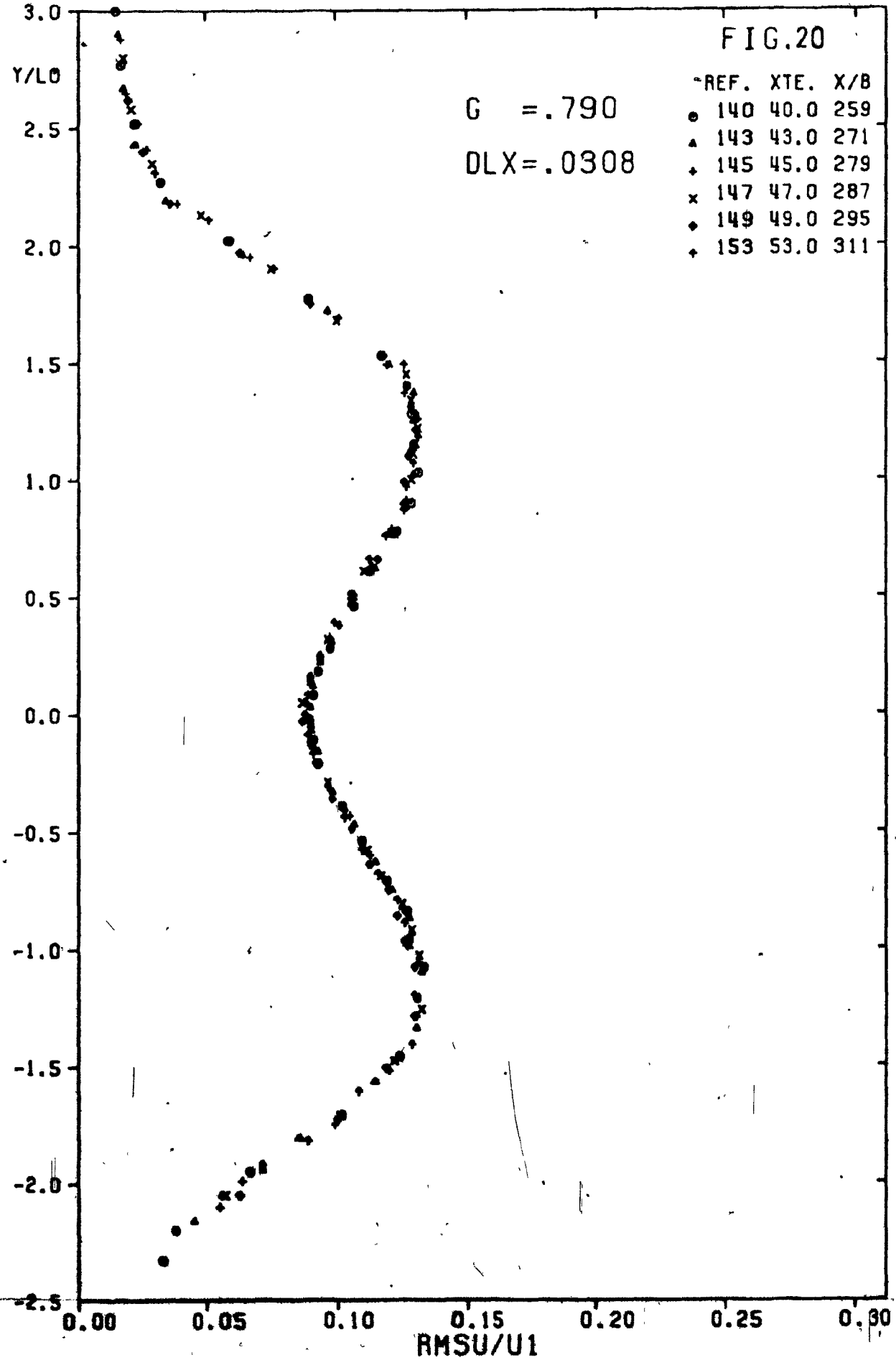
FIG.20
G =.790
DLX=.0308
REF. XTE. X/B
140 40.0 259
143 43.0 271
145 45.0 279
147 47.0 287
149 49.0 295
153 53.0 311
Y/LO
3.0
2.5
2.0
1.5
1.0
0.5
0.0
-0.5
-1.0
-1.5
-2.0
-2.5
0.00
0.05
0.10
0.15
0.20
0.25
0.30
RMSU/U1

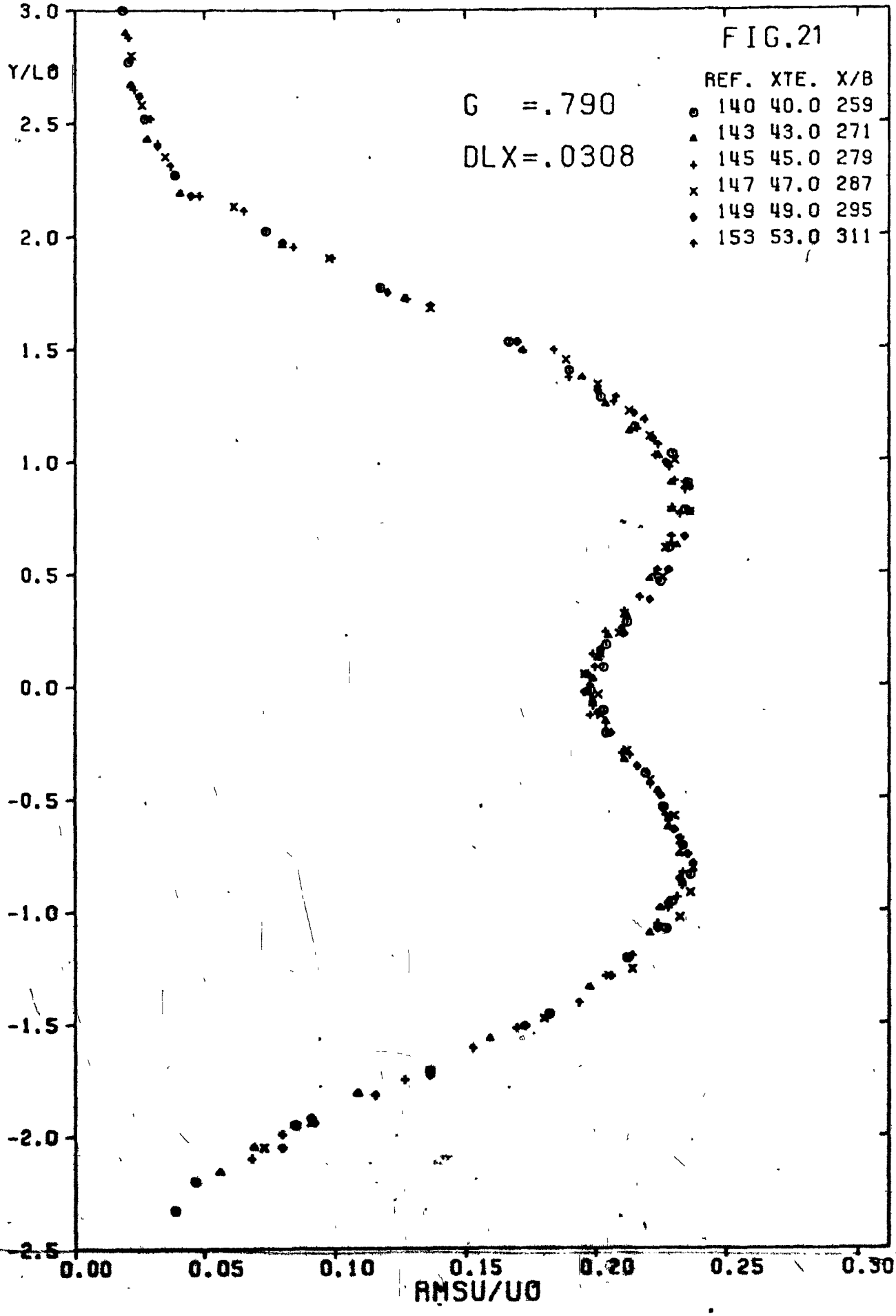
FIG.21
G =.790
DLX=.0308
REF. XTE. X/B
140 40.0 259
143 43.0 271
145 45.0 279
147 47.0 287
149 49.0 295
153 53.0 311
Y/L0
3.0
2.5
2.0
1.5
1.0
0.5
0.0
-0.5
-1.0
-1.5
-2.0
-2.5
0.00
0.05
0.10
0.15
0.20
0.25
0.30
RMSU/U0

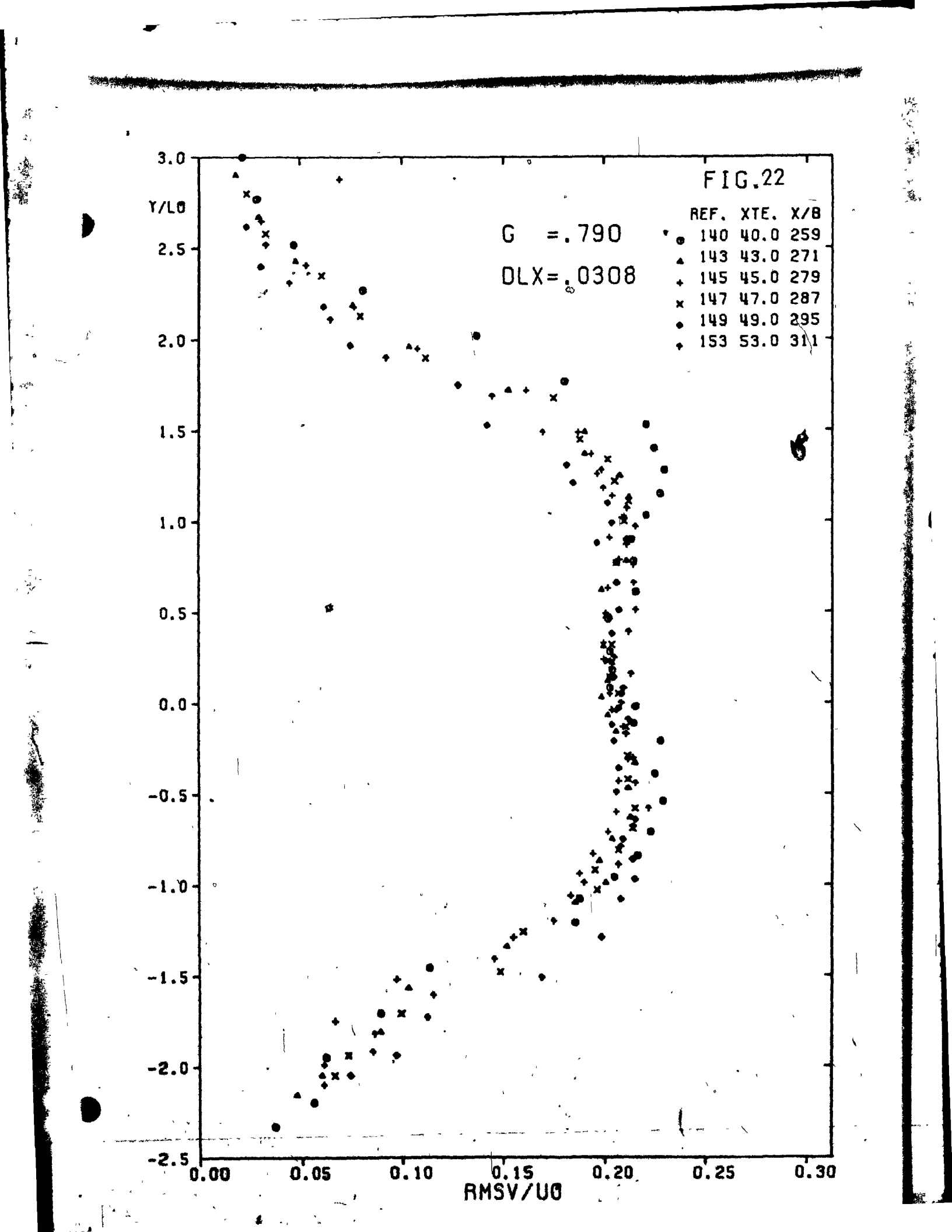
FIG.22
G =.790
DLX=.0308
REF. XTE. X/B
140 40.0 259
143 43.0 271
145 45.0 279
147 47.0 287
149 49.0 295
153 53.0 311
Y/L0
RMSV/U0
3.0
2.5
2.0
1.5
1.0
0.5
0.0
-0.5
-1.0
-1.5
-2.0
-2.5
0.00
0.05
0.10
0.15
0.20
0.25
0.30

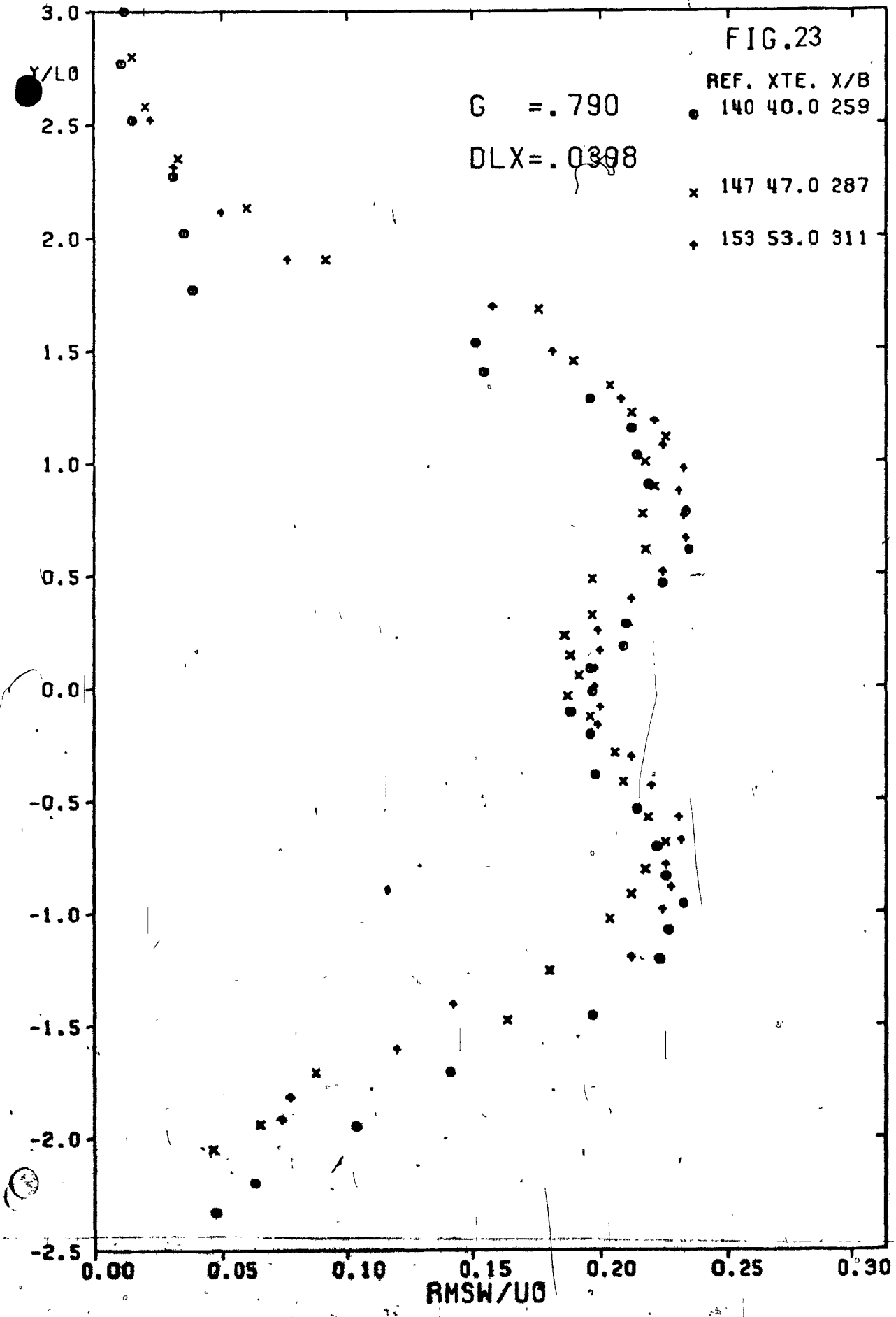
FIG.23
REF. XTE. X/B
140 40.0 259
147 47.0 287
153 53.0 311
G =.790
DLX=.0398
Y/L0
RMSW/U0
3.0
2.5
2.0
1.5
1.0
0.5
0.0
-0.5
-1.0
-1.5
-2.0
-2.5
0.00
0.05
0.10
0.15
0.20
0.25
0.30

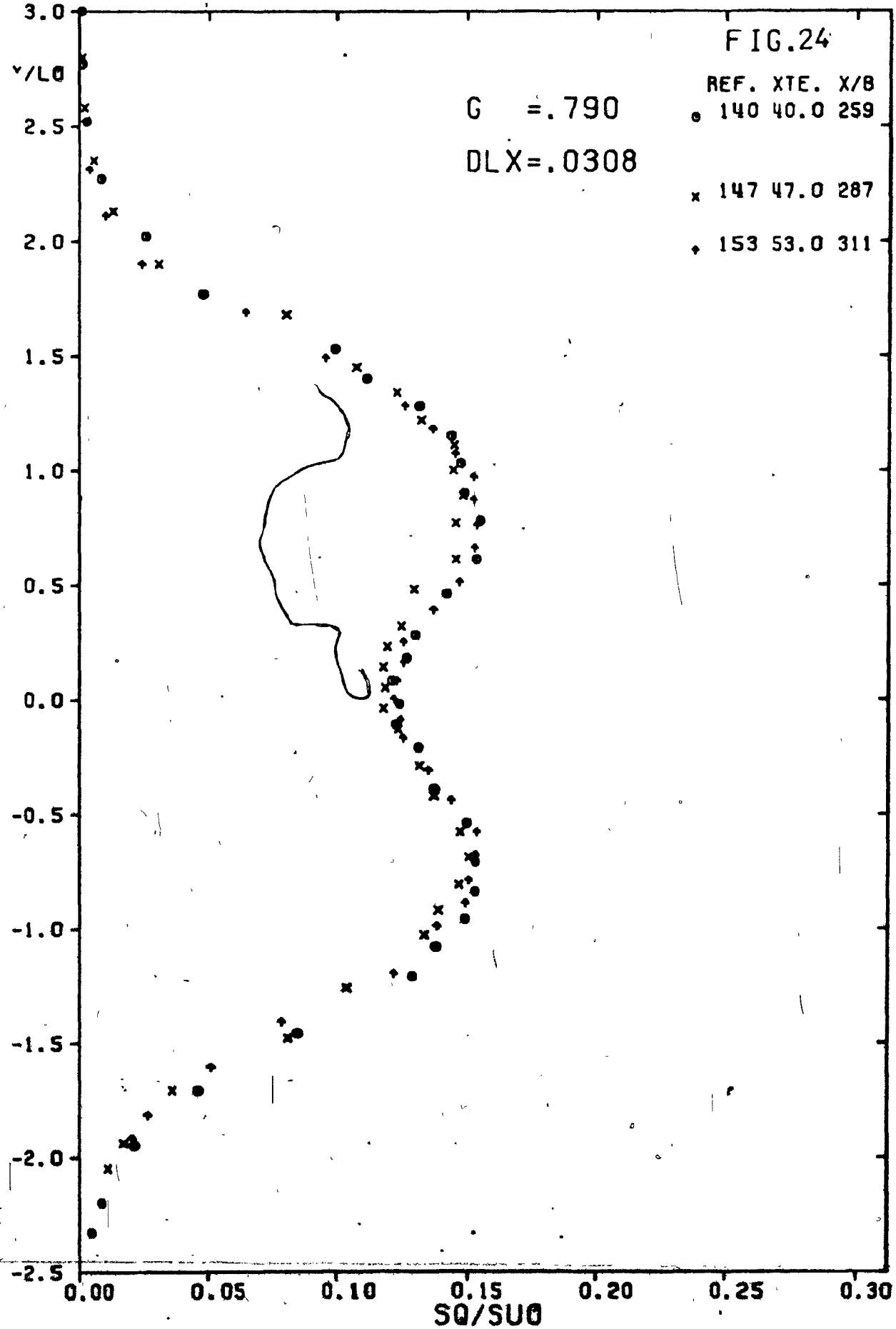
FIG.24
REF. XTE. X/B
140 40.0 259
147 47.0 287
153 53.0 311
G =.790
DLX=.0308
U/LO
SQ/SUO
3.0
2.5
2.0
1.5
1.0
0.5
0.0
-0.5
-1.0
-1.5
-2.0
-2.5
0.00
0.05
0.10
0.15
0.20
0.25
0.30

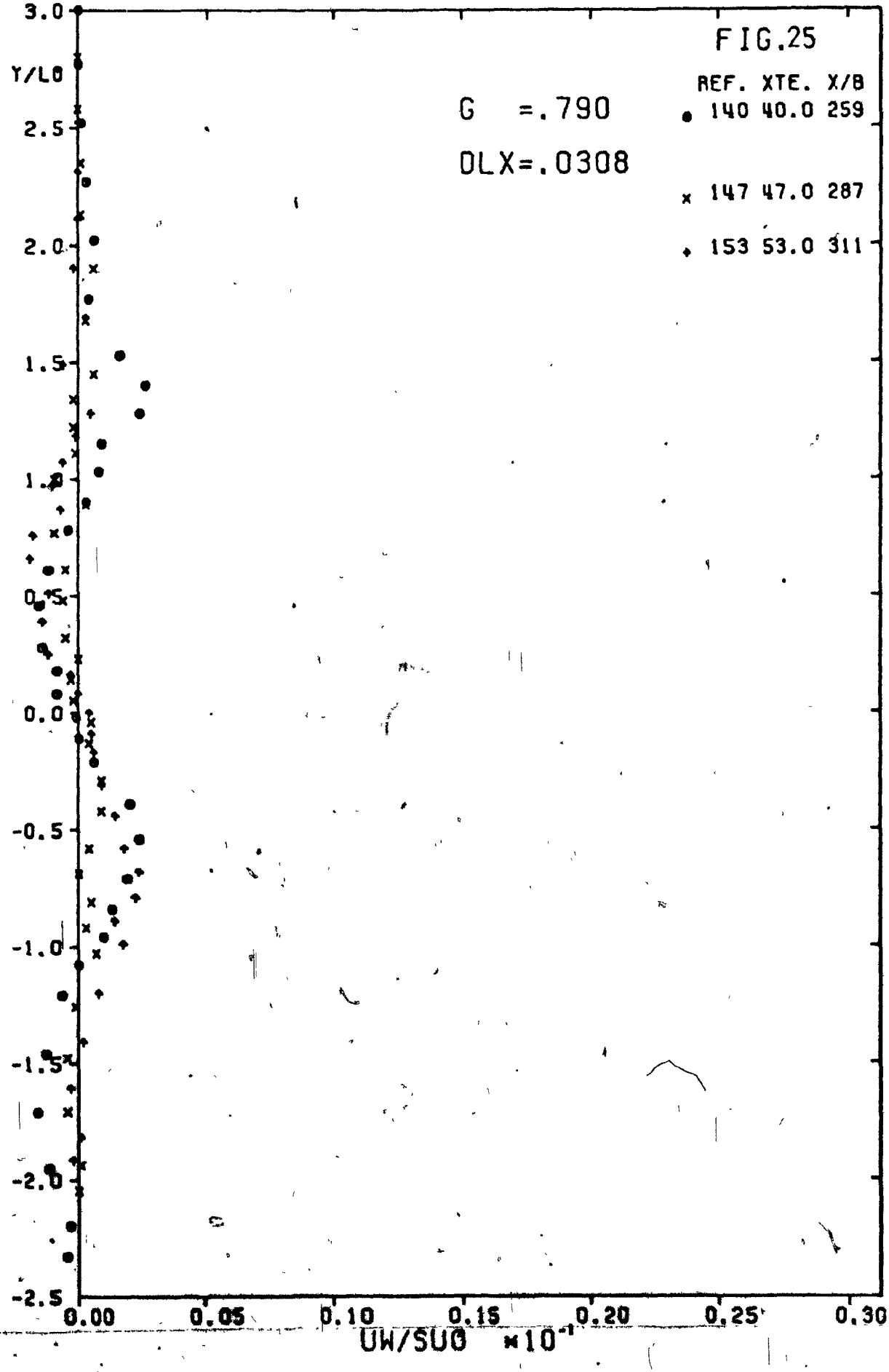
FIG.25
G =.790
DLX=.0308
REF. XTE. X/B
140 40.0 259
147 47.0 287
153 53.0 311
Y/L0
UW/SU0 ×10⁻¹
3.0
2.5
2.0
1.5
1.0
0.5
0.0
-0.5
-1.0
-1.5
-2.0
-2.5
0.00
0.05
0.10
0.15
0.20
0.25
0.30

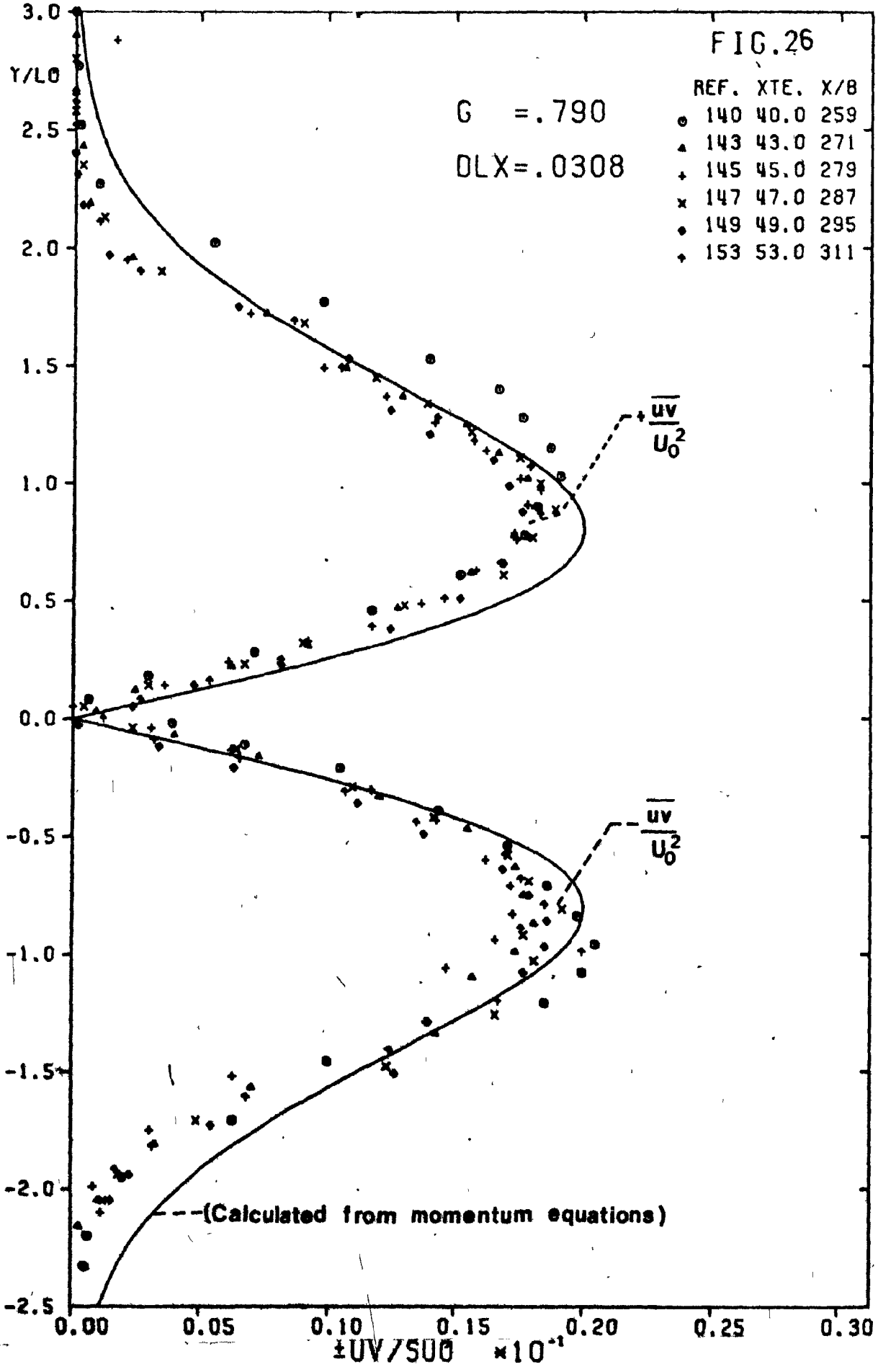
FIG.26
G =.790
DLX=.0308
REF. XTE. X/8
140 40.0 259
143 43.0 271
145 45.0 279
147 47.0 287
149 49.0 295
153 53.0 311
Y/L0
3.0
2.5
2.0
1.5
1.0
0.5
0.0
-0.5
-1.0
-1.5
-2.0
-2.5
0.00
0.05
0.10
0.15
0.20
0.25
0.30
±UV/500 ×10⁻¹
+uv/U0²
-uv/U0²
---(Calculated from momentum equations)

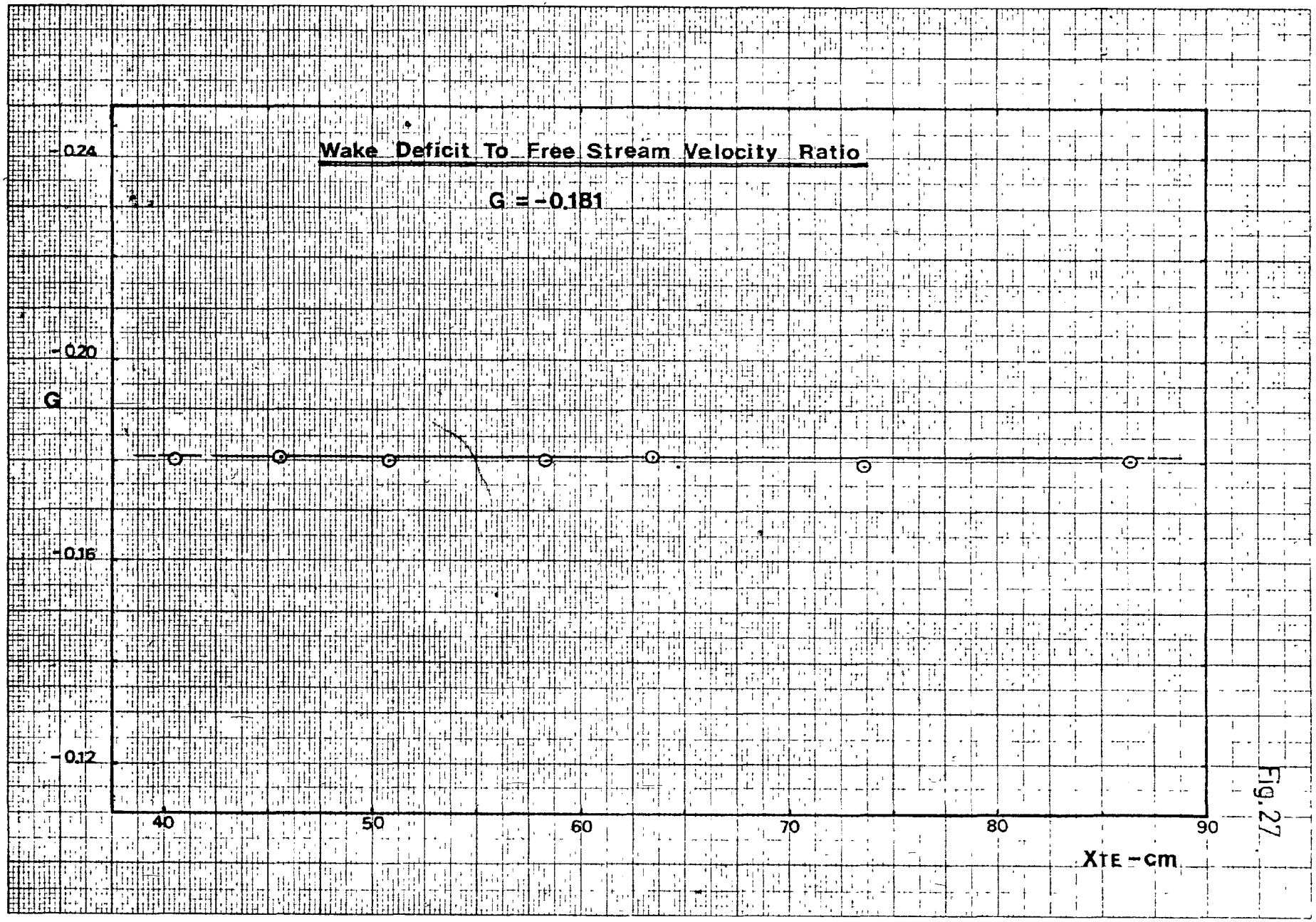
Wake Deficit To Free Stream Velocity Ratio
G = -0.181
-0.24
-0.20
-0.16
-0.12
G
40
50
60
70
80
90
XTE - cm

Fig. 27

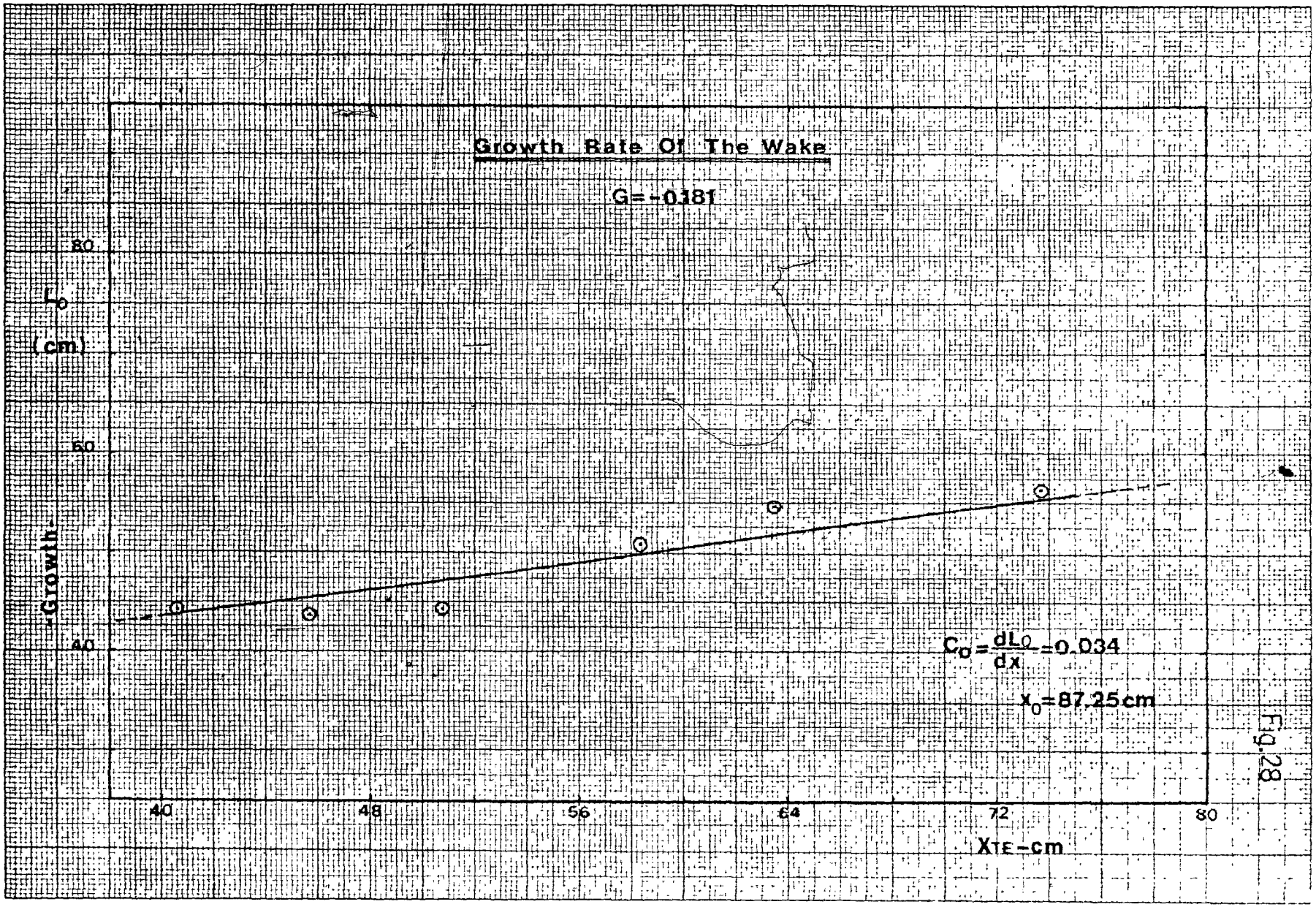

Fig.28

VELOCITY DECAY

Fig.29

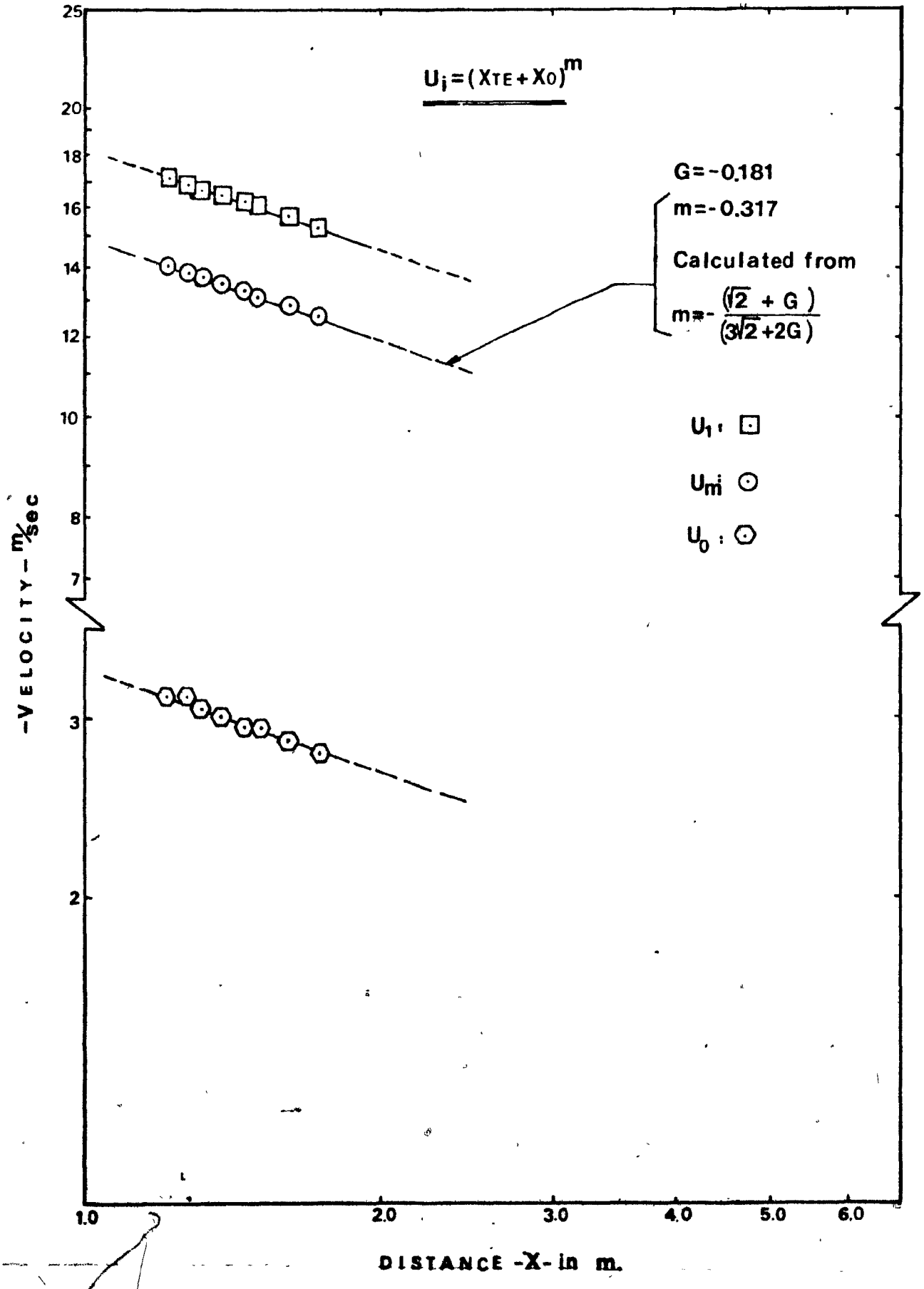

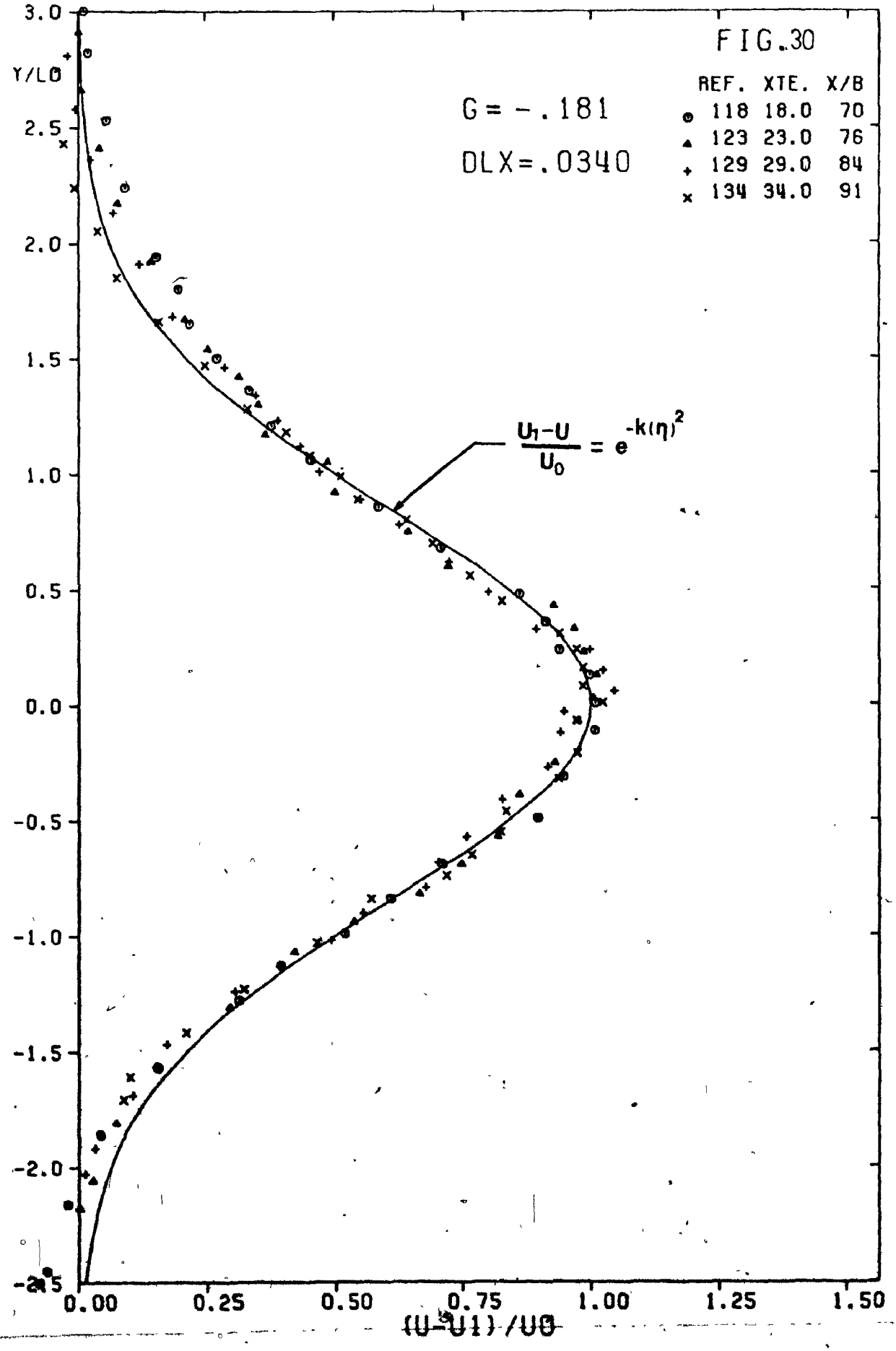
FIG.30
G = -.181
DLX=.0340
REF. XTE. X/B
118 18.0 70
123 23.0 76
129 29.0 84
134 34.0 91
$\frac{U_1-U}{U_0} = e^{-k(\eta)^2}$
Y/L0
3.0
2.5
2.0
1.5
1.0
0.5
0.0
-0.5
-1.0
-1.5
-2.0
-2.5
0.00
0.25
0.50
0.75
1.00
1.25
1.50
(U-U1)/U0

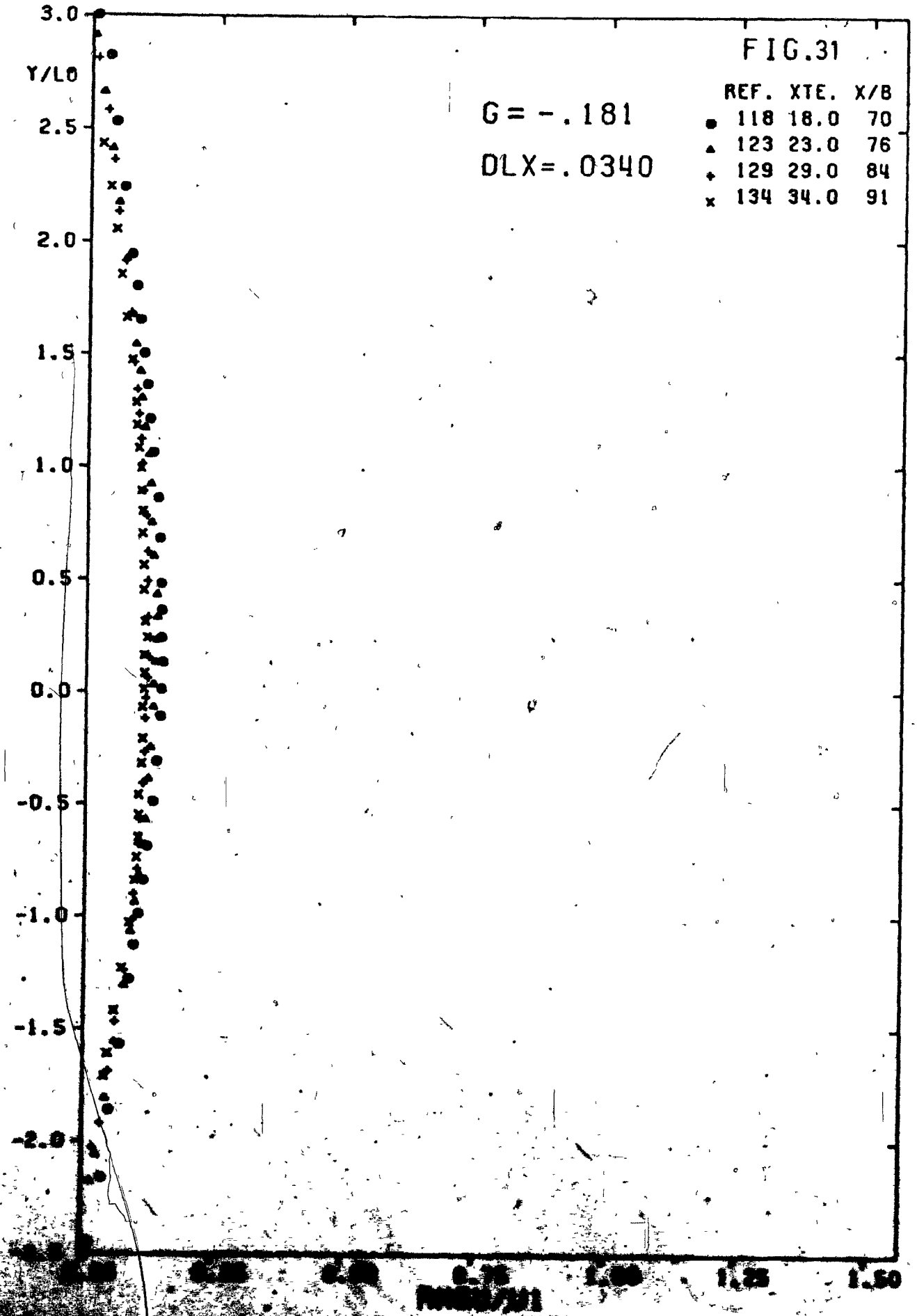
FIG.31
G = -.181
DLX=.0340
REF. XTE. X/B
118 18.0 70
123 23.0 76
129 29.0 84
134 34.0 91
Y/LO
3.0
2.5
2.0
1.5
1.0
0.5
0.0
-0.5
-1.0
-1.5
-2.0
1.25
1.50

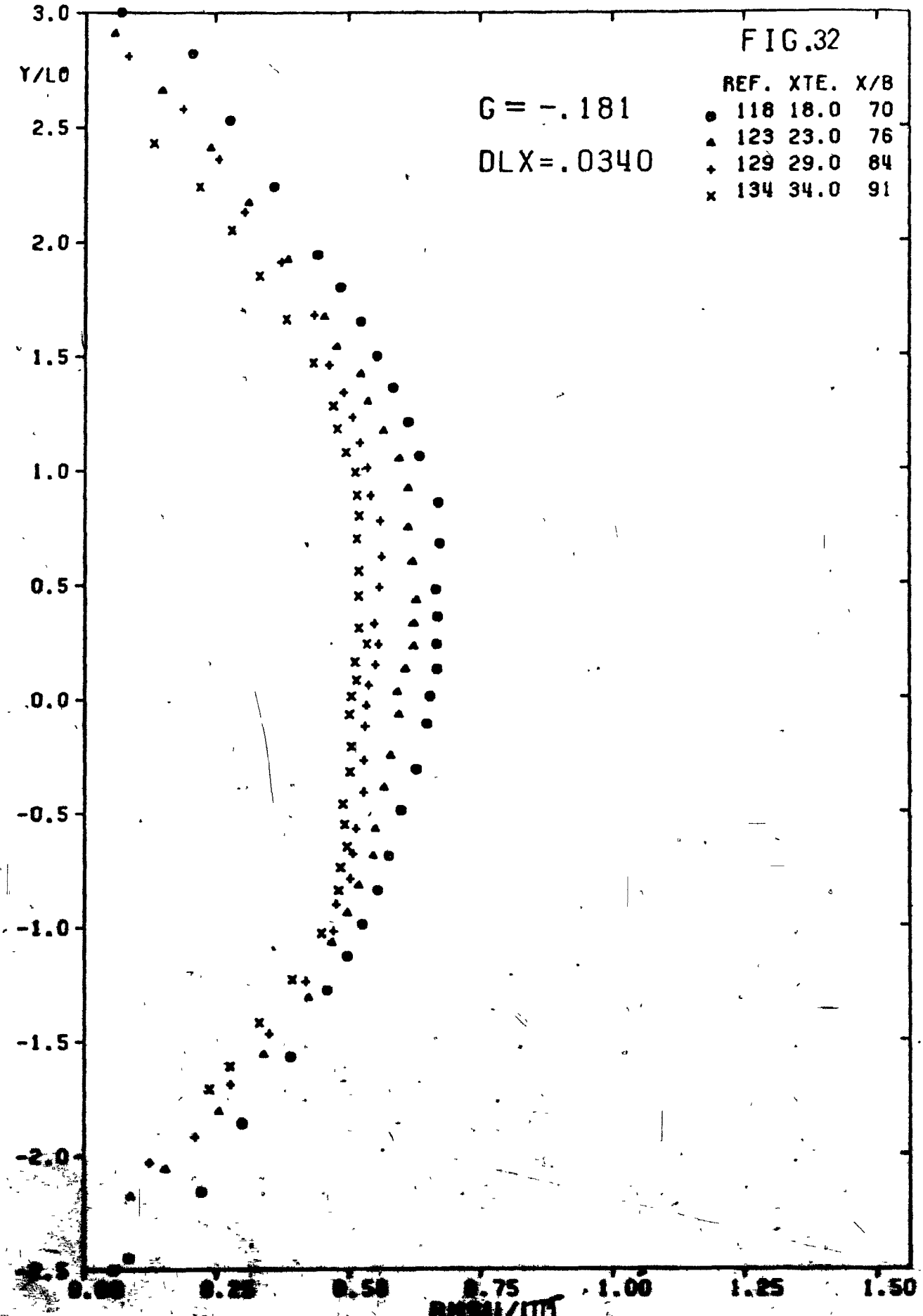
FIG.32
G = -.181
DLX=.0340
REF. XTE. X/B
118 18.0 70
123 23.0 76
129 29.0 84
134 34.0 91
Y/LO
3.0
2.5
2.0
1.5
1.0
0.5
0.0
-0.5
-1.0
-1.5
-2.0
-2.5
0.00
0.25
0.50
0.75
1.00
1.25
1.50

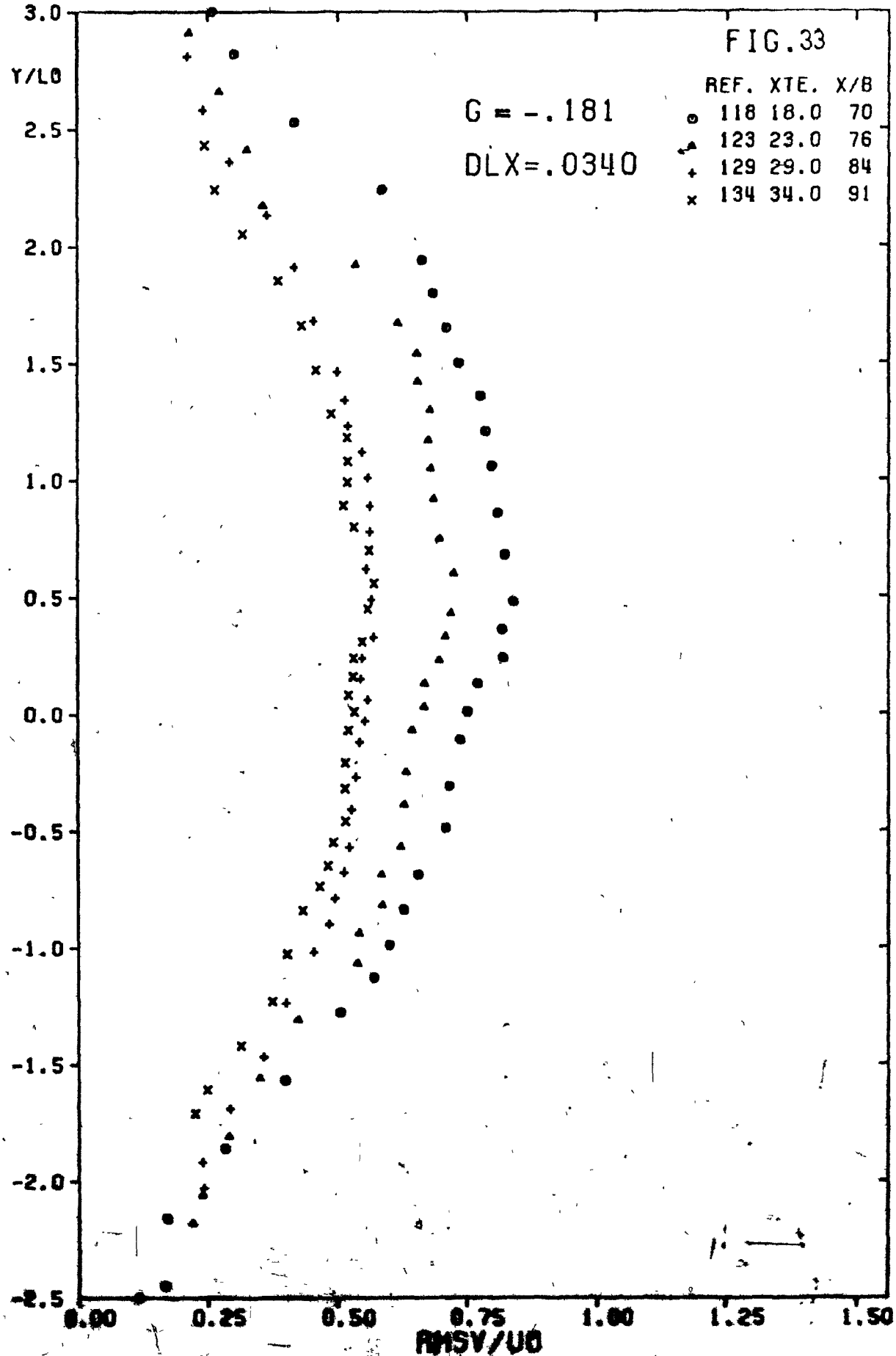
FIG.33
G = -.181
DLX=.0340
REF. XTE. X/B
118 18.0 70
123 23.0 76
129 29.0 84
134 34.0 91
Y/LO
RMSV/UO
3.0
2.5
2.0
1.5
1.0
0.5
0.0
-0.5
-1.0
-1.5
-2.0
-2.5
0.00
0.25
0.50
0.75
1.00
1.25
1.50

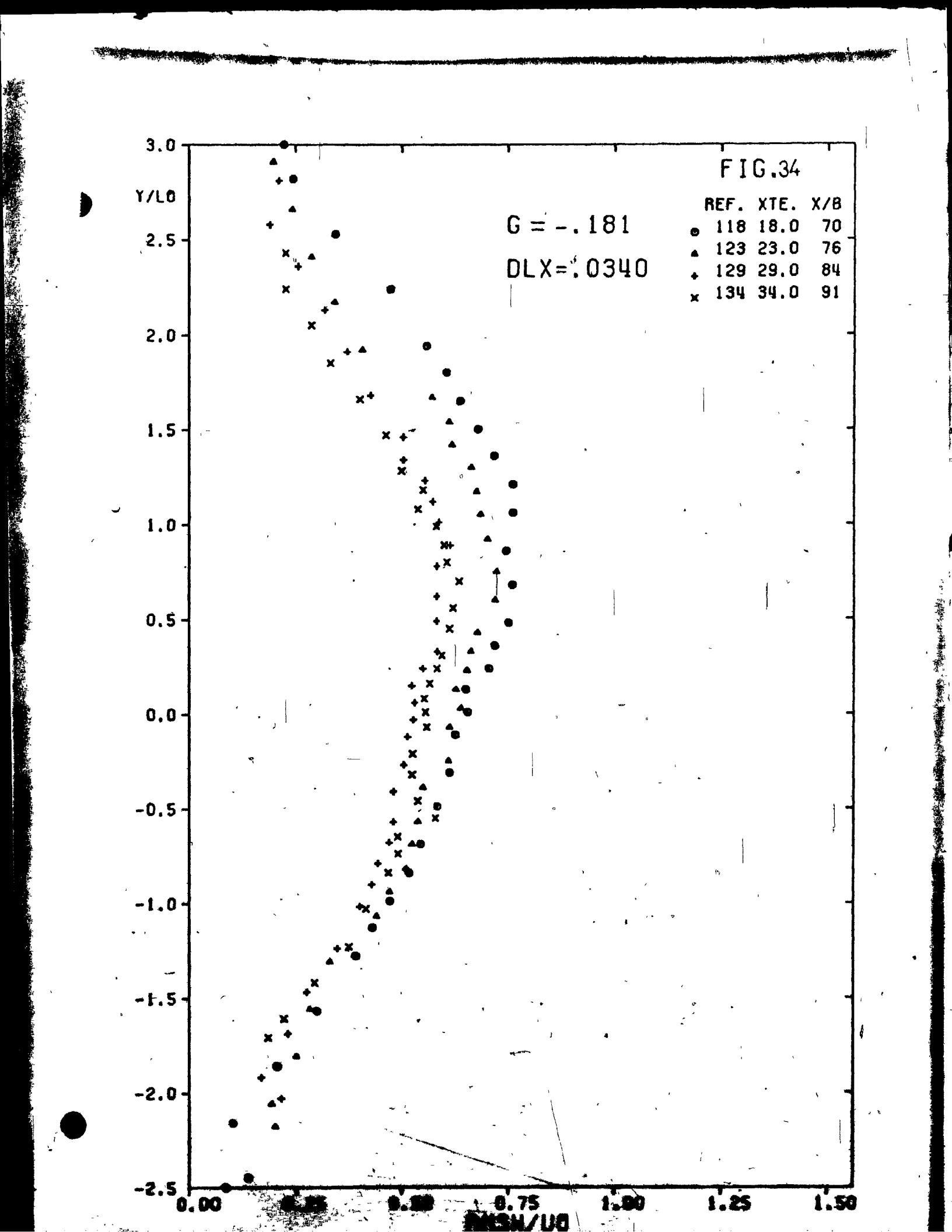
FIG.34
G = -.181
DLX=.0340
REF. XTE. X/B
118 18.0 70
123 23.0 76
129 29.0 84
134 34.0 91
Y/L0
3.0
2.5
2.0
1.5
1.0
0.5
0.0
-0.5
-1.0
-1.5
-2.0
-2.5
0.00
0.75
1.00
1.25
1.50

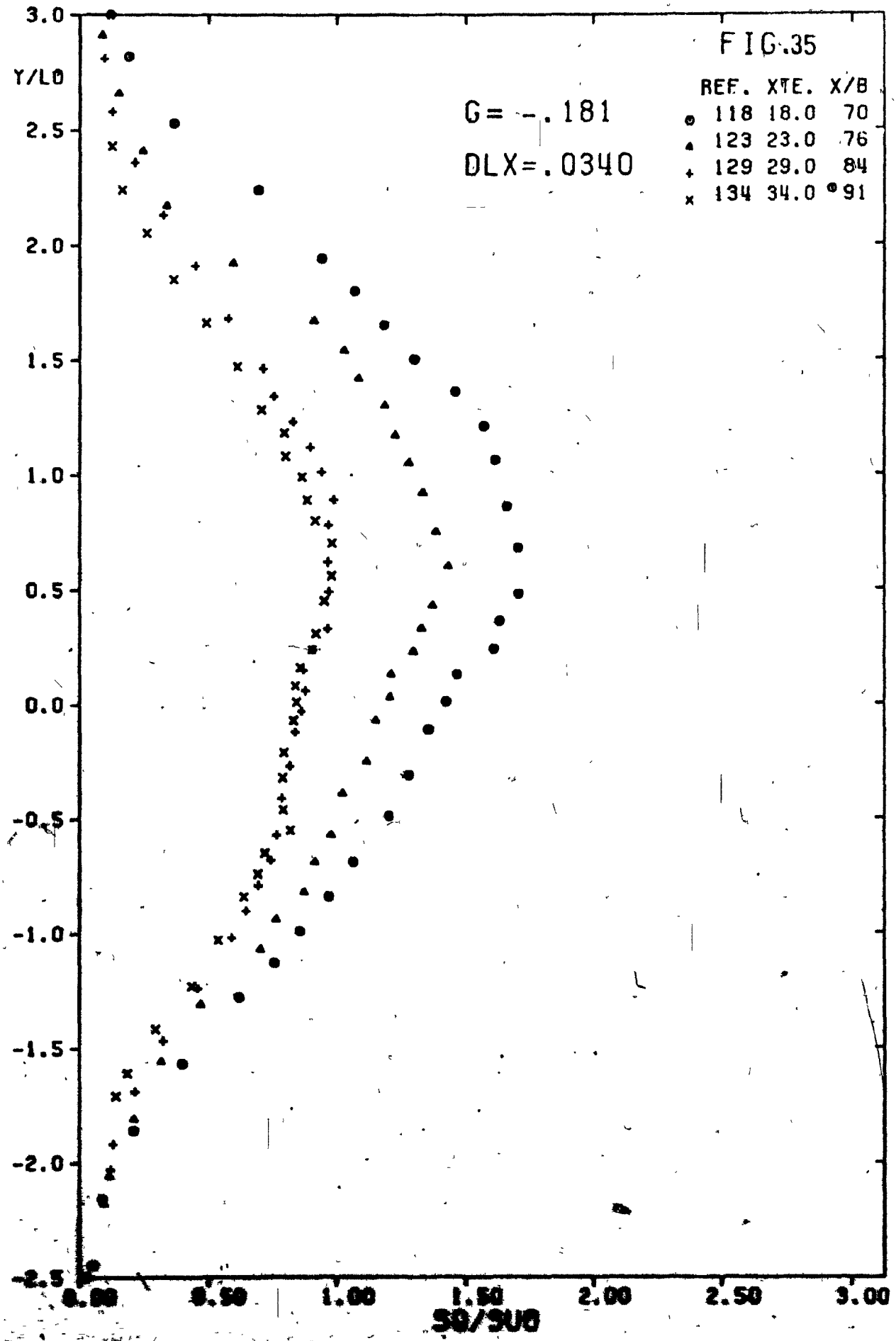
FIG.35
G= -.181
DLX=.0340
REF. XTE. X/B
118 18.0 70
123 23.0 76
129 29.0 84
134 34.0 91
Y/LO
3.0
2.5
2.0
1.5
1.0
0.5
0.0
-0.5
-1.0
-1.5
-2.0
-2.5
0.00
0.50
1.00
1.50
2.00
2.50
3.00
SO/SUO

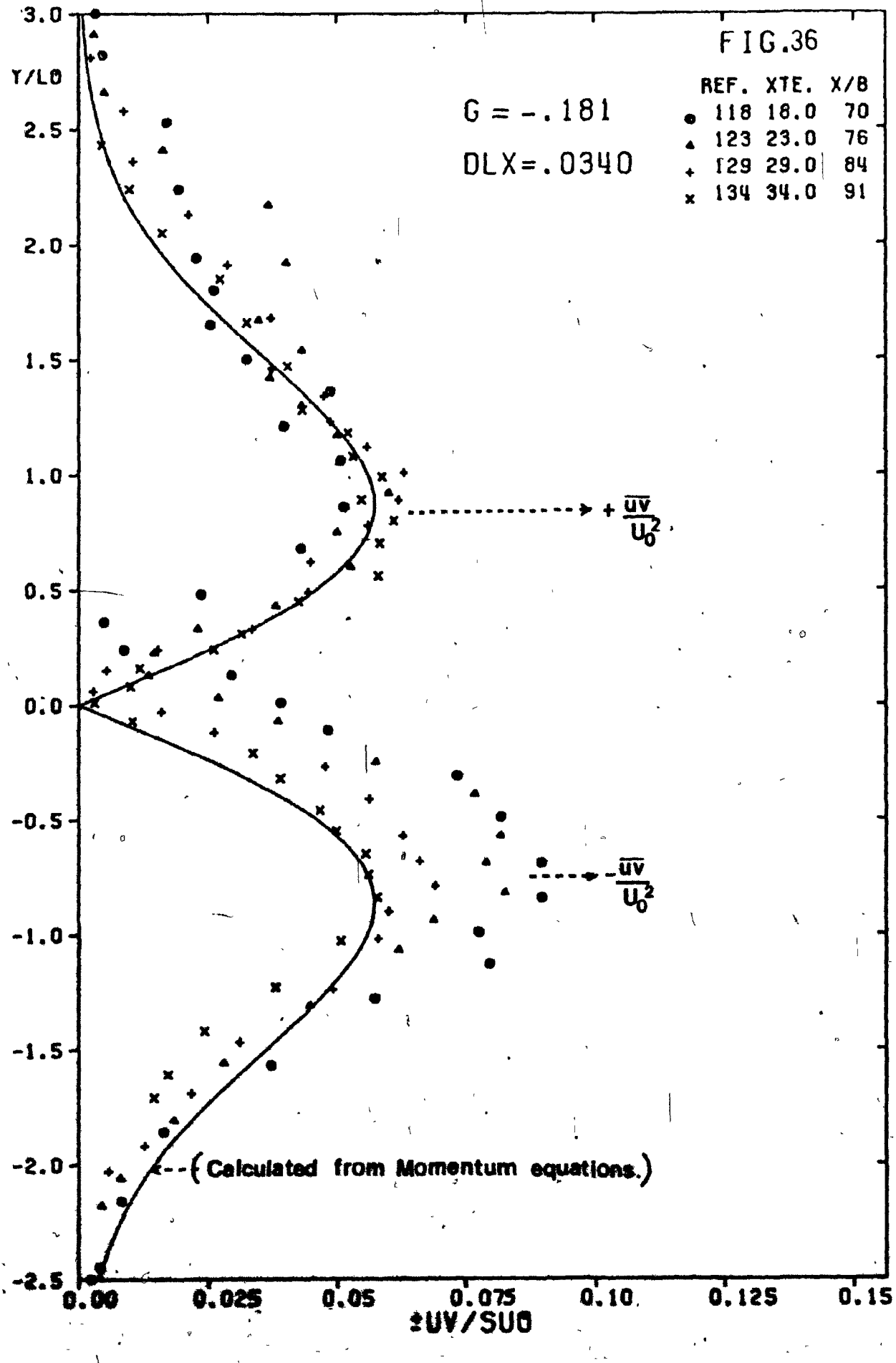
FIG.36
G = -.181
DLX=.0340
REF. XTE. X/8
118 18.0 70
123 23.0 76
129 29.0 84
134 34.0 91
Y/L0
3.0
2.5
2.0
1.5
1.0
0.5
0.0
-0.5
-1.0
-1.5
-2.0
-2.5
+ $\frac{\overline{uv}}{U_0^2}$
- $\frac{\overline{uv}}{U_0^2}$
(Calculated from Momentum equations.)
0.00
0.025
0.05
0.075
0.10
0.125
0.15
±UV/SU0

Fig.37

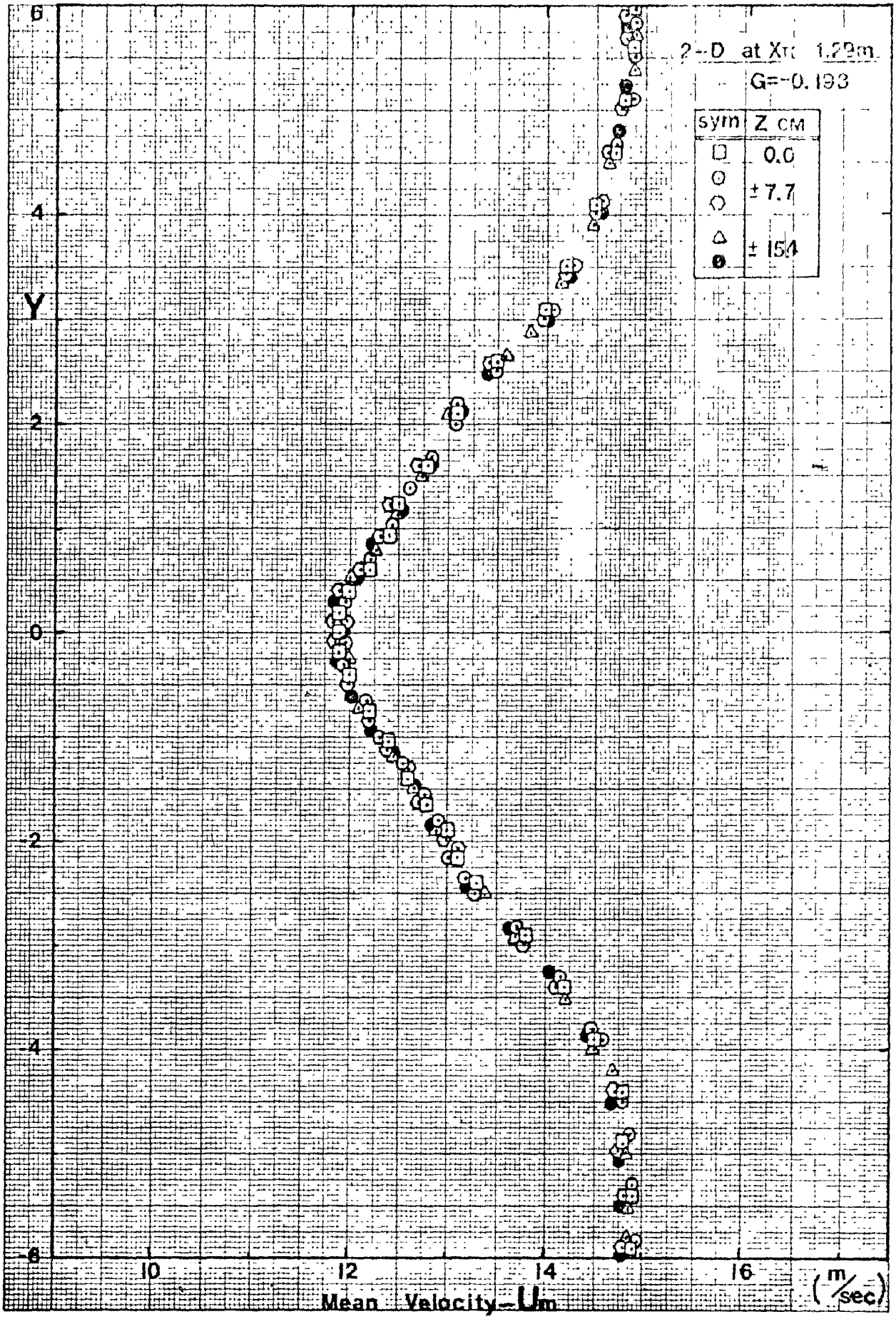

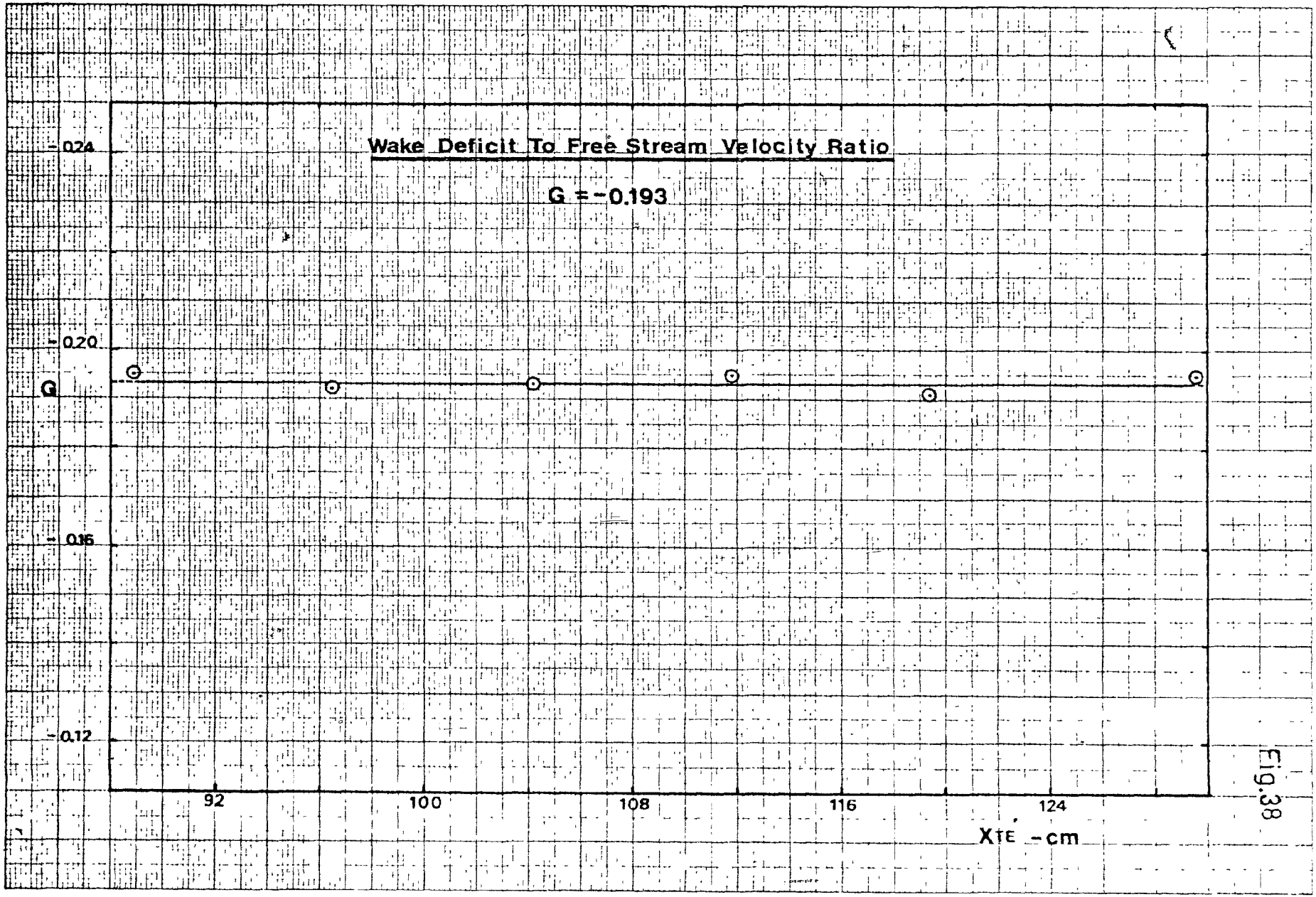

Fig. 38

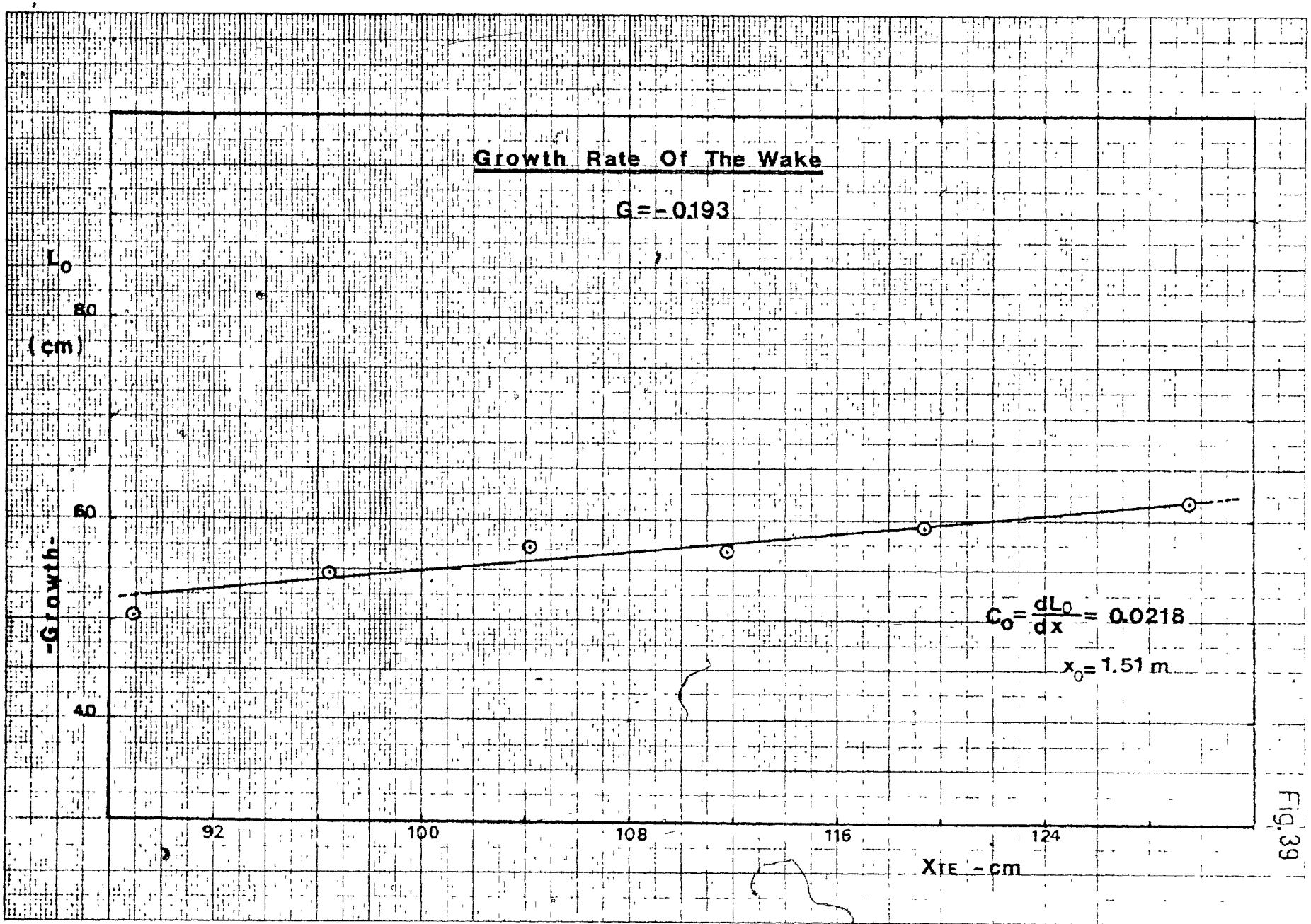

Fig. 39

VELOCITY DECAY

Fig 40

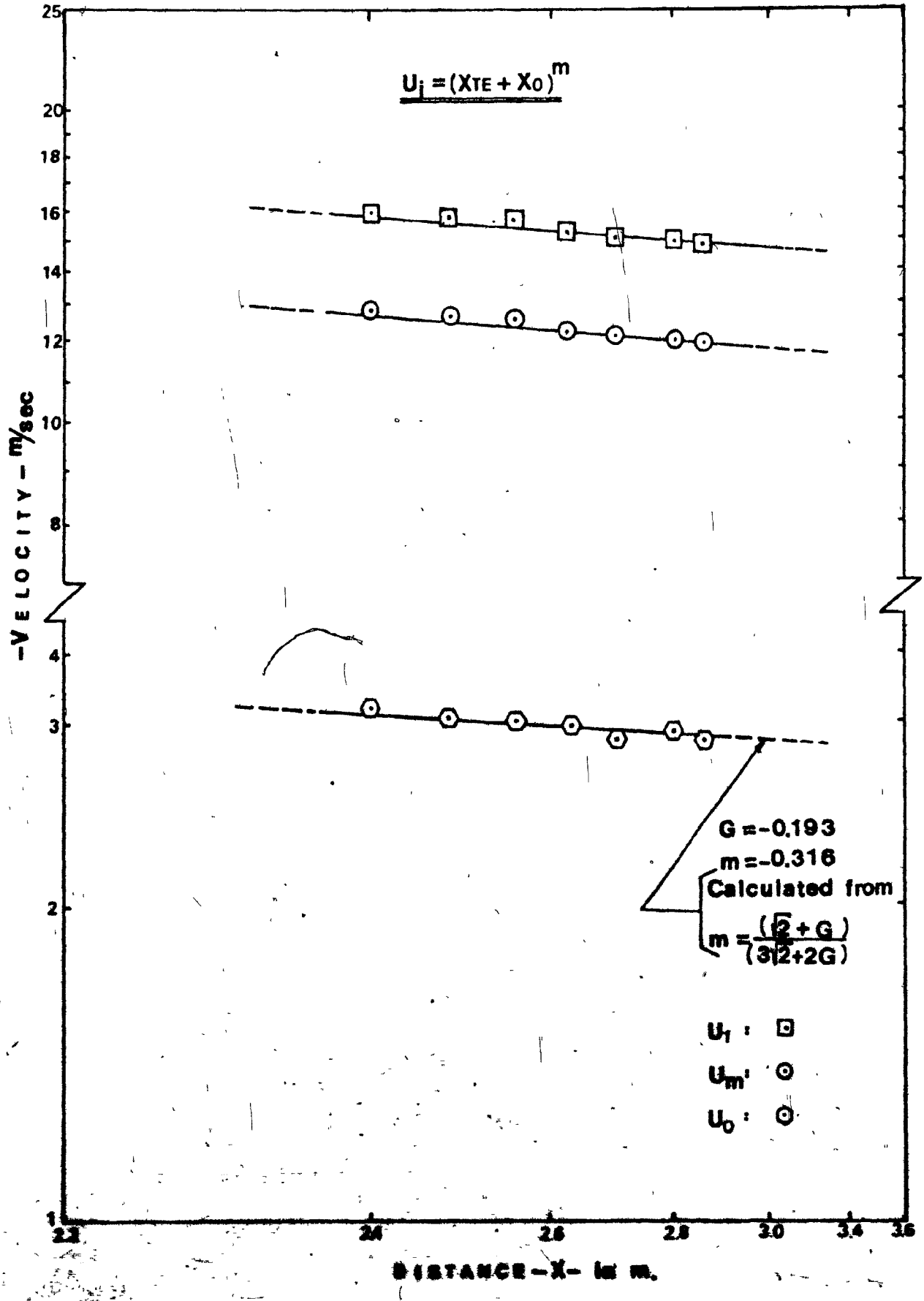

FIG.41

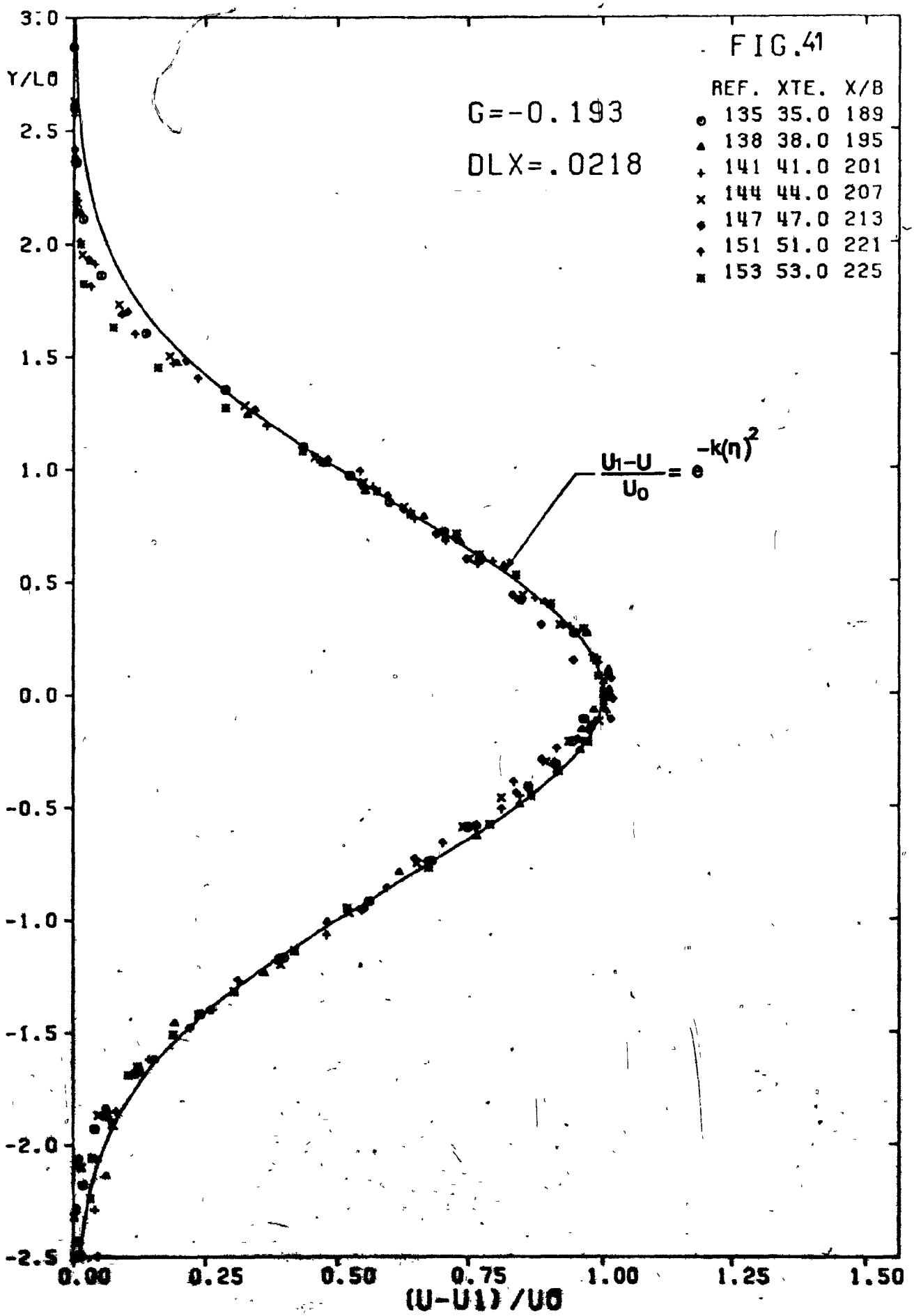
G=-0.193
DLX=.0218
REF. XTE. X/B
135 35.0 189
138 38.0 195
141 41.0 201
144 44.0 207
147 47.0 213
151 51.0 221
153 53.0 225
$\frac{U_1-U}{U_0} = e^{-k(\eta)^2}$
Y/L0
3.0
2.5
2.0
1.5
1.0
0.5
0.0
-0.5
-1.0
-1.5
-2.0
-2.5
0.00
0.25
0.50
0.75
1.00
1.25
1.50
(U-U1)/U0

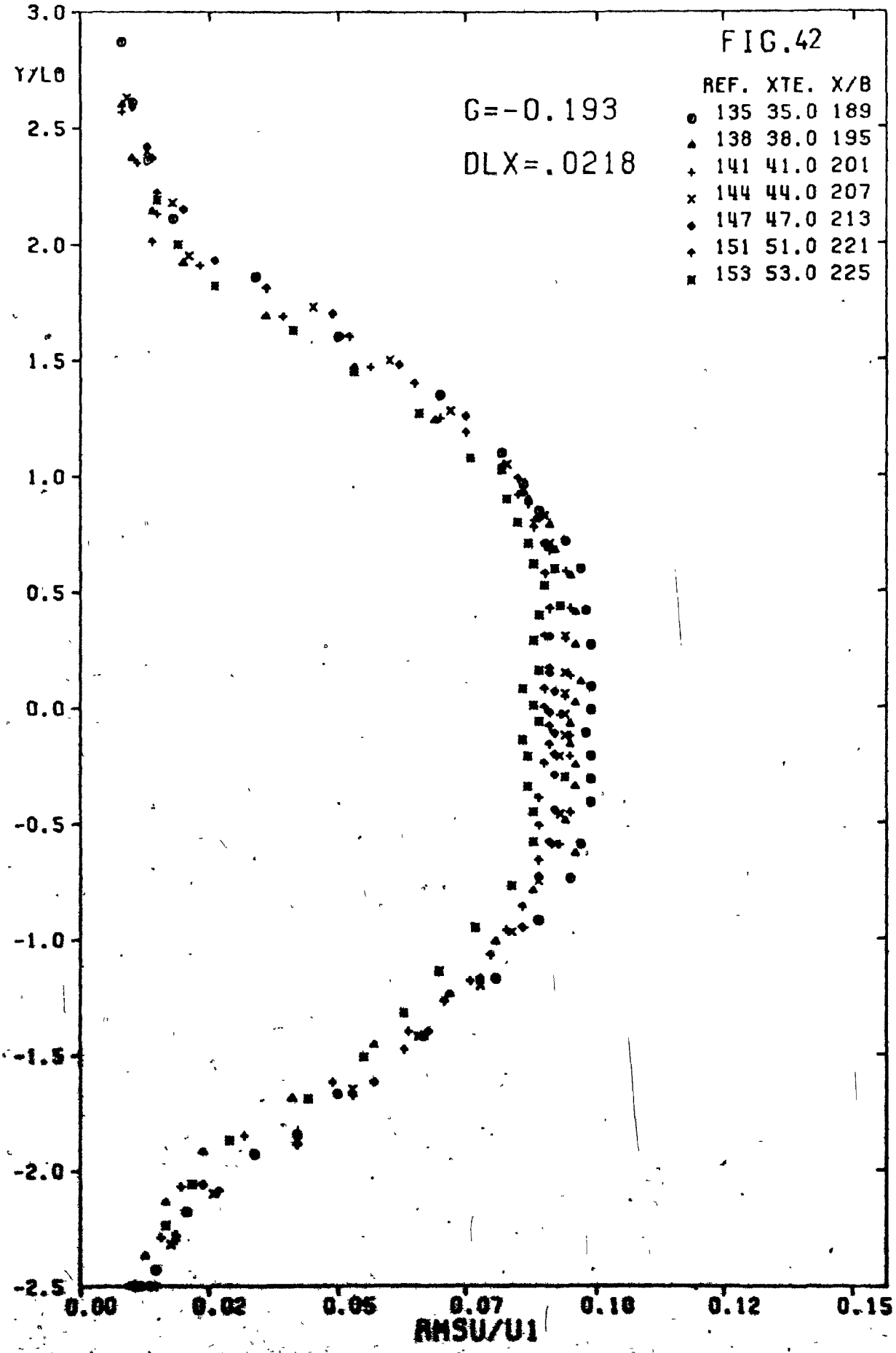
FIG.42
G=-0.193
DLX=.0218
REF. XTE. X/B
135 35.0 189
138 38.0 195
141 41.0 201
144 44.0 207
147 47.0 213
151 51.0 221
153 53.0 225
Y/L0
3.0
2.5
2.0
1.5
1.0
0.5
0.0
-0.5
-1.0
-1.5
-2.0
-2.5
0.00
0.02
0.05
0.07
0.10
0.12
0.15
RMSU/U1

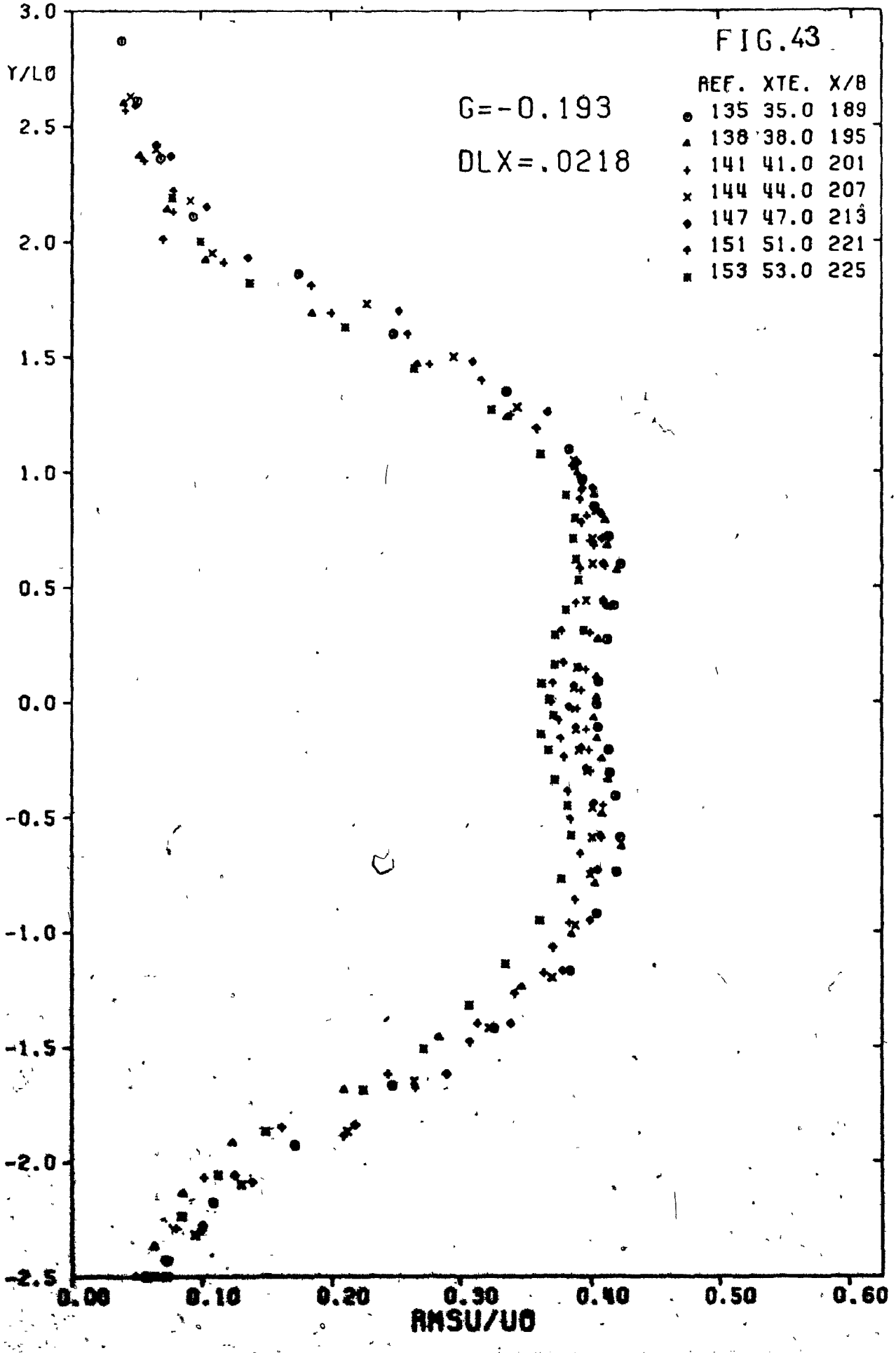
FIG.43
G=-0.193
DLX=.0218
REF. XTE. X/B
135 35.0 189
138 38.0 195
141 41.0 201
144 44.0 207
147 47.0 213
151 51.0 221
153 53.0 225
Y/L0
3.0
2.5
2.0
1.5
1.0
0.5
0.0
-0.5
-1.0
-1.5
-2.0
-2.5
0.00
0.10
0.20
0.30
0.40
0.50
0.60
RMSU/U0

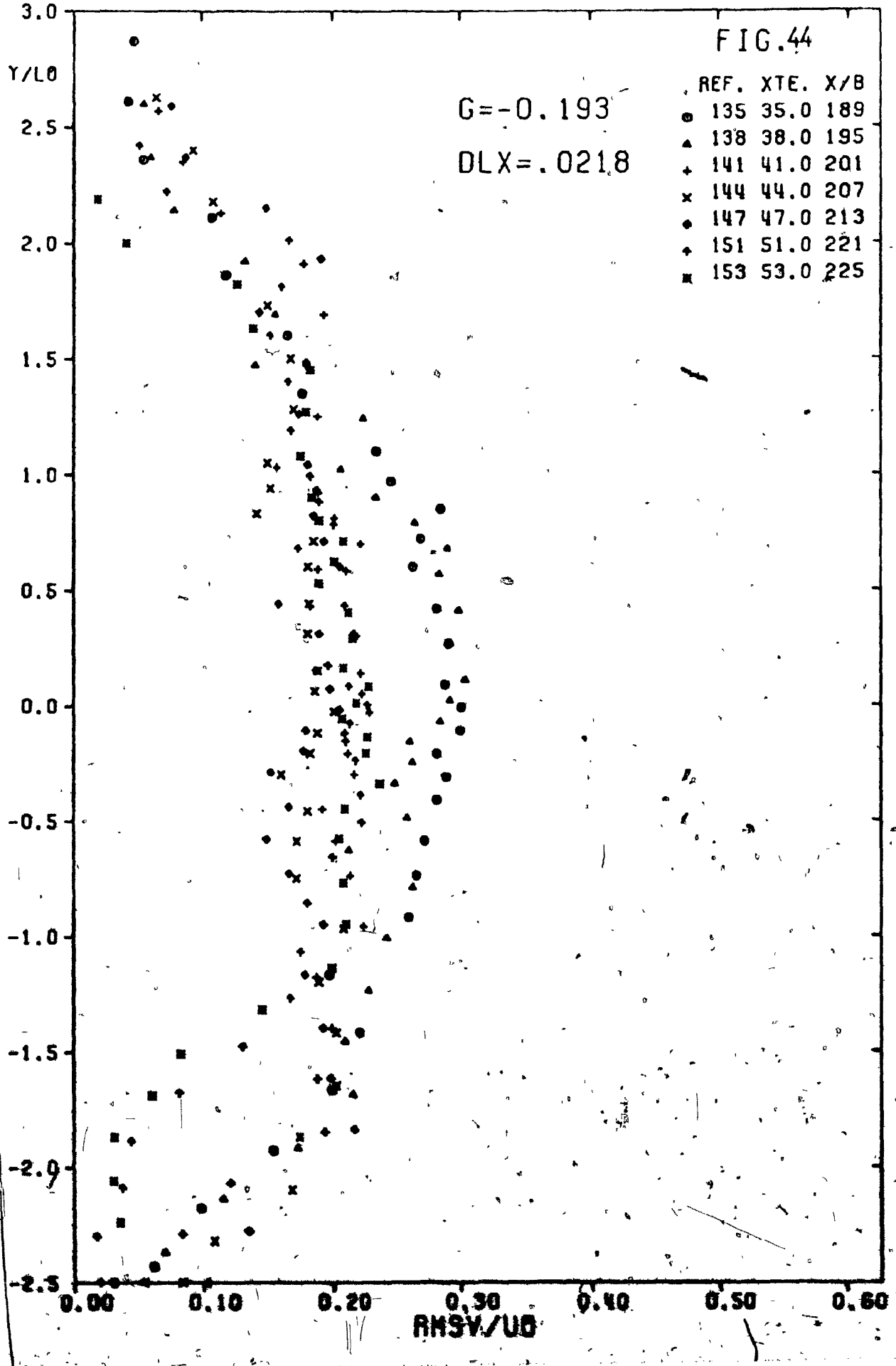
FIG.44
G=-0.193
DLX=.0218
REF. XTE. X/B
135 35.0 189
138 38.0 195
141 41.0 201
144 44.0 207
147 47.0 213
151 51.0 221
153 53.0 225
Y/L0
3.0
2.5
2.0
1.5
1.0
0.5
0.0
-0.5
-1.0
-1.5
-2.0
-2.5
0.00
0.10
0.20
0.30
0.40
0.50
0.60
RMSV/U0

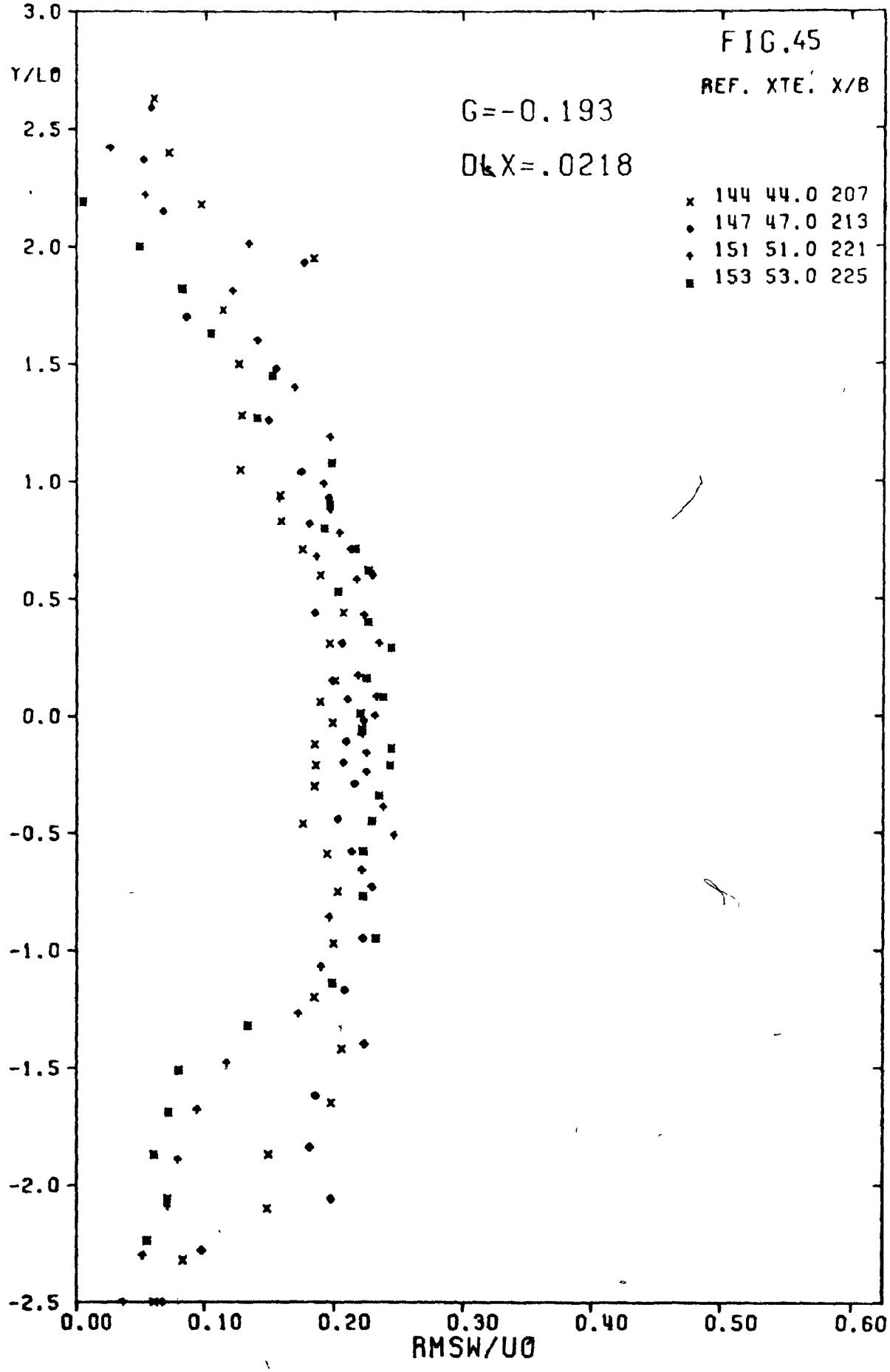
FIG.45
REF. XTE. X/B
G=-0.193
DLX=.0218
144 44.0 207
147 47.0 213
151 51.0 221
153 53.0 225
Y/L0
RMSW/U0
3.0
2.5
2.0
1.5
1.0
0.5
0.0
-0.5
-1.0
-1.5
-2.0
-2.5
0.00
0.10
0.20
0.30
0.40
0.50
0.60

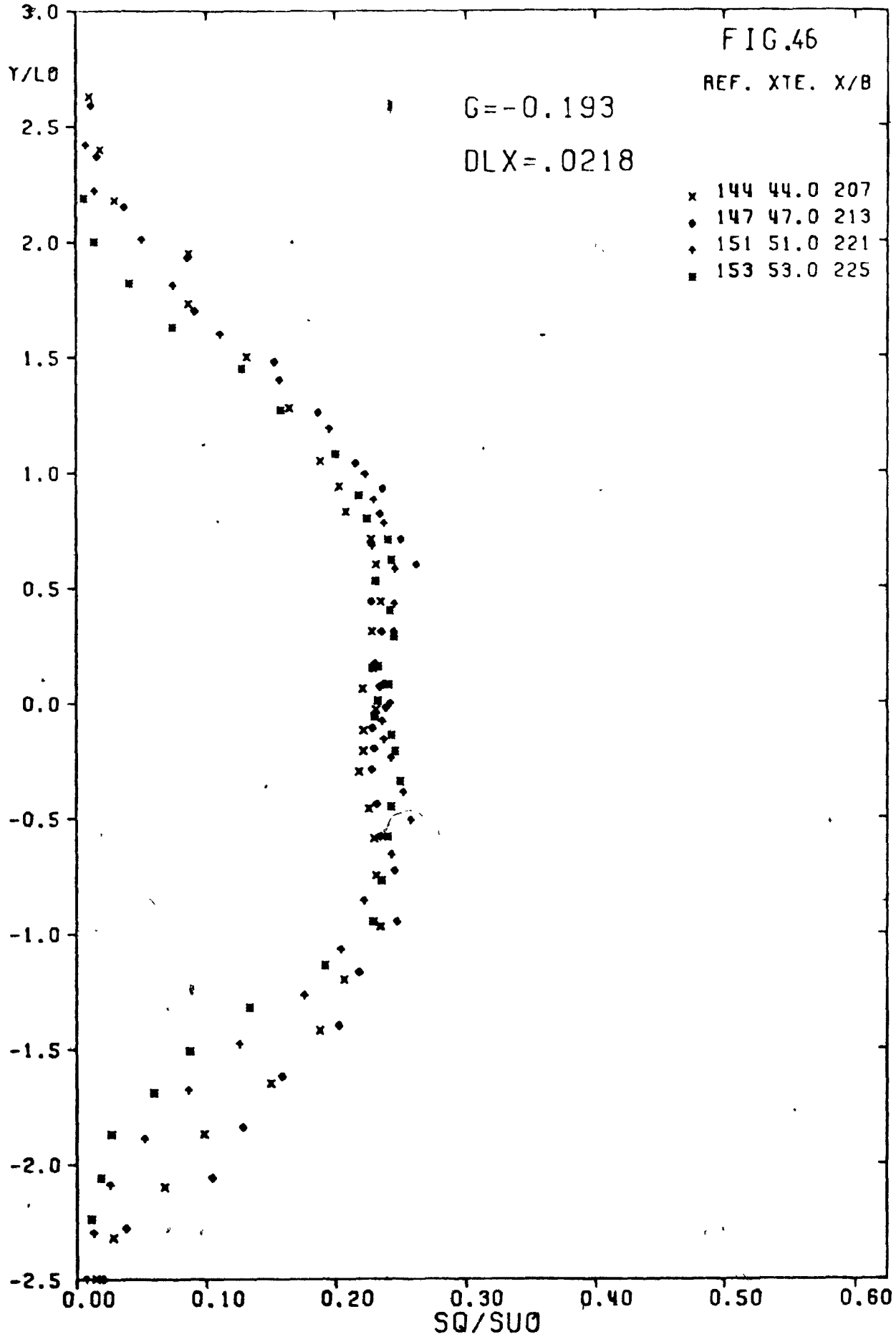
FIG.46
REF. XTE. X/B
G=-0.193
DLX=.0218
144 44.0 207
147 47.0 213
151 51.0 221
153 53.0 225
Y/L0
SQ/SU0
3.0
2.5
2.0
1.5
1.0
0.5
0.0
-0.5
-1.0
-1.5
-2.0
-2.5
0.00
0.10
0.20
0.30
0.40
0.50
0.60

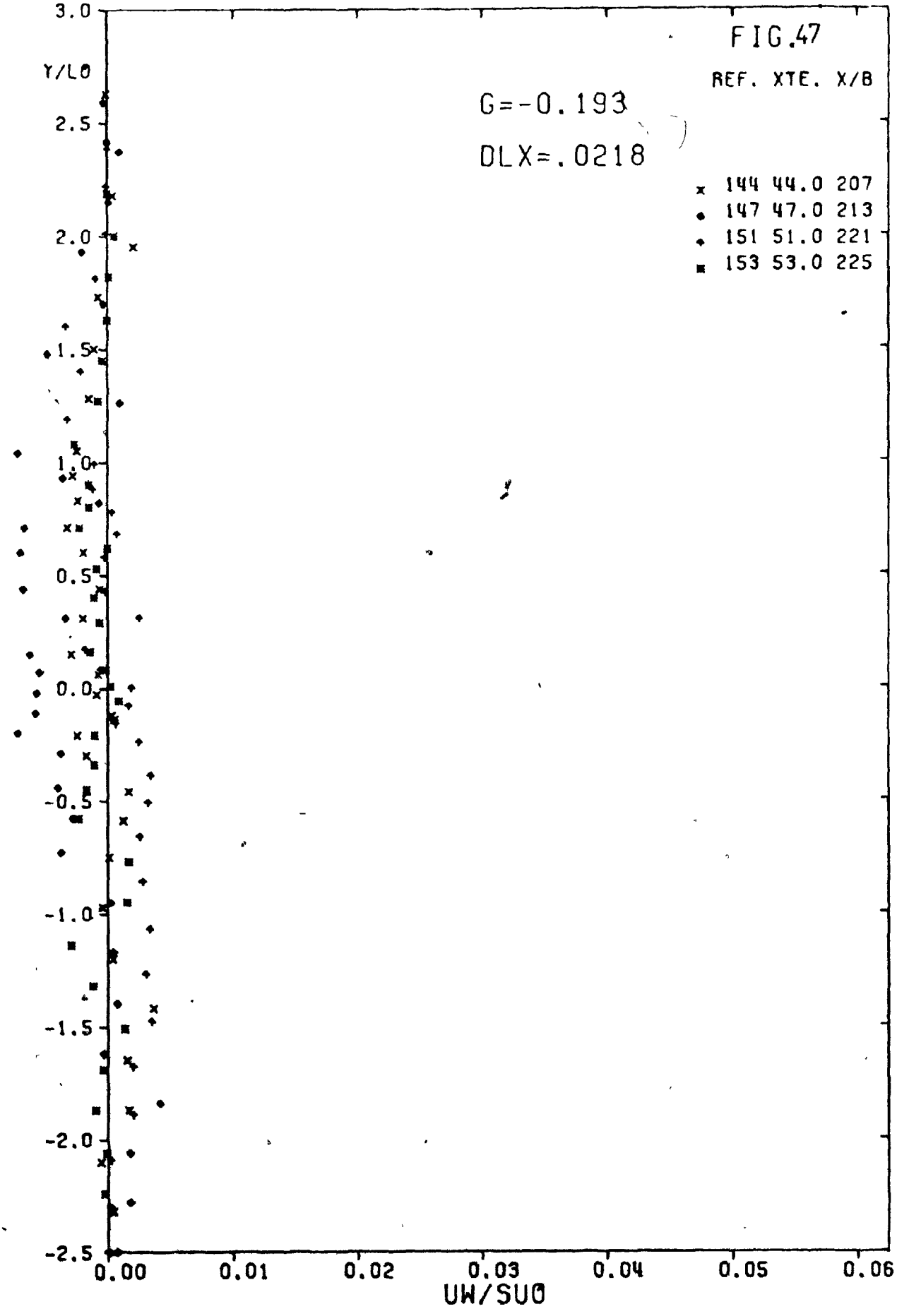
FIG.47
REF. XTE. X/B
G=-0.193
DLX=.0218
144 44.0 207
147 47.0 213
151 51.0 221
153 53.0 225
Y/L0
UW/SU0
3.0
2.5
2.0
1.5
1.0
0.5
0.0
-0.5
-1.0
-1.5
-2.0
-2.5
0.00
0.01
0.02
0.03
0.04
0.05
0.06

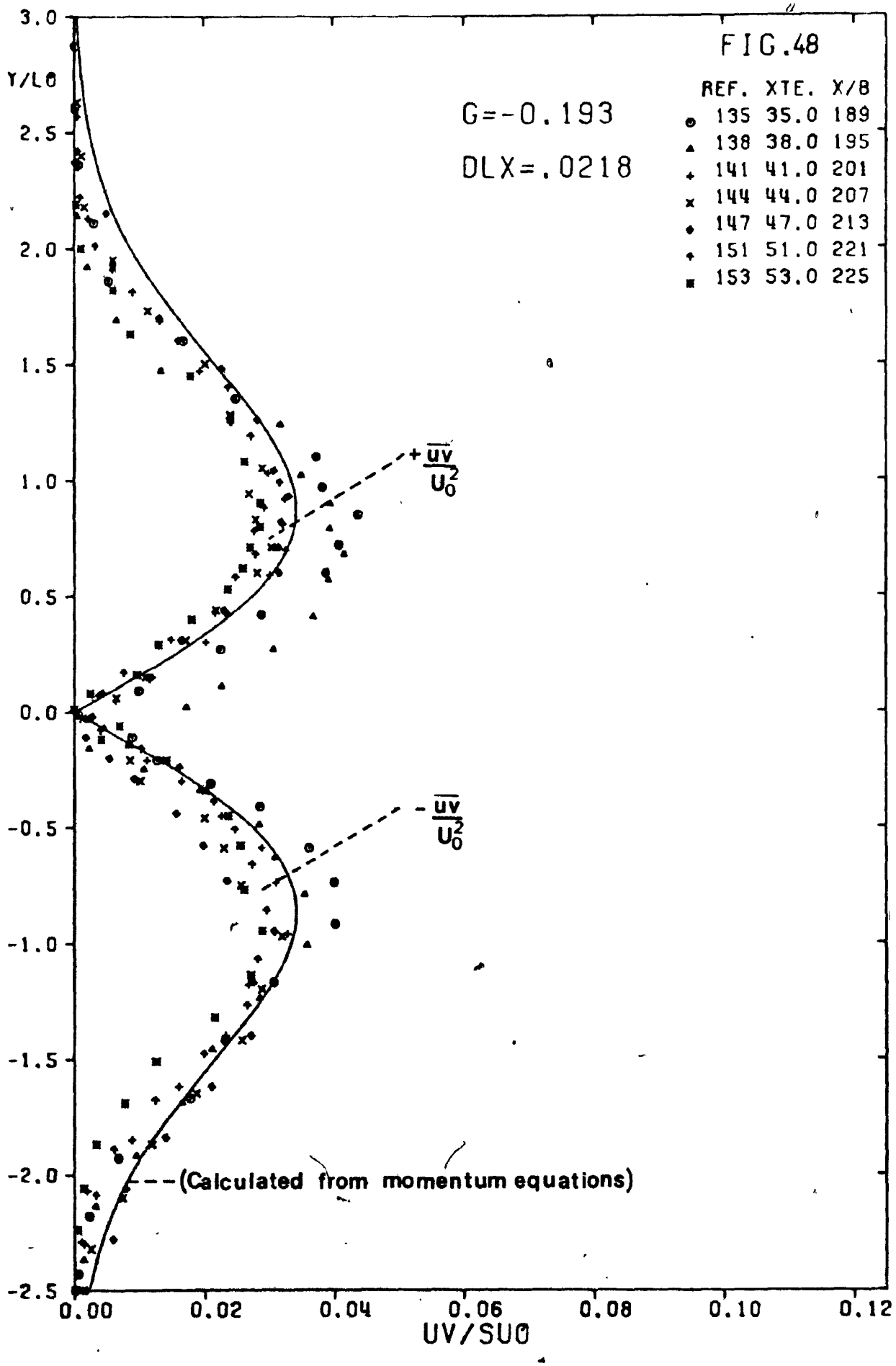
FIG.48
G=-0.193
DLX=.0218
REF. XTE. X/B
135 35.0 189
138 38.0 195
141 41.0 201
144 44.0 207
147 47.0 213
151 51.0 221
153 53.0 225
Y/L0
3.0
2.5
2.0
1.5
1.0
0.5
0.0
-0.5
-1.0
-1.5
-2.0
-2.5
+ $\frac{\overline{uv}}{U_0^2}$
- $\frac{\overline{uv}}{U_0^2}$
---(Calculated from momentum equations)
0.00
0.02
0.04
0.06
0.08
0.10
0.12
UV/SU0

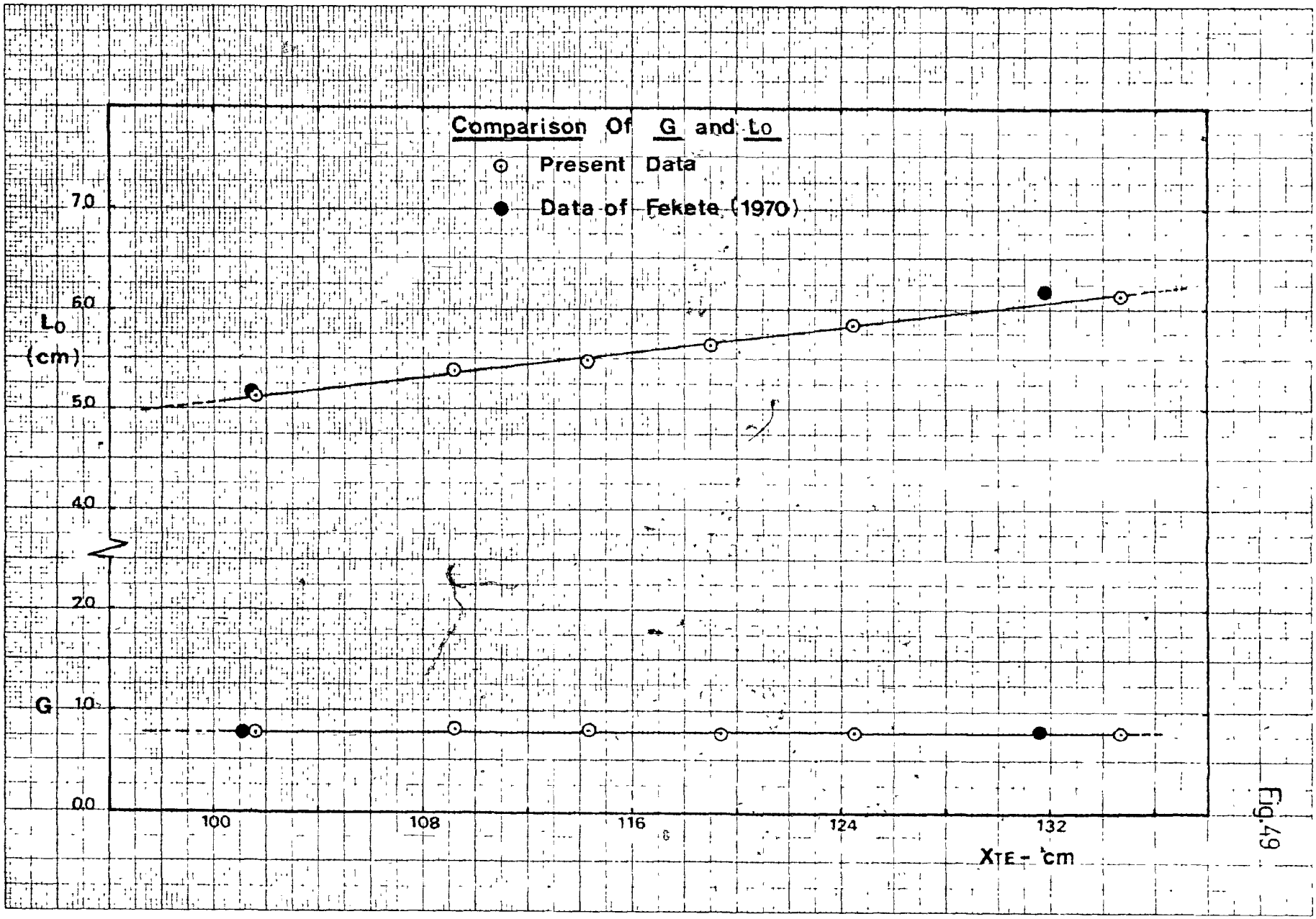
Comparison Of G and Lo
Present Data
Data of Fekete (1970)
Lo (cm)
7.0
6.0
5.0
4.0
2.0
G 1.0
0.0
100
108
116
124
132
XTE - cm

Fig. 49

Fig. 50

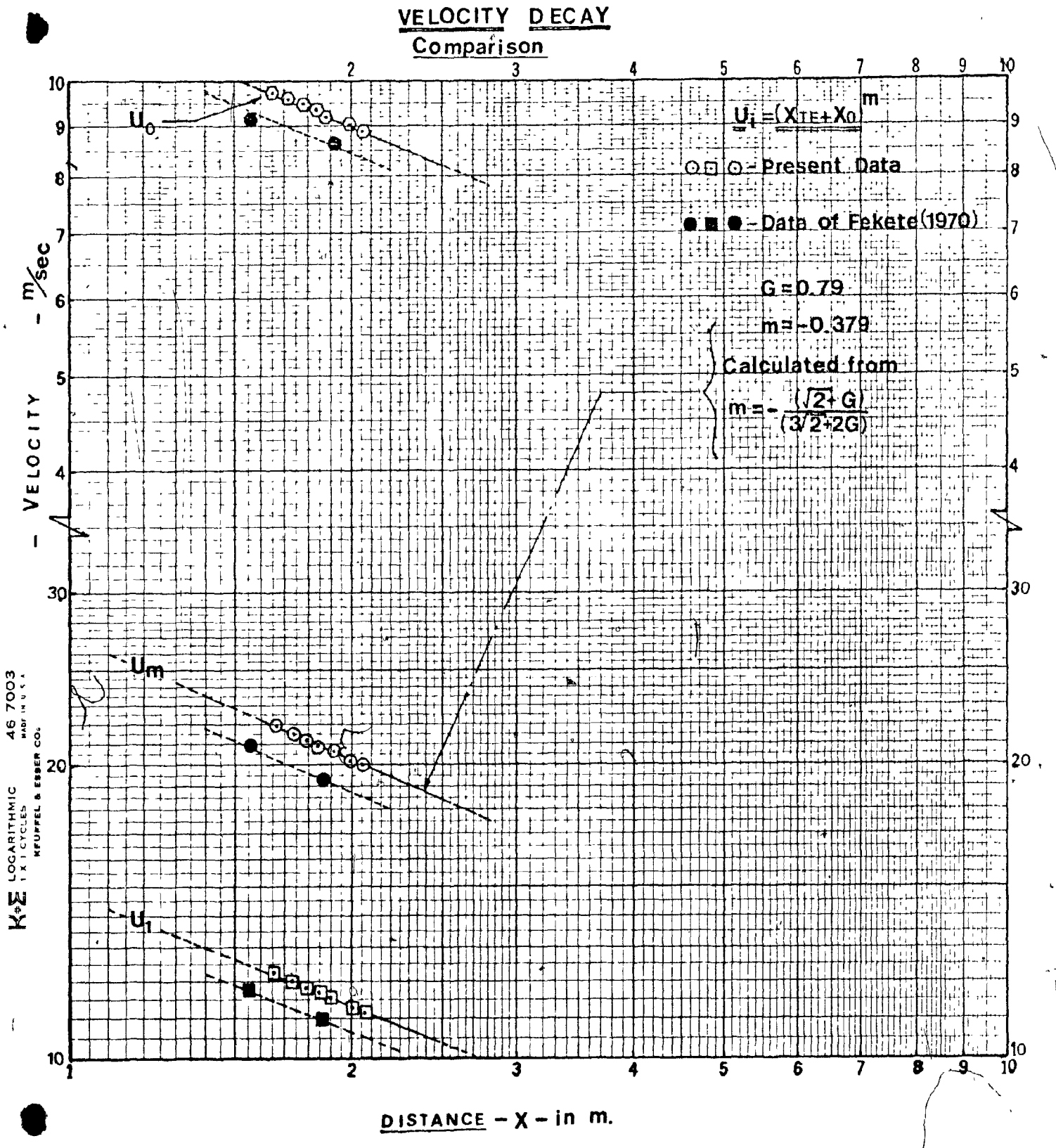
VELOCITY DECAY
Comparison
$U_i = \frac{(X_{TE}+X_0)}{}^m$
○□⊙ - Present Data
●■● - Data of Fekete (1970)
G = 0.79
m = -0.379
Calculated from
$m = -\frac{(\sqrt{2}+G)}{(3\sqrt{2}+2G)}$
U_0
U_m
U_1
- VELOCITY - m/sec
DISTANCE - X - in m.
K+E LOGARITHMIC 1 X 1 CYCLES KEUFFEL & ESSER CO. 46 7003

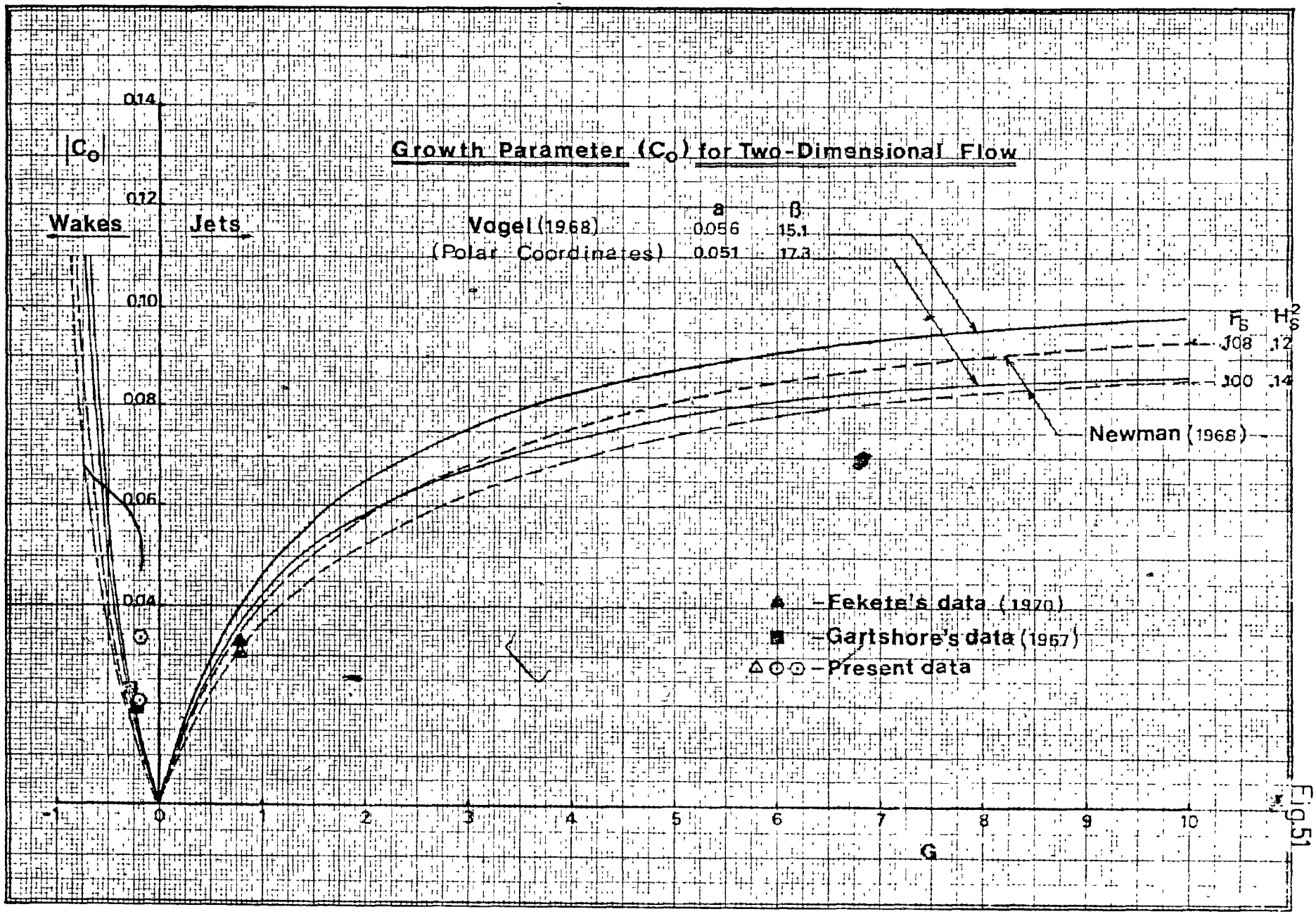

Fig.51

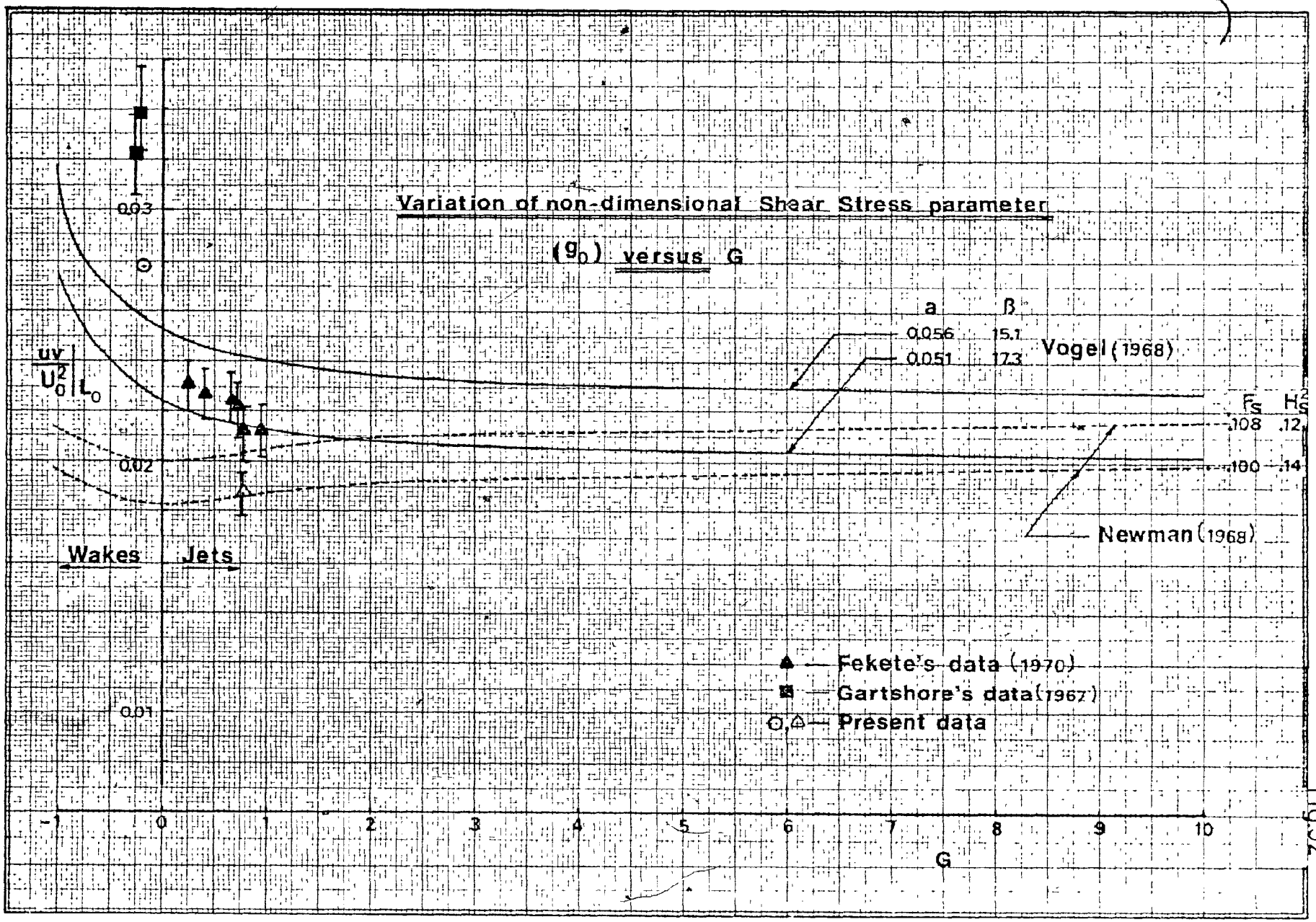
Variation of non-dimensional Shear Stress parameter
(g_0) versus G
$\frac{uv}{U_0^2}\Big|_{L_0}$
0.03
0.02
0.01
a
ß
0.056
15.1
0.051
17.3
Vogel (1968)
Fs
Hs
.108
.12
.100
.14
Newman (1968)
Wakes
Jets
Fekete's data (1970)
Gartshore's data (1967)
Present data
-1
0
1
2
3
4
5
6
7
8
9
10
G

Fig.52

LEAVES 53 AND 54 OMITTED IN PAGE NUMBERING.

Fig. 53a

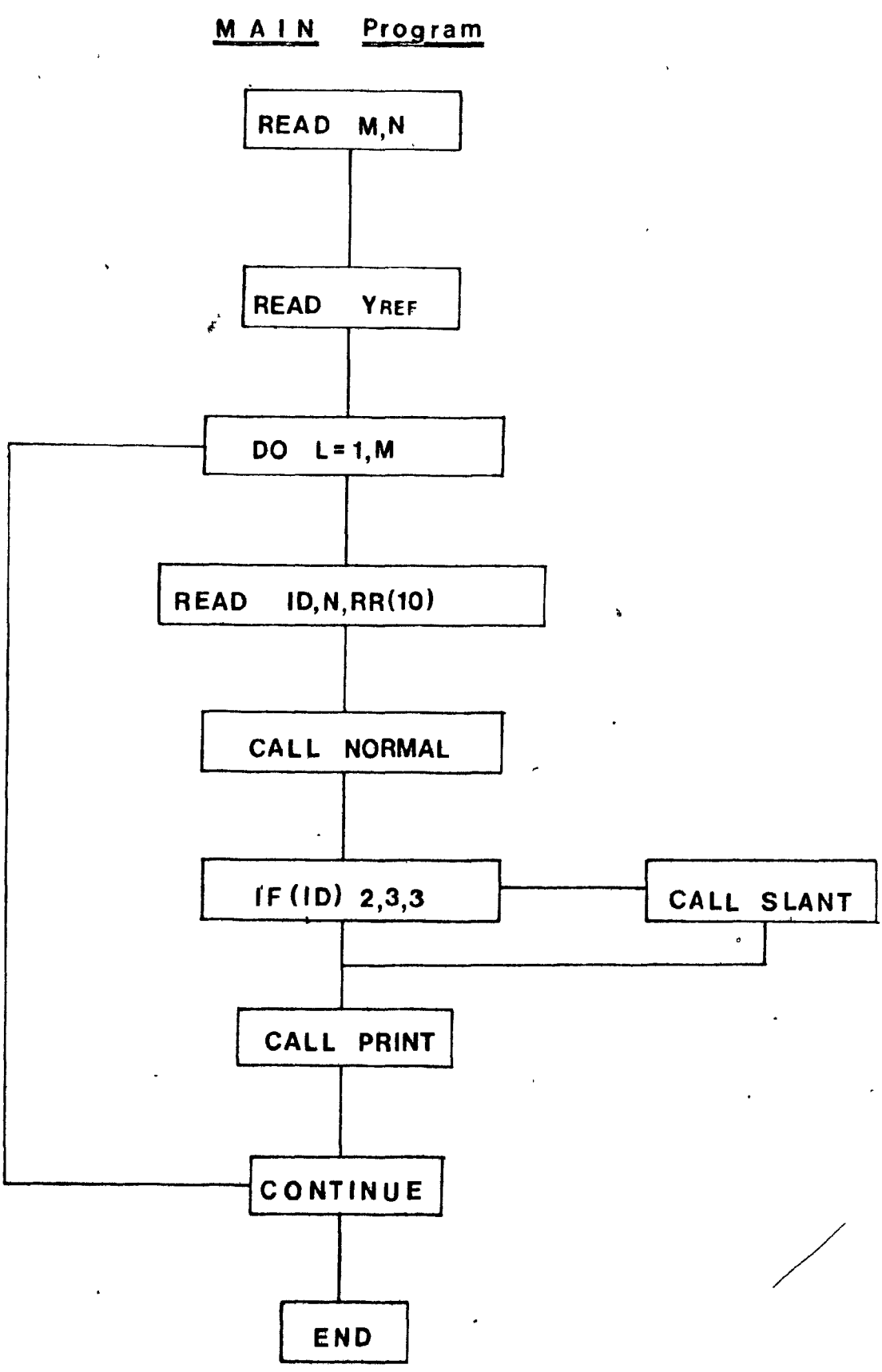
MAIN Program
READ M,N
READ YREF
DO L=1,M
READ ID,N,RR(10)
CALL NORMAL
IF(ID) 2,3,3
CALL SLANT
CALL PRINT
CONTINUE
END

Fig.53b

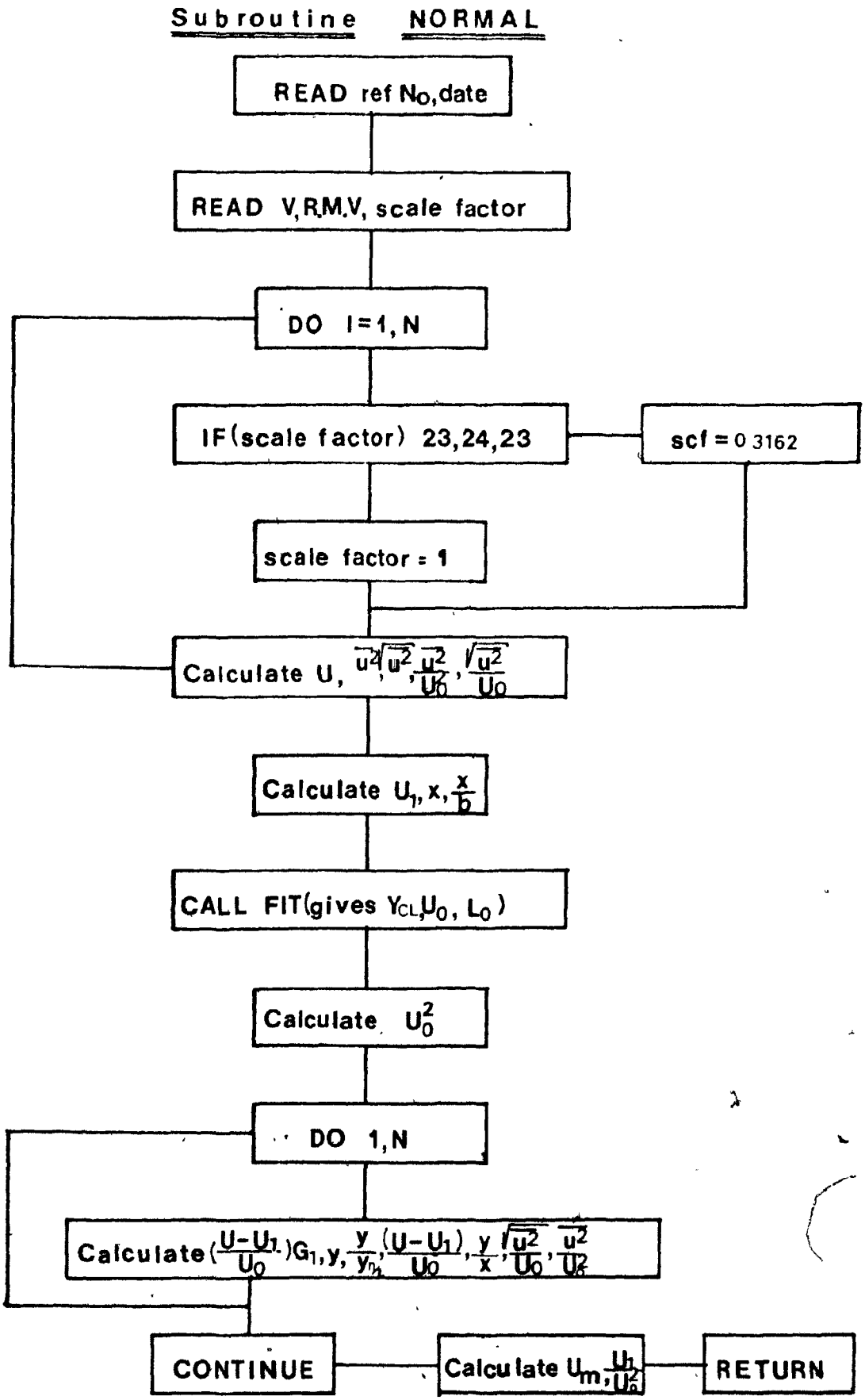
Subroutine NORMAL
READ ref No, date
READ V, R.M.V, scale factor
DO I=1, N
IF(scale factor) 23,24,23
scf = 0 3162
scale factor = 1
Calculate U, $\overline{u^2}$, $\sqrt{\overline{u^2}}$, $\frac{\overline{u^2}}{U_0^2}$, $\frac{\sqrt{\overline{u^2}}}{U_0}$
Calculate U_1, x, $\frac{x}{b}$
CALL FIT(gives Y_{CL}, U_0, L_0)
Calculate U_0^2
DO 1, N
Calculate $(\frac{U-U_1}{U_0})G_1$, y, $\frac{y}{y_{\frac{1}{2}}}$, $\frac{(U-U_1)}{U_0}$, $\frac{y}{x}$, $\frac{\sqrt{\overline{u^2}}}{U_0}$, $\frac{\overline{u^2}}{U_0^2}$
CONTINUE
Calculate U_m, $\frac{U_1}{U_0}$
RETURN

Fig.53c

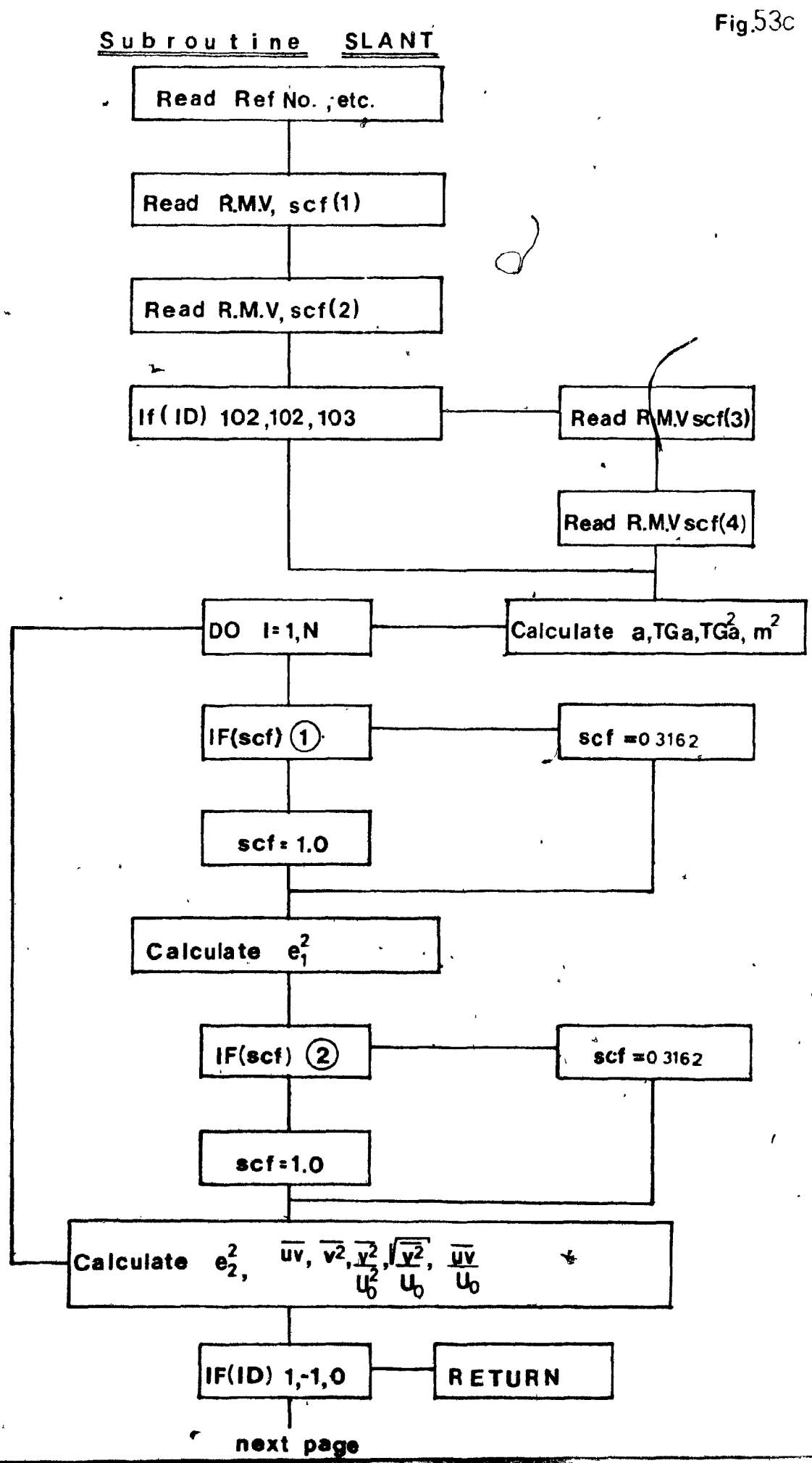
Subroutine SLANT
Read Ref No. ;etc.
Read R.M.V, scf(1)
Read R.M.V, scf(2)
If (ID) 102 ,102 , 103
Read R.M.V scf(3)
Read R.M.V scf(4)
DO I= 1,N
Calculate a,TGa,TGa², m²
IF(scf) ①
scf =0 3162
scf = 1.0
Calculate e₁²
IF(scf) ②
scf =0 3162
scf =1.0
Calculate e₂², uv, v², v²/u₀², √v²/u₀, uv/u₀
IF(ID) 1,-1,0
RETURN
next page

Fig. 53d

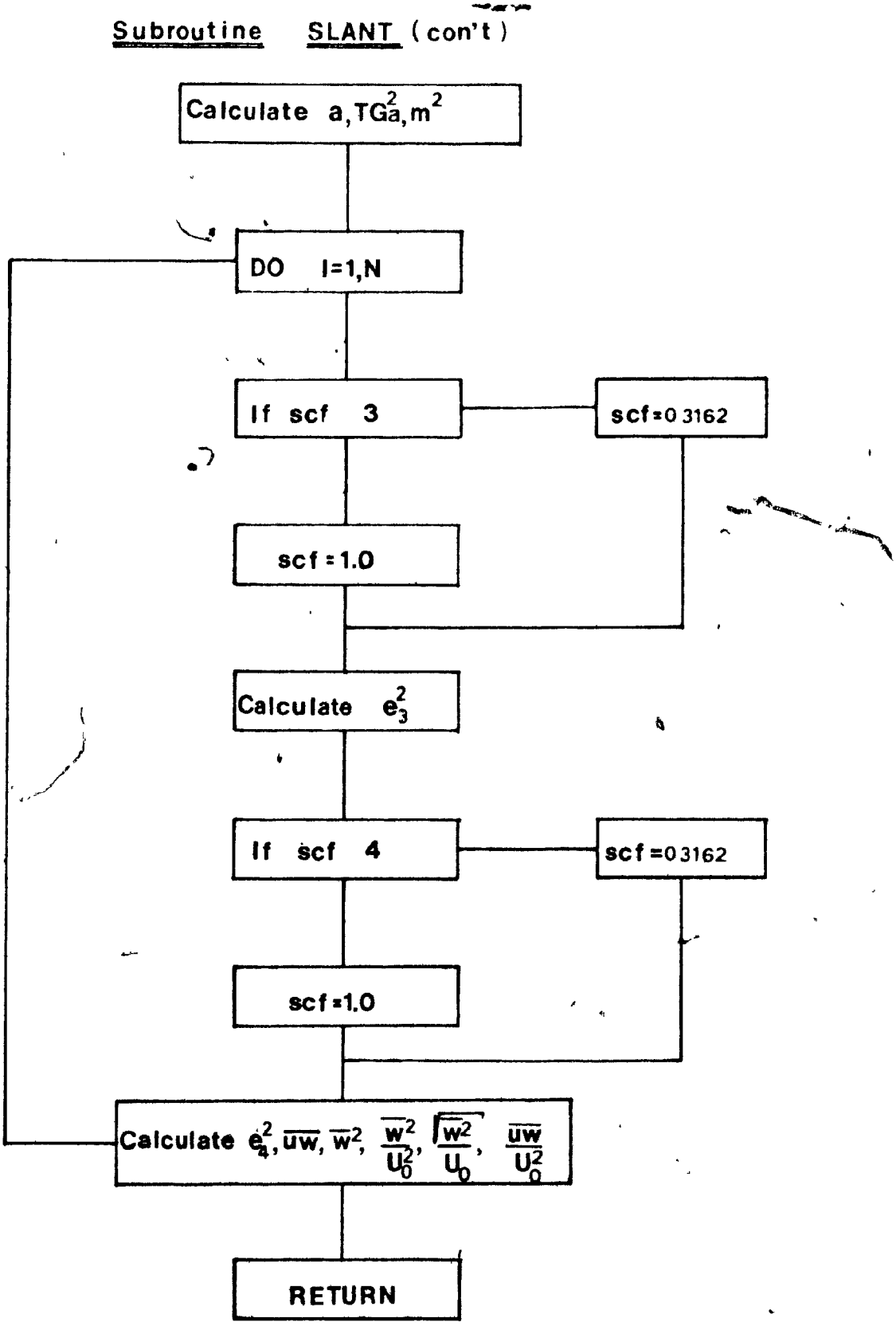
Subroutine SLANT (con't)
Calculate a, TG_a^2, m^2
DO I=1,N
If scf 3
scf=0.3162
scf=1.0
Calculate e_3^2
If scf 4
scf=0.3162
scf=1.0
Calculate e_4^2, $\overline{uw}$, $\overline{w^2}$, $\frac{\overline{w^2}}{U_0^2}$, $\frac{\sqrt{\overline{w^2}}}{U_0}$, $\frac{\overline{uw}}{U_0^2}$
RETURN

REF.NO.	XTE	DAY	MO	YR	WIRE NO.	WIRE MTL.	WIRE DIA.IN	WIRE ANGLE	WIRE CALIBRATION DV/DU	WIRE CALIBRATION INTERCEPT	EFF.VEL. RATIO
147	47.0	25	9	76	1	1	0.0032	90.00	0.3010	-0.2139	
147	47.0	27	9	76	1	2	0.0002	43.55	0.3509	-0.2710	1.01
147	47.0	27	9	76	1	2	0.0002	45.55	0.3509	-0.2710	1.01

REF. ORDINATE	MEAN VOLTAGE	N WIRE RMS VOLTS	SCALE FACTR	UV1 RMS VOLTS	SCALE FACTR	UV2 RMS VOLTS	SCALE FACTR	UW1 RMS VOLTS	SCALE FACTR	UW2 RMS VOLTS	SCALE FACTR
1 7.50	4.7000	0.15530	10.	0.24520	1.	0.24640	1.	0.20730	1.	0.22430	1.
1 8.00	4.3010	0.19750	10.	0.30820	1.	0.30050	1.	0.26570	1.	0.30010	1.
1 8.50	4.3000	0.27500	10.	0.10920	0.	0.19310	0.	0.27180	1.	0.44290	1.
1 9.00	4.2940	0.10800	0.	0.18920	0.	0.25450	0.	0.20030	0.	0.21430	0.
1 9.50	4.2380	0.18880	0.	0.23410	0.	0.32410	0.	0.25180	0.	0.27760	0.
1-0.00	4.1580	0.25130	0.	0.27070	0.	0.33630	0.	0.26230	0.	0.32740	0.
1-0.50	4.0700	0.29330	0.	0.30220	0.	0.43470	0.	0.38420	0.	0.38740	0.
1-1.00	3.9580	0.32630	0.	0.33790	0.	0.46110	0.	0.41290	0.	0.41480	0.
1-1.50	3.8200	0.34610	0.	0.35850	0.	0.48840	0.	0.43730	0.	0.43490	0.
1-2.00	3.7340	0.35000	0.	0.37710	0.	0.47300	0.	0.45280	0.	0.43960	0.
1 2.25	3.6340	0.35180	0.	0.37900	0.	0.45340	0.	0.44790	0.	0.43720	0.
1-2.65	3.5700	0.34750	0.	0.38460	0.	0.45500	0.	0.44190	0.	0.42660	0.
1 3.00	3.5280	0.34250	0.	0.39320	0.	0.43380	0.	0.44060	0.	0.42100	0.
1-3.20	3.4720	0.33870	0.	0.40520	0.	0.42880	0.	0.44040	0.	0.41240	0.
1-3.40	3.4180	0.33520	0.	0.41040	0.	0.41800	0.	0.43490	0.	0.41200	0.
1 3.60	3.4150	0.33070	0.	0.42340	0.	0.41130	0.	0.43450	0.	0.41190	0.
1-3.80	3.4170	0.33420	0.	0.42670	0.	0.41010	0.	0.43340	0.	0.41110	0.
1-4.00	3.4780	0.33690	0.	0.44330	0.	0.43180	0.	0.43400	0.	0.40640	0.
1-4.35	3.5290	0.34110	0.	0.45690	0.	0.38720	0.	0.43490	0.	0.42700	0.
1-4.65	3.5770	0.35390	0.	0.47400	0.	0.37670	0.	0.44830	0.	0.42270	0.
1-5.00	3.6300	0.35400	0.	0.50190	0.	0.37230	0.	0.46280	0.	0.43700	0.
1 5.25	3.7000	0.35240	0.	0.49690	0.	0.36640	0.	0.45520	0.	0.43910	0.
1 5.50	3.7540	0.35180	0.	0.49500	0.	0.36180	0.	0.43300	0.	0.43040	0.
1 5.75	3.8260	0.34670	0.	0.49300	0.	0.35320	0.	0.42790	0.	0.42440	0.
1 6.00	3.8800	0.33660	0.	0.47770	0.	0.34330	0.	0.42790	0.	0.39870	0.
1 6.50	3.9990	0.31570	0.	0.45150	0.	0.32080	0.	0.38200	0.	0.38620	0.
1 7.00	4.1110	0.26740	0.	0.39770	0.	0.27640	0.	0.34530	0.	0.32140	0.
1 7.50	4.2050	0.21800	0.	0.31660	0.	0.23190	0.	0.26190	0.	0.25950	0.
1 8.00	4.2690	0.11680	0.	0.23230	0.	0.13010	0.	0.20740	0.	0.11000	0.
1 8.50	4.2990	0.26470	10.	0.18740	0.	0.40940	1.	0.37090	1.	0.37770	1.
1 9.00	4.2940	0.20660	10.	0.33120	1.	0.32730	1.	0.24410	1.	0.30030	1.
1 9.50	4.2900	0.13750	10.	0.26260	1.	0.24590	1.	0.23260	1.	0.20670	1.

Fig. 54a

REF.NO.	XTE	DAY	MO	YR	WIRE NO.	WIRE MTL.	WIRE DIA.IN	WIRE ANGLE	WIRE CALIBRATION DY/DU	WIRE CALIBRATION INTERCEPT	REF.VEL. RATIO
147	47.0	25	9	76	1	1	0.0002	90.00	0.3019	-0.2139	
147	47.0	27	9	76	1	2	0.0002	45.55	0.1509	-0.2710	1.01
147	47.0	27	9	76	1	2	0.0002	45.55	0.1509	-0.2710	1.01

X	X/B	LD	UO	UM	U1	UO/U1	YCL	XO
106.6	213.	2.26	2.857	12.076	14.933	0.191	143.65	59.6

YREF	Y	U	U-U1	/U-U1/G	RMSU	MSU	MSV	MSW	UV	UW
1 7.50	-6.15	15.0	-0.0	0.0	0.163	0.026	0.034	0.013	-0.000	0.002
1 7.00	-5.65	15.0	-0.0	0.0	0.207	0.043	0.063	0.027	-0.014	0.005
1 6.50	-5.15	15.0	-0.0	0.1	0.288	0.083	0.109	0.058	-0.044	0.012
1 6.00	-4.65	14.9	0.0	0.2	0.360	0.130	0.208	0.235	-0.061	0.012
1 5.50	-4.15	14.7	0.2	0.3	0.625	0.391	0.281	0.198	-0.106	0.029
1 5.00	-3.65	14.5	0.5	0.5	0.832	0.693	0.294	0.204	-0.140	-0.000
1 4.50	-3.15	14.2	0.7	0.7	0.972	0.944	0.334	0.300	-0.205	0.035
1 4.00	-2.65	13.8	1.1	1.1	1.081	1.168	0.190	0.200	-0.208	0.037
1 3.50	-2.15	13.4	1.5	1.5	1.143	1.307	0.224	0.207	-0.232	0.002
1 3.00	-1.65	13.1	1.9	2.0	1.150	1.344	0.165	0.314	-0.178	-0.027
1 2.75	-1.30	12.7	2.2	2.3	1.165	1.358	0.132	0.275	-0.150	-0.030
1 2.55	-1.00	12.5	2.4	2.5	1.151	1.325	0.105	0.247	-0.118	-0.028
1 3.00	-0.55	12.4	2.5	2.7	1.134	1.287	0.138	0.279	-0.071	-0.027
1 3.20	-0.45	12.2	2.7	2.8	1.122	1.259	0.110	0.259	-0.060	-0.030
1 3.40	-0.25	12.0	2.9	2.8	1.110	1.233	0.105	0.264	-0.013	-0.041
1 3.60	-0.05	12.0	2.9	2.9	1.095	1.200	0.257	0.206	0.021	-0.040
1 3.80	0.15	12.0	2.9	2.8	1.107	1.225	0.234	0.265	0.029	-0.038
1 4.00	0.35	12.2	2.7	2.8	1.116	1.245	0.212	0.279	0.001	-0.044
1 4.25	0.70	12.4	2.5	2.7	1.130	1.277	0.217	0.254	0.134	-0.033
1 4.65	1.00	12.6	2.4	2.5	1.172	1.374	0.119	0.209	0.170	-0.047
1 5.00	1.35	12.8	2.1	2.2	1.173	1.375	0.252	0.315	0.230	-0.043
1 5.25	1.60	13.0	2.0	2.0	1.167	1.363	0.265	0.273	0.208	-0.047
1 5.50	1.85	13.1	1.8	1.8	1.165	1.358	0.207	0.194	0.241	-0.004
1 5.75	2.10	13.4	1.6	1.6	1.148	1.319	0.213	0.230	0.250	-0.025
1 6.00	2.35	13.6	1.4	1.4	1.115	1.243	0.158	0.181	0.233	-0.051
1 6.50	2.85	14.0	1.0	0.9	1.046	1.094	0.184	0.134	0.213	-0.007
1 7.00	3.35	14.3	0.5	0.5	0.866	0.795	0.104	0.143	0.173	-0.074
1 7.50	3.85	14.6	0.3	0.4	0.722	0.521	0.121	0.043	0.098	-0.003
1 8.00	4.35	14.8	-0.1	0.2	0.397	0.158	0.218	0.185	0.046	-0.015
1 8.50	4.85	14.9	-0.0	0.1	0.259	0.099	0.131	0.028	0.039	0.001
1 9.00	5.35	14.9	0.0	0.1	0.216	0.047	0.046	0.016	0.001	0.006
1 9.50	5.85	14.9	0.0	0.0	0.144	0.021	0.034	0.020	0.002	-0.002

Fig 5.4 b

REF.NO.	XTE	DAY MO YR	WIRE NO.	WIRE MTL.	WIRE DIA.IN	WIRE ANGLE	WIRE CALIBRATION DV/DU	INTERCEPT	REF.VEL. RATIO
147	47.0	25 9 76	1	1	0.0002	90.00	0.3019	-0.2179	
147	47.0	27 9 76	1	2	0.0002	45.55	0.3509	-0.2710	1.01
147	47.0	27 9 76	1	2	0.0002	45.55	0.3509	-0.2710	1.01

X	X/B	LO	UO	UM	U1	UO/U1	YCL	XO	DLX	G
106.6	213.	2.26	2.857	12.076	14.933	0.191	143.65	[illegible]	.0218C	-.1930

YREF	Y/LO	Y/X	U-U1 / UO	/U-U1/G / UO	RMSU / U	RMSU / UO	RMSV / UO	RMSW / UC	MSU / SU	MSU / SUO	MSV / SUO	MSW / SUO	Q2 / SUO	UV / SUO	MUV / SUO	UW / SUO	Y/LOX
137.5	-2.72	-.0577	-.007	0.006	0.011	0.057	0.059	0.043	0.0001	0.0032	0.0035	0.0019	0.009	-.0000	0.0011	0.0002	-2.65
138.0	-2.50	-.0530	-.008	0.013	0.014	0.072	0.096	0.062	0.0002	0.0052	0.0093	0.0079	0.018	-.0018	0.0023	0.0007	-2.43
138.5	-2.28	-.0433	-.007	0.027	0.019	0.101	0.125	0.091	0.0004	0.0107	0.0156	0.0082	0.034	-.0030	0.0044	0.0016	-2.22
139.0	-2.06	-.0436	0.012	0.053	0.024	0.126	0.206	0.187	0.0006	0.0159	0.0426	0.0176	0.092	-.0091	0.0077	0.0016	[illegible]
139.5	-1.84	-.0389	0.065	0.096	0.042	0.219	0.201	0.168	0.0018	0.0479	0.0402	0.0283	0.116	-.0140	0.0127	0.0038	-1.79
140.0	-1.62	-.0343	0.158	0.163	0.057	0.291	0.184	0.172	0.0073	0.0349	0.0340	0.0297	0.149	-.0212	0.0182	-.0003	-1.57
140.5	-1.40	-.0296	0.260	0.259	0.068	0.340	0.179	0.207	0.0047	0.1156	0.0320	0.0423	0.191	-.0272	0.0247	0.0037	-1.36
141.0	-1.17	-.0249	0.390	0.384	0.078	0.378	0.166	0.193	0.0061	0.1431	0.0275	0.0372	0.201	-.0275	0.0305	0.0033	-1.14
141.5	-0.95	-.0202	0.530	0.533	0.086	0.400	0.179	0.206	0.0077	0.1601	0.0320	0.0424	0.234	[illegible]	[illegible]	0.0032	[illegible]
142.0	-0.73	-.0155	0.650	0.690	0.089	0.406	0.154	0.212	0.0079	0.1547	0.0357	0.0495	0.233	[illegible]	[illegible]	[illegible]	-0.71
142.3	-0.58	-.0122	0.766	0.794	0.091	0.408	0.137	0.198	0.00 4	0.1664	0.0138	0.0303	[illegible]	[illegible]	[illegible]	[illegible]	[illegible]
142.6	-0.44	-.0094	0.840	0.872	0.092	0.403	0.154	0.188	0.0014	0.1523	0.0036	0.0353	0.221	-.0136	[illegible]	-.0037	[illegible]
143.0	-0.29	-.0061	0.889	0.944	0.092	0.397	0.140	0.200	0.00 4	0.1577	0.0137	0.0359	0.217	-.0094	0.0177	-.0015	-0.28
143.2	-0.20	-.0042	0.957	0.973	0.092	0.393	0.165	0.192	0.00 4	0.1542	0.0272	0.0370	0.216	-.0055	0.0126	-.0057	-0.19
143.4	-0.11	-.0024	1.016	0.991	0.092	0.394	0.167	0.194	0.00 5	0.1510	0.0340	0.0377	0.217	-.0019	0.0072	-.0054	-0.11
143.6	-0.02	-.0005	1.020	1.000	0.091	0.393	0.190	0.206	0.00 3	0.1370	0.0361	0.0423	0.225	0.0028	0.0015	-.0053	-0.02
143.8	0.07	0.0014	1.017	0.987	0.092	0.387	0.193	0.195	0.00 5	0.1501	[illegible]	0.0379	[illegible]	[illegible]	0.0042	-.0071	[illegible]
144.0	0.15	0.0033	0.946	0.984	0.091	0.391	0.174	0.184	0.0013	0.1326	0.0304	0.0340	0.217	0.0120	0.0098	-.0058	0.15
144.3	0.31	0.0065	0.897	0.936	0.091	0.395	0.176	0.191	0.0053	0.1564	0.0311	0.0363	0.224	0.0154	0.0139	-.0071	[illegible]
144.6	0.44	0.0094	0.872	0.873	0.093	0.410	0.146	0.171	0.0047	0.1644	0.0212	[illegible]	0.214	[illegible]	0.0251	[illegible]	0.43
145.0	0.60	0.0126	0.747	0.761	0.092	0.410	0.190	0.212	0.0014	0.1685	[illegible]	[illegible]	[illegible]	[illegible]	[illegible]	[illegible]	[illegible]
145.2	0.71	0.0150	0.639	0.767	0.090	[illegible]	0.179	0.197	0.0011	0.1569	[illegible]	[illegible]	[illegible]	[illegible]	[illegible]	[illegible]	[illegible]
145.5	0.82	0.0173	0.626	0.629	0.089	0.408	0.172	0.167	0.0019	0.1664	[illegible]	[illegible]	0.224	[illegible]	0.0341	-.0036	[illegible]
145.7	0.93	0.0197	0.543	0.550	0.086	0.402	0.174	0.191	0.00 4	0.1516	0.0304	[illegible]	0.275	0.0730	0.0340	-.0077	[illegible]
146.0	1.04	0.0220	0.480	0.473	0.082	0.390	0.168	0.161	0.0018	0.1523	[illegible]	0.0254	[illegible]	[illegible]	0.0329	-.0067	1.01
146.5	1.26	0.0267	0.342	0.332	0.075	0.360	0.152	0.138	[illegible]	0.1140	0.0253	0.0171	[illegible]	[illegible]	[illegible]	[illegible]	1.23
147.0	1.48	0.0314	0.213	0.218	0.062	0.310	0.167	0.143	0.0018	0.0901	0.0278	[illegible]	0.144	0.0228	[illegible]	-.0045	1.44
147.5	1.70	0.0361	0.104	0.134	0.049	0.253	0.132	0.079	0.00 4	0.0539	0.0173	0.0062	[illegible]	0.0130	0.0153	-.0073	[illegible]
148.0	1.93	0.0408	0.029	0.077	0.026	0.155	0.177	0.163	0.0017	0.0183	0.0312	[illegible]	0.076	0.0061	0.0102	-.0019	1.87
148.5	2.15	0.0455	-.005	0.041	0.020	0.104	0.137	0.063	0.0014	0.0109	0.0147	0.0040	0.034	0.0051	0.0062	0.0001	[illegible]
149.0	2.37	0.0502	0.000	0.020	0.014	0.076	0.090	0.048	0.0012	0.0057	0.0064	0.0023	0.014	0.0001	0.0035	0.0007	[illegible]
149.5	2.59	0.0549	0.005	0.010	0.010	0.050	0.070	0.054	0.0011	0.0025	0.0043	0.0079	0.010	0.0002	0.0018	-.0003	2.52

Fig. 54c

Fig.55

```
$WATFIV                PAGES=60,LINES=60
C
C          THIS PROGRAM SETS THE LOUVRES FOR AN APPROPRIATE
C          ........ .... .. PRESSURE GRADIENT..........
C* * * * *                 ........ .....                   ........
C          .....         G=(M-U)/U)=-0.24     .....
C          ......        M=-0.312
C          .....F=(H-PREF)/(H-P2)=1.32
      DIMENSION XS(50),S(50)
      X0= 30.25
      XREF=9.0
      READ(5,100)PF,PLM,FK
  100 FORMAT(3F10.4)
      PF=PF*(XREF-X0)**(2.0*PLM)
      FT=0.7071/(1.0-PLM)
      XS(1)=9.0
      DO 1 I=1,40
      SLAT=2.50
      IF(I.EQ.1)GO TO 2
      IF(I/5*5.EQ.I)SLAT=3.375
      XS(I)=(S(I-1)+(S(I-1)+1.0))*SLAT
    2 F=SQRT(PF/(XS(I)-X0)**(2.0*PLM)-1.0+FK)*FT
      S(I)=-1.0/(F*(XS(I)-X0)+1.0)
      IF(XS(I).GT.96.0)GO TO 3
    1 CONTINUE
    3 N=I
      WRITE(6,200)PF,PLM,FK
  200 FORMAT(1H0,16H(H-P2)/(H-PREF)=,F10.4/1H0,2HM=,F10.4/1H0,2HK=,F10.4
     1//)
      WRITE(6,201)(I,XS(I),S(I),I=1,N)
  201 FORMAT(1H0,8HSLAT NO.,12X,1HX,10X,3HS/L/(1H0,4X,I2,7X,F12.2,F12.4)
     1 )
      STOP
      END
```

$DATA

(H-P2)/(H-PREF)= 0.1337

M= -0.3120

K= 0.7000

SLAT NO.	X	S/L
1	9.00	0.2334
2	12.08	0.2051
3	15.10	0.1829
4	18.05	0.1630
5	21.99	0.1455
6	24.85	0.1338
7	27.68	0.1237
8	30.49	0.1150
9	33.28	0.1074
10	37.02	0.0995
11	39.76	0.0927
12	42.50	0.0876
13	45.21	0.0829
14	47.92	0.0787
15	51.56	0.0736
16	54.25	0.0702
17	56.92	0.0671
18	59.59	0.0642
19	62.25	0.0616
20	65.83	0.0583
21	68.48	0.0561
22	71.12	0.0540